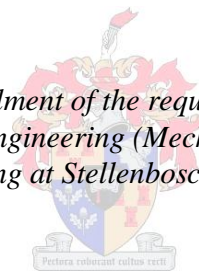


Quantification of the normal patellofemoral shape and its clinical applications

by
Kyung Jin Cho

*Thesis presented in fulfilment of the requirements for the degree of
Master of Science in Engineering (Mechanical) in the Faculty of
Engineering at Stellenbosch University*



Supervisor: Dr. Jacobus Hendrik Müller
Prof. Cornie Scheffer

March 2013

DECLARATION

By submitting this thesis electronically, I declare that the entirety of the work contained therein is my own, original work, that I am the sole author thereof (save to the extent explicitly otherwise stated), that reproduction and publication thereof by Stellenbosch University will not infringe any third party rights and that I have not previously in its entirety or in part submitted it for obtaining any qualification.

Signature:

Kyung Jin Cho

Date:

ABSTRACT

The shape of the knee's trochlear groove is a very important factor in the overall stability of the knee. However, a quantitative description of the normal three-dimensional geometry of the trochlea is not available in the literature. This is also reflected in the poor outcomes of patellofemoral arthroplasty (PFA). In this study, a standardised method for femoral parameter measurements on three-dimensional femur models was established. Using software tools, virtual femur models were aligned with the mechanical and the posterior condylar planes and this framework was used to measure the femoral parameters in a repeatable way. An artificial neural network (ANN), incorporating the femoral parameter measurements and classifications done by experienced surgeons, was used to classify knees into normal and abnormal categories. As a result, 15 knees in the database were classified by the ANN as being normal. Furthermore, the geometry of the normal knees was analysed by fitting B-spline curves and circular arcs on their sagittal surface curves to prove and reconfirm that the groove has a circular shape on a sagittal plane. Self-organising maps (SOM), which is a type of ANN, was trained with the acquired data of the normal knees and in this way the normal trochlear geometry could be predicted. The prediction of the anterior-posterior (AP) distance and the trochlear heights showed an average agreement of 97 % between the actual and the predicted normal geometries. A case study was conducted on four types of trochlear dysplasia to determine a normal geometry for these knees, and a virtual surface reconstruction was performed on them. The study showed that the trochlea was deepened after the surface reconstruction, having an average trochlea depth of 5.5 mm compared to the original average value of 2.9 mm. In summary, this research proposed a quantitative method for describing and predicting the normal geometry of a knee by making use of ANN and the femoral parameters that are unaffected by trochlear dysplasia.

UITTREKSEL

Die vorm van die trogleêre keep is 'n belangrike faktor in patella-stabiliteit. Tog is 'n kwantitatiewe beskrywing van die normale driedimensionele geometrie van die troglea nog nie beskikbaar nie, wat duidelik blyk uit die swak uitkomstes van patellofemorale artroplastie (PFA). In hierdie studie is 'n gestandaardiseerde metode vir die meting van femorale parameters op grond van driedimensionele femurmodelle ontwikkel. Die femurmodel is in lyn gebring met die meganiese en posterior kondilêre vlak, welke raamwerk gebruik is om die femorale parameters op 'n herhaalbare wyse te meet. Die normale knieë is geklassifiseer met 'n kunsmatige neurale netwerk (ANN), wat die femorale parameter-mate sowel as die chirurgiese klassifikasie ingesluit het, en 15 knieë is gevolglik as normaal aangewys. Die normale knie-geometrie is ontleed deur B-lat-krommes en sirkelboë op die sagittale oppervlak-kurwes aan te bring om te bewys en te herbevestig dat die keep uit 'n sirkelvorm op 'n sagittale vlak bestaan. Die ingesamelde data van die normale knieë is ingevoer by selfreëlende kaarte (SOM), synde 'n soort ANN, wat die navorser in staat gestel het om die normale trogleêre geometrie te voorspel. Die voorspelling van die anterior-posterior (AP) afstand en die trogleêre hoogtes toon 'n gemiddelde ooreenkoms van meer as 97 % tussen die werklike en voorspelde normale geometrie. 'n Gevallestudie is op vier soorte trogleêre displasie uitgevoer om die normale geometrie te voorspel en 'n oppervlakrekonstruksie daarop uit te voer. Hierdie studie het getoon dat die troglea ná oppervlakrekonstruksie verdiep was, met 'n gemiddelde trogleadiepte van 5.5 mm in vergelyking met die aanvanklike gemiddelde waarde van 2.9 mm. Hierdie navorsing het dus 'n metode aan die hand gedoen vir die kwantitatiewe beskrywing en voorspelling van normale geometrie met behulp van ANN sowel as met die femorale parameters wat nie deur die trogleêre displasie geraak word nie.

ACKNOWLEDEMENTS

Special thanks to:

- my supervisors, Dr. J.H. Müller and Prof. C. Scheffer, for providing guidance and understanding throughout the project, and without whom I would not have been able to complete this project;
- orthopaedic surgeon, Dr. P.J. Erasmus, for inspiring discussions and the clinical input;
- Kiran Dellimore for proofreading and encouragement;
- BERG; and
- my friends and family.

DEDICATIONS

모든 것을 창조한 전능자 그리고 불쌍한 길 잃은 내 영혼에게

TABLE OF CONTENTS

	Page
DECLARATION	I
ABSTRACT	III
UITTREKSEL	IV
ACKNOWLEDEMENTS.....	V
DEDICATIONS	VI
LIST OF FIGURES	X
LIST OF TABLES.....	XII
NOMENCLATURE.....	XIV
1 INTRODUCTION.....	1
1.1 BACKGROUND.....	1
1.2 MOTIVATION	3
1.3 OBJECTIVES	3
1.4 SCOPES AND LIMITATIONS	4
1.5 THESIS LAYOUT	5
2 LITERATURE REVIEW	6
2.1 ANATOMICAL TERMS AND REFERENCES OF THE PATELLOFEMORAL JOINT.....	6
2.1.1 <i>Orientation and the movement of the patellofemoral joint.....</i>	<i>6</i>
2.1.2 <i>Referencing axes on the femur.....</i>	<i>7</i>
2.2 THE FACTORS AFFECTING PATELLOFEMORAL JOINT STABILITY.....	9
2.2.1 <i>Soft tissues and their functions</i>	<i>9</i>
2.2.2 <i>Shape of the trochlea</i>	<i>12</i>
2.3 IDENTIFICATION OF TROCHLEAR DYSPLASIA.....	13
2.3.1 <i>Qualitative methods for identifying trochlear dysplasia</i>	<i>13</i>
2.3.2 <i>Quantitative methods for identifying trochlear dysplasia.....</i>	<i>15</i>
3 THREE-DIMENSIONAL MODEL GENERATION AND FEMORAL PARAMETER MEASUREMENTS	25
3.1 ETHICAL APPROVAL AND STUDY POPULATION	25
3.2 VALIDATION OF THE THREE-DIMENSIONAL MODEL GENERATION AND MEASUREMENT SYSTEMS.....	25
3.2.1 <i>Segmentation techniques from CT Scans</i>	<i>25</i>

3.2.2	<i>Testing the effect of the smoothing tool on the accuracy of the model</i>	26
3.2.1	<i>Validation of the measurement system with repeatability and reproducibility (R&R) test</i>	28
3.3	FEMORAL PARAMETER MEASUREMENTS AND THE FINDINGS.....	29
3.3.1	<i>Reference and coordinate system</i>	29
3.3.2	<i>Femoral parameter measurement techniques</i>	33
3.3.3	<i>Findings from the femoral parameter measurements</i>	37
3.4	DISCUSSION.....	39
4	CLINICAL CLASSIFICATION OF NORMAL AND ABNORMAL KNEES	40
4.1	QUANTITATIVE CLASSIFICATION WITH FEMORAL PARAMETERS.....	40
4.2	QUALITATIVE CLASSIFICATION BY SURGEONS.....	40
4.3	CLASSIFICATION WITH ARTIFICIAL NEURAL NETWORKS PATTERN RECOGNITION TOOL	41
4.3.1	<i>Overview of the procedure</i>	42
4.3.2	<i>Selection of optimum number of input parameters and number of hidden layer neurons</i>	43
4.4	ANALYSIS OF CLASSIFICATION METHODS	44
4.5	DISCUSSION.....	45
5	ANALYSES FOR NORMAL TROCHLEA PREDICTION	47
5.1	SAGITTAL SURFACE CURVE ANALYSIS.....	47
5.1.1	<i>Sagittal surface curve generation and selection methods</i>	47
5.1.2	<i>Generation of B-spline curves and finding the centres of the curvatures</i>	48
5.1.3	<i>Circular arc fitting using least squares theorem</i>	49
5.1.4	<i>Results of the curve analysis</i>	51
5.1.5	<i>Plane fitting to the centre points of the least squares circular arcs</i>	51
5.2	VALIDATION FOR NORMAL TROCHLEA GEOMETRY PREDICTION METHOD: SELF-ORGANIZING MAPS (SOM)	53
5.2.1	<i>Introduction</i>	53
5.2.2	<i>Materials and methods</i>	53
5.2.3	<i>Results and discussion</i>	55
5.3	OVERVIEW OF THE NORMAL TROCHLEAR GEOMETRY ANALYSES AND PREDICTION.....	57
6	CASE STUDY: RECONSTRUCTION OF THE TROCHLEAR GROOVE OF THE DYSPLASTIC KNEES USING NEURAL NETWORKS	59
6.1	MATERIALS AND METHODS	59
6.2	RESULTS AND DISCUSSION OF THE SURFACE PREDICTION AND REMODELLING.....	60
6.3	CLINICAL SUGGESTIONS AND TROCHLEOPLASTY SELECTION	63
6.4	OVERVIEW OF THE CASE STUDY	65

7	CONCLUSIONS.....	67
7.1	SUMMARY OF METHODS IN CONTEXT OF THE LITERATURE STUDY	67
7.1.1	<i>Three-dimensional model generation</i>	67
7.1.2	<i>Reference framework</i>	67
7.1.3	<i>Parameter measurement</i>	68
7.1.4	<i>Sagittal curve analysis method</i>	68
7.1.5	<i>Artificial neural networks (ANN)</i>	68
7.2	SUMMARY OF OUTCOMES AND MAJOR CONCLUSIONS.....	69
7.2.1	<i>Standardised three-dimensional model measurement system</i>	69
7.2.2	<i>Trochlear dysplasia identification</i>	69
7.2.3	<i>Normal geometry</i>	70
7.3	CLINICAL APPLICATIONS	70
7.3.1	<i>Prosthesis design</i>	70
7.3.2	<i>Surgical planning</i>	71
7.4	LIMITATIONS AND FUTURE WORK.....	71
7.4.1	<i>Number of the samples</i>	71
7.4.2	<i>Cartilaginous geometry of the trochlea</i>	72
7.4.3	<i>Relative patellar position and geometry to the femur</i>	72
7.4.4	<i>Alignment of the lower limb</i>	72
8	REFERENCES.....	74
	APPENDIX A: MEASUREMENTS OF PATELLAR PARAMETERS	79
	APPENDIX B: CLASSIFICATION RESULTS.....	81
	APPENDIX C: TESTING FOR OPTIMAL RUNNING CONDITION OF ARTIFICIAL NEURAL NETWORKS (ANN) PATTERN RECOGNITION	83
	APPENDIX D: EQUATIONS FOR B-SPLINES	85
	APPENDIX E: SAGITTAL CURVE ANALYSES RESULTS.....	87
	APPENDIX F: SAGITTAL CURVES OF THE NORMAL KNEES	94
	APPENDIX G: COMPARISON OF THE SULCUS ANGLE MEASUREMENT METHODS	115

LIST OF FIGURES

FIGURE 1.1: ANTERIOR VIEW OF PATELLOFEMORAL JOINT	1
FIGURE 2.1: THREE ANATOMICAL VIEWS OF THE LEFT KNEE WITH THE ANATOMICAL DIRECTIONAL TERMS	6
FIGURE 2.2: ILLUSTRATION OF THE MOVEMENT OF THE PATELLOFEMORAL JOINT	7
FIGURE 2.3: ANATOMICAL LANDMARKS AND REFERENCE AXES ON THE TRANSVERSE VIEW OF DISTAL FEMUR EDITED FROM ASANO ET AL. (2004)	8
FIGURE 2.4: DEFINING ANATOMICAL AXES (RED AND BLUE) AND MECHANICAL AXIS (GREEN).....	8
FIGURE 2.5: CARTILAGE ON THE KNEE JOINT AND THE MENISCI.....	10
FIGURE 2.6: MEDIAL ANATOMY OF THE PATELLA STABILISERS EDITED FROM AMIS ET AL. (2003).....	11
FIGURE 2.7: ANTERIOR VIEW OF THE SOFT TISSUE STABILISERS EDITED FROM O’NEIL (1997).....	11
FIGURE 2.8: ANATOMY OF THE TROCHLEA	12
FIGURE 2.9: ILLUSTRATION OF PATELLOFEMORAL ARTHROPLASTY (PFA) ADAPTED FROM FARR ET AL. (2008)	13
FIGURE 2.10: CLASSIFICATION OF TROCHLEAR DYSPLASIA DEVELOPED BY H. DEJOUR ET AL. (1990) ADAPTED FROM ZAFFAGNINI ET AL. (2010)	14
FIGURE 2.11: TROCHLEAR DYSPLASIA CLASSIFICATION REPRODUCED FROM D. DEJOUR ET AL. (2007).....	14
FIGURE 2.12: THREE-DIMENSIONAL MODEL OF THE DISTAL FEMUR ADAPTED FROM BIEDERT ET AL. (2011)	15
FIGURE 2.13: MR IMAGE OF TROCHLEAR GROOVE ON DISTAL AND PROXIMAL PLANE ADAPTED FROM TEICHTAHL ET AL. (2007)....	16
FIGURE 2.14: THE ROMAN ARCH IS VISIBLE ON THE TRANSVERSE SLICE.....	17
FIGURE 2.15: MR IMAGE OF MEASUREMENT PLANES OF THE SAME FEMUR.....	18
FIGURE 2.16: (A) TROCHLEAR DEPTH (B) ANTERIOR-POSTERIOR (AP) DISTANCES ON A TRANSVERSE SLICE.....	18
FIGURE 2.17: SULCUS ANGLE MEASUREMENT ON A TRANSVERSE SLICE	20
FIGURE 2.18: LATERAL TROCHLEAR FACET INCLINATION (LTI) MEASUREMENT	21
FIGURE 2.19: MEASUREMENT OF LATERAL AND MEDIAL TROCHLEAR FACET LENGTHS	22
FIGURE 2.20: VENTRAL TROCHLEAR PROMINENCE (VTP) MEASUREMENT EDITED FROM PFIRRMANN ET AL. (2000)	23
FIGURE 3.1: THREE-DIMENSIONAL MODEL WAS GENERATED BY SEGMENTING CT SCANS	26
FIGURE 3.2: THE ASSUMPTIONS MADE TO ESTIMATE THE EFFECT OF THE CHANGE IN VOLUME DUE TO THE SMOOTHING EFFECT ON THE MODEL FEATURES	27
FIGURE 3.3: MEASUREMENT OF THE SULCUS ANGLES AND MAXIMUM DISTANCE BETWEEN THE SURFACE CURVES.....	27
FIGURE 3.4: HIGHLIGHTED REGION OF THE FEMORAL SHAFT	30
FIGURE 3.5: GENERATION OF THE BEST FIT SPHERE TO THE HIGHLIGHTED SURFACE OF THE FEMORAL HEAD	30
FIGURE 3.6: GENERATION OF THE ANATOMICAL AND MECHANICAL AXES.....	30
FIGURE 3.7: CONSTRUCTION OF THE POSTERIOR CONDYLAR PLANE	31
FIGURE 3.8: ILLUSTRATION OF THE DISTAL AND MEASUREMENT PLANES.....	32
FIGURE 3.9: THE COORDINATE SYSTEM FOR THE FEMUR MODEL	32

FIGURE 3.10: MEASUREMENT OF THE TROCHLEAR DEPTH	33
FIGURE 3.11: MEASUREMENT OF THE SULCUS ANGLE	34
FIGURE 3.12: MEASUREMENT OF LATERAL TROCHLEAR INCLINATION (LTI).....	34
FIGURE 3.13: ILLUSTRATION OF THE TROCHLEAR ASYMMETRY RATIO MEASUREMENT METHOD.....	35
FIGURE 3.14: MEASUREMENT OF THE ANTERIOR-POSTERIOR (AP) DISTANCES	36
FIGURE 3.15: MEDIAL-LATERAL (ML) DISTANCE MEASUREMENT	36
FIGURE 3.16: SCHEMATIC OF THE MECHANICAL MIDDLE AND POSTERIOR CONDYLAR PLANES.....	37
FIGURE 3.17: LATERAL VIEW FOR DEFINING VENTRAL TROCHLEAR PROMINENCE (VTP).....	37
FIGURE 4.1: (A) LATERAL VIEW OF THE DISTAL FEMUR, (B) FIRST TRANSVERSE CT SLICE ON WHICH THE ROMAN ARCH IS VISIBLE WHEN EXAMINED FROM THE DISTAL SIDE.	41
FIGURE 4.2: CLASSIFICATION METHOD USING PATTERN RECOGNITION FUNCTION OF ARTIFICIAL NEURAL NETWORKS (ANN).....	42
FIGURE 4.3: BOX-WHISKER PLOT FOR TROCHLEAR DEPTH, SULCUS ANGLE AND MIDDLE AP/ML	44
FIGURE 5.1: MECHANICAL MIDDLE PLANE (RED) AND OTHER SAGITTAL SLICING PLANES (BLUE).....	47
FIGURE 5.2: SELECTION OF THE PORTION OF THE CURVE TO BE ANALYSED (RED) A) ON A LATERAL SLICE (L3) AND B) MEDIAL SLICE (M1).....	48
FIGURE 5.3: CENTRE OF CURVATURE ESTIMATION METHOD.....	49
FIGURE 5.4: CENTRES OF THE CURVATURES FOR THE POINTS ON B-SPLINE CURVE FIT TO A SAGITTAL SURFACE CURVE (M2)	49
FIGURE 5.5: SELECTING THE CIRCULAR PORTION OF A SAGITTAL SURFACE CURVE (M2)	50
FIGURE 5.6: (A) TROCHLEAR FLEXION ANGLE AND (B) RADIUS FOR THE CIRCULAR REGION (BLUE LINE)	50
FIGURE 5.7: CENTRE PLANE POSITION	52
FIGURE 5.8: A) TROCHLEAR DYSPLASIA INDEPENDENT PARAMETERS B) TROCHLEAR HEIGHTS.....	54
FIGURE 5.9: SCHEMATIC OF TESTING NORMAL GEOMETRY PREDICTION METHOD USING SELF-ORGANISING MAPS (SOM) FOR ONE SAMPLE	55
FIGURE 5.10: SOM PATTERN OF THE TROCHLEAR DYSPLASIA INDEPENDENT PARAMETERS AND ANTERIOR-POSTERIOR (AP) DISTANCES	56
FIGURE 5.11: SOM PATTERN OF THE TROCHLEAR DYSPLASIA INDEPENDENT PARAMETERS AND THE TROCHLEAR HEIGHTS	56
FIGURE 6.1: SKETCH ON A MEDIAL SAGITTAL PLANE (M2) SHOWING THE PREDICTION OF THE ANTERIOR PORTION USING SOM ESTIMATION	60
FIGURE 6.2: ANTERIOR VIEW OF DYSPLASTIC FEMURS BEFORE AND AFTER SURFACE REMODELLING	62
FIGURE 6.3: THE ANTERIOR VIEW OF TYPE D DYSPLASTIC FEMUR BEFORE AND AFTER VIRTUAL TROCHLEOPLASTY (THE LIGHT BLUE LINES SHOW THE GUIDELINES FOR THE SURFACE MORPHING)	65
FIGURE D1: B-SPLINE CURVE.....	85
FIGURE G1: SULCUS ANGLE MEASUREMENTS ON A CT SCAN AND ON A THREE-DIMENSIONAL (3D) MODEL.....	115

LIST OF TABLES

TABLE 2.1: TRANSVERSE MEASUREMENT PLANES	17
TABLE 2.2: TROCHLEAR DEPTH MEASUREMENT ON DYSPLASTIC KNEES BY DIFFERENT RESEARCHERS	19
TABLE 2.3: SUMMARY OF SULCUS ANGLE MEASUREMENTS ON DYSPLASTIC KNEES FROM VARIOUS STUDIES	20
TABLE 2.4: LATERAL TROCHLEAR INCLINATION (LTI) MEASUREMENT ON DYSPLASTIC KNEES BY DIFFERENT RESEARCHERS	21
TABLE 2.5: TROCHLEAR FACET ASYMMETRY MEASUREMENT ON DYSPLASTIC KNEES BY DIFFERENT RESEARCHERS	22
TABLE 2.6: ANTERIOR-POSTERIOR TO MEDIAL-LATERAL RATIO RESULTS FROM BIEDERT ET AL. (2009)	23
TABLE 2.7: SUMMARY OF VENTRAL TROCHLEAR PROMINENCE MEASUREMENTS ON DYSPLASTIC KNEES FROM VARIOUS STUDIES	24
TABLE 3.1: THE PARAMETERS OF THE MODEL BEFORE AND AFTER SMOOTHING EFFECT.....	28
TABLE 3.2: GUIDELINE FOR ACCEPTANCE OF THE MEASUREMENT SYSTEM REPEATABILITY AND REPRODUCIBILITY	29
TABLE 3.3: RESULT FOR REPEATABILITY AND REPRODUCIBILITY (R&R) TEST	29
TABLE 3.4: COMPARISON BETWEEN RIGHT AND LEFT FEMURS.....	38
TABLE 3.5: COMPARISON BETWEEN MALE AND FEMALE GROUPS.....	39
TABLE 4.1: CUT-OFF VALUES FOR IDENTIFICATION OF TROCHLEAR DYSPLASIA FOR DIFFERENT FEMORAL MEASUREMENTS.....	40
TABLE 4.2: SELECTED PARAMETERS FOR NETWORK TRAINING AND THEIR STATISTICAL OVERLAP FACTOR	43
TABLE 4.3: AGREEMENT BETWEEN ANN AND OTHER CLASSIFICATION METHODS	44
TABLE 4.4: THE MEAN AND STANDARD DEVIATION OF THE INPUT PARAMETERS FOR THE NORMAL AND DYSPLASTIC GROUPS.....	45
TABLE 4.5: SENSITIVITY AND SPECIFICITY FOR IDENTIFYING TROCHLEAR DYSPLASIA	45
TABLE 5.1: RESULTS OF CURVE ANALYSIS	51
TABLE 5.2: SUMMARY OF CENTRE PLANE FITTING RESULT.....	52
TABLE 5.3: STATISTICAL DIFFERENCE BETWEEN NORMAL AND DYSPLASTIC GROUPS.....	54
TABLE 5.4: AVERAGE % AGREEMENT BETWEEN THE MEASURED AND PREDICTED VALUES OF RADIUS AND AP DISTANCE.....	55
TABLE 5.5: AVERAGE % AGREEMENT BETWEEN THE MEASURED AND PREDICTED VALUES OF LOCATION OF PLANE AND TROCHLEAR HEIGHTS	56
TABLE 6.1: KEY FEMORAL PARAMETERS FOR DYSPLASTIC FEMURS BEFORE AND AFTER VIRTUAL SURFACE RECONSTRUCTION.....	61
TABLE 6.2: TROCHLEAR HEIGHT DIFFERENCE BETWEEN THE MEASUREMENT AND THE PREDICTION.....	61
TABLE 6.3: FEMORAL PARAMETERS BEFORE AND AFTER THE VIRTUAL DEPRESSION TROCHLEOPLASTY	64
TABLE A1: PATELLAR PARAMETERS FOR RIGHT KNEES	79
TABLE A2: PATELLAR PARAMETERS FOR LEFT KNEES	80
TABLE B1: QUANTITATIVE AND QUALITATIVE CLASSIFICATION FOR TROCHLEAR DYSPLASIA OF RIGHT KNEES (A: DYSPLASTIC FEMUR N: NORMAL FEMUR)	81
TABLE B2: QUANTITATIVE AND QUALITATIVE CLASSIFICATION FOR TROCHLEAR DYSPLASIA OF LEFT KNEES (A: DYSPLASTIC FEMUR N: NORMAL FEMUR)	82
TABLE C1: AVERAGE AGREEMENT OVER 15 RUNS.....	83

TABLE C2: STANDARD DEVIATION OF THE AGREEMENT OVER 15 RUNS.....	83
TABLE C3: AVERAGE GOAL FUNCTION OVER 15 RUNS.....	83
TABLE C4: STANDARD DEVIATION OF THE GOAL FUNCTION OVER 15 RUNS	84
TABLE E1: RADIUS OF CIRCULAR ARC	87
TABLE E2: TROCHLEAR FLEXION ANGLE OF CIRCULAR ARC.....	87
TABLE E3: MAXIMUM ERROR BETWEEN DATA POINT AND LEAST SQUARES CIRCLE	88
TABLE E4: AVERAGE DISTANCE BETWEEN THE CENTRE POINTS OF THE B-SPLINE AND CIRCULAR ARC.....	88
TABLE E5: CENTRE PLANE LOCATION.....	89
TABLE E6: AVERAGE % AGREEMENT BETWEEN THE PREDICTION AND THE MEASURED ANTERIOR-POSTERIOR (AP).....	90
TABLE E7: AVERAGE % AGREEMENT BETWEEN THE PREDICTION AND THE MEASURED RADIUS OF THE CIRCULAR ARCS.....	91
TABLE E8: AVERAGE % AGREEMENT BETWEEN THE PREDICTION AND THE MEASURED RADIUS OF THE TROCHLEAR HEIGHTS	92
TABLE E8: AVERAGE % AGREEMENT BETWEEN THE PREDICTION AND THE MEASURED RADIUS OF THE PLANE LOCATION	93
TABLE F1: B-SPLINE CURVE AND LEAST SQUARES CIRCULAR ARC FITTING TO THE SAGITTAL SURFACE CURVES OF THE NORMAL KNEES	94
TABLE G1: SULCUS ANGLE MEASUREMENTS ON A CT SCAN AND ON A THREE-DIMENSIONAL MODEL	115

NOMENCLATURE

Abbreviation	Description
ANN	Artificial neural network
AP	Anterior-posterior
BMU	Best matching unit
CT	Computed tomography
DM	Distal plane-mechanical plane angle
L	Lateral
LCL	Lateral collateral ligament
LP	Lateral epicondylar prominence
LPFL	Lateral patellofemoral ligament
LR	Lateral retinaculum
LRR	Lateral retinacular release
LTI	Lateral trochlear inclination
M	Medial
MA	Mechanical axis-anatomical axis angle
MCL	Medial collateral ligament
MD	Measurement plane-distal plane distance
ML	Medial-lateral
MP	Medial epicondylar prominence
MPFL	Medial patellofemoral ligament
MR	Magnetic resonance
MS	Medial epicondylar sulcus
PFA	Patellofemoral arthroplasty
PT	Patella tendon
QT	Quadriceps tendon
RF	Rectus femoris
SOF	Statistical overlap factor
SOM	Self-organising maps
TD	Trochlear depth
TFA	Trochlear facet asymmetry
TKA	Total knee arthroplasty
VI	Vastus intermedius

VL	Vastus lateralis
VLL	Vastus lateralis longus
VLO	Vastus lateralis obliquus
VM	Vastus medialis
VML	Vastus medialis longus
VMO	Vastus medialis obliquus
VTP	Ventral trochlear prominence

Symbol	Description
C	B-spline curve
d	Chord length
N	Normalised B-spline basis function
P	Control point of B-spline
U	Knot vector
Q	Data points of sagittal curve

1 INTRODUCTION

1.1 Background

The knee is the largest and the most complex joint in the lower extremity. It is prone to injury because it bears heavy loads during every day and athletic activities. In double leg stance each knee takes 50 % of the body weight, in single leg stance it increases to four times the body weight while in activities like running and squatting it can increase up to seven times the body weight (Merchant, 1988; Wilk et al., 1998).

The knee joint basically consists of three compartments; there are two compartments between the upper and lower legs and the third compartment between kneecap (patella) and the front of the upper leg (femur) is the patellofemoral joint (Figure 1.1). The patella slides on the groove of the femur, the trochlea, as the knee bends (flexes) and straightens (extends). The focus of this thesis will be on the patellofemoral joint.

In the patellofemoral joint, the bony structures are held together by strong ligaments and the muscles of extensor mechanism to provide joint stability (Birrer and O'connor, 2004). The articular surfaces of the bones are covered with articular cartilage which is the weight bearing surface of the joint. In situations like osteoarthritis, the joint surfaces can wear away to an extent that there is a bone on bone articulation which causes pain and impair joint mobility (Enderle et al., 2005).

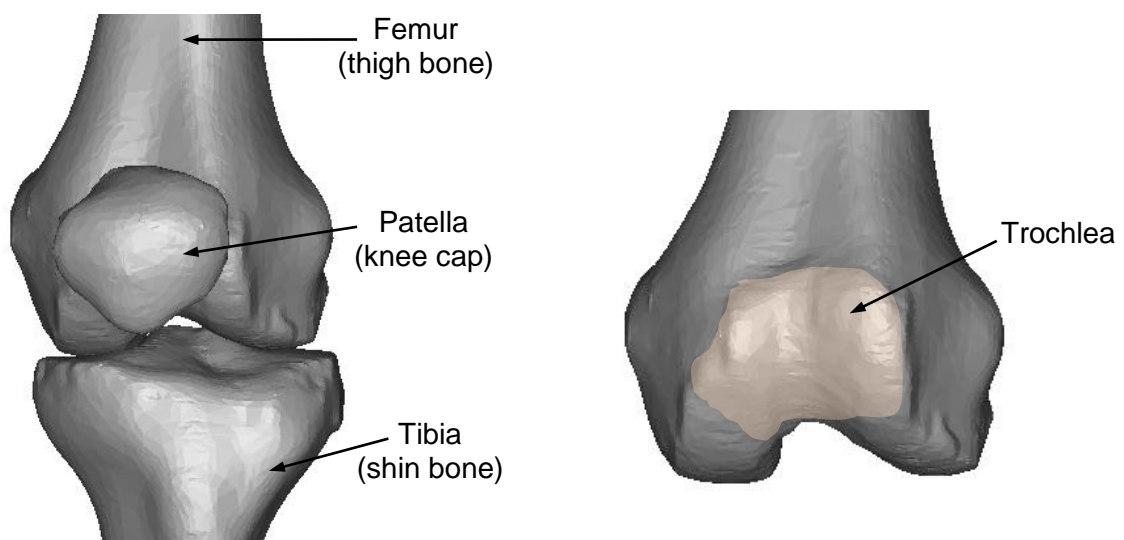


Figure 1.1: Anterior view of patellofemoral joint

Patellofemoral joint disorders are commonly found in all age groups and are one of the most common sport injuries that clinicians encounter (Zaffagnini et al., 2010). About 15 to 33 % of active adults and 21 to 45 % of adolescents suffer from patellofemoral pain (Wilk et al., 1998). Approximately 11 % of males and 24 % of females over 55 years old have isolated patellofemoral arthritis (Davies et al., 2002). These studies show that there is a large scope for investigating the cause and the treatments of patellofemoral disorders.

Patellofemoral pain is a predisposing factor to patellofemoral osteoarthritis (Utting et al., 2005) and mainly caused by overloading (Juhn, 1999). An overloaded patellofemoral joint is caused by malalignment and instability between the patella and the trochlea. The high pressure developed in the joint leads to articular cartilage damage, which causes pain. Patellar instability is caused by an inadequate soft tissue (the muscles and the ligaments) support, or by an abnormally shaped trochlea, or in most cases by a combination of the two.

There is a high correlation between the shape of the trochlea and the patellofemoral joint function (Balcarek et al., 2010; Balcarek et al., 2011). 85 % of patients who suffered from recurrent patellar dislocation also had trochlear dysplasia (abnormally shaped trochlea) (Dejour et al., 1994). Trochlear dysplasia was identified in 16 % of patients with anterior knee pain, whereas only 2.7 % of the normal group had trochlear dysplasia (Keser et al., 2008). These studies show the importance of the patellofemoral joint shape, especially of the trochlea, in the optimal functioning of the joint.

The depth of the trochlear groove, the flatness of the lateral facets, and the existence of a bump on the anterior trochlea were found to be the key factors that cause an unstable patella (Balcarek et al., 2010). Orthopaedic surgeons make a quantitative measurement of these features by using radiographs, computed tomography (CT), and magnetic resonance (MR) images in order to identify trochlear dysplasia. Trochlear dysplasia can also be qualitatively identified by looking for certain indications such as the “crossing sign” from the side view of x-rays and a sagittal slice of the MR or CT scans (Dejour et al., 1994).

The main cause of the patellofemoral pain and instability should be identified to select an appropriate treatment regime. If the shape of the trochlea is the key factor, a bony surgical procedure such as trochleoplasty (correcting the shape of the trochlea) can be considered. On the other hand, if the major problem is an inefficiency of the soft tissue support, a surgical reinforcement of the soft tissues can be done. It is important to be able to identify the major component contributing to the instability and address that in order to have a satisfactory surgical result.

1.2 Motivation

The following factors are the motivation for this study:

- researchers are not in agreement on the groove orientation, trochlear length and the condyle curvatures;
- the measurements on CT or MR scans are influenced on the alignment of the femur during scanning. A measurement method which is not influenced by the orientation of the femur is needed;
- there are considerable geometrical differences between normal trochleas and the current prostheses designs (Varadarajan et al., 2011). This is reflected in the poor outcomes of patellofemoral arthroplasty (PFA), requiring surgical revisions or conversion to total knee arthroplasty (TKA) (Donell and Glasgow, 2007);
- the shape of the trochlea of the total knee arthroplasty (TKA) prosthesis design is the main determinant factor for the success of the procedure (D'Lima et al., 2003; Kulkarni et al., 2000). Better understanding of the normal trochlea geometry leads to better prosthesis design;
- a comprehensive knowledge for the normal groove geometry is needed including its orientation, length and the curvatures to design a custom fit prosthesis that can restore the normal trochlea for the specific geometry and size of the patient's knee; and
- surgeons require a guideline for selecting an appropriate treatment regime during surgical planning. With better understanding of the normal trochlea shape, surgeons can decide whether or whether not the trochlea shape has to be altered as the treatment.

1.3 Objectives

If a measurement dataset describing the three-dimensional geometry of the normal trochlea is available, the normal geometry of a dysplastic femur can be predicted. This prediction can show which features are responsible for trochlear dysplasia and can help orthopaedic surgeons to plan the knee surgery better and choose a suitable treatment

regime. The predicted normal geometry can also be used as the guideline for trochleoplasty by showing where and to what extent it has to be resurfaced. This study aims therefore to quantify the normal trochlea geometry by:

- reviewing literature in order to determine and summarise the current techniques used to quantify the trochlea shape;
- generating three-dimensional femoral models from CT scans;
- standardising the measurement method on three-dimensional femoral models to acquire femoral parameters;
- comparing three different trochlea classification methods (qualitative, quantitative and artificial neural networks (ANN));
- conducting a curvature analysis by means of a sagittal curve fitting to the trochlea;
- testing the accuracy of the normal geometry prediction method using self-organising maps (SOM); and
- conducting a case study to suggest an appropriate treatment regime for knees with trochlear dysplasia.

1.4 Scopes and Limitations

The scope of this study is restricted to:

- a description of the osseous (i.e., bones only) geometry of the trochlea;
- the identification of the proximal trochlear dysplasia (trochlear dysplasia refers to proximal dysplasia in general terms); and
- the suggestion of a treatment regime that alters the bony geometry of the trochlea.

It is also important to note the limitations of this study:

- only the osseous geometry of the trochlea is analysed and soft tissue was excluded because only CT scans were available (unlike bones, soft tissue is not easily discernible for segmentation purposes);
- the relative position of the patella to the femur (e.g., the patellar height) was not investigated since its position is dependent on the knee flexion angle; and

- the influence of the distal dysplasia on the patellofemoral function is not yet well researched, therefore, this study was restricted to the proximal dysplasia which has been shown to cause patellar instability.

1.5 Thesis Layout

This chapter has introduced the concept of the patellofemoral joint shape and outlined the main challenges and objectives associated with describing a normal trochlea shape. An outline of the rest of the study follows.

Chapter 2 presents a comprehensive review of the literature on the shape of the patellofemoral joint. Emphasis is placed on previous clinical findings, theories and methodological contributions quantifying the shape of the patellofemoral joint. In Chapter 3, the methods for three-dimensional femoral model generations from CT scans, as well as the standardised method for measuring femoral parameters of these models are described. This is followed by an illustration of three different methods for identifying trochlear dysplasia and a comparison of the results (Chapter 4), while an outline of the method and results for validating a normal trochlea geometry prediction tool is provided in Chapter 5. Chapter 6 presents a case study on which the normal geometry prediction tool is applied to knees with trochlear dysplasia. Chapter 7 summarises the major conclusions and the key contributions of this thesis as well as the limitations of this research, leading to the recommendations for future work.

2 LITERATURE REVIEW

This chapter starts with the basic anatomy and the biomechanics associated with the patellofemoral joint function. The shape of the normal trochlea is described, followed by the various methods that identify trochlear dysplasia.

2.1 Anatomical Terms and References of the Patellofemoral Joint

2.1.1 Orientation and the movement of the patellofemoral joint

There are three anatomical planes that pass through the body and that are perpendicular to each other, namely the sagittal, transverse, and coronal planes. On these planes, the anatomical directional terms describe the position of the anatomical structures (Figure 2.1).

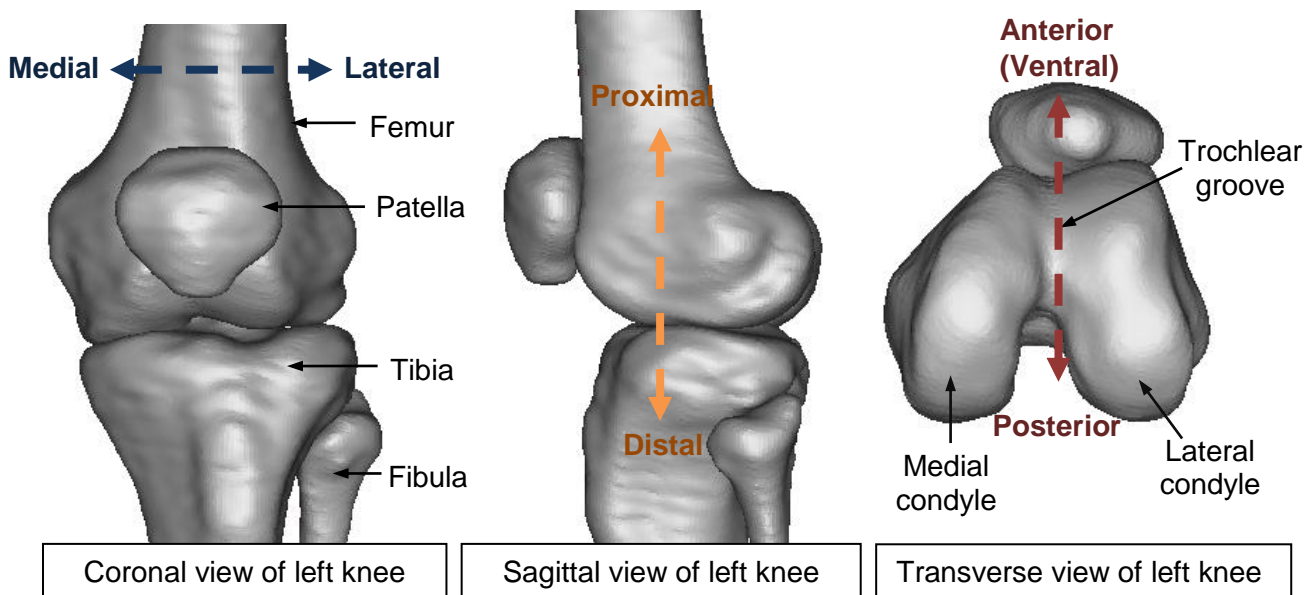


Figure 2.1: Three anatomical views of the left knee with the anatomical directional terms

The main patellofemoral movements are the flexion (bending) and extension (straightening) motions. At full extension, the patella rests above the femoral groove and as the knee flexes, the patella slides onto the distal groove (Figure 2.2). The patella undergoes three translational movements (medial-lateral, anterior-posterior, proximal-distal) as well as three rotational movements (flexion-extension, medial-lateral, and internal-external), while the femur flexes and extends on the tibia (Katchburian et al., 2003).

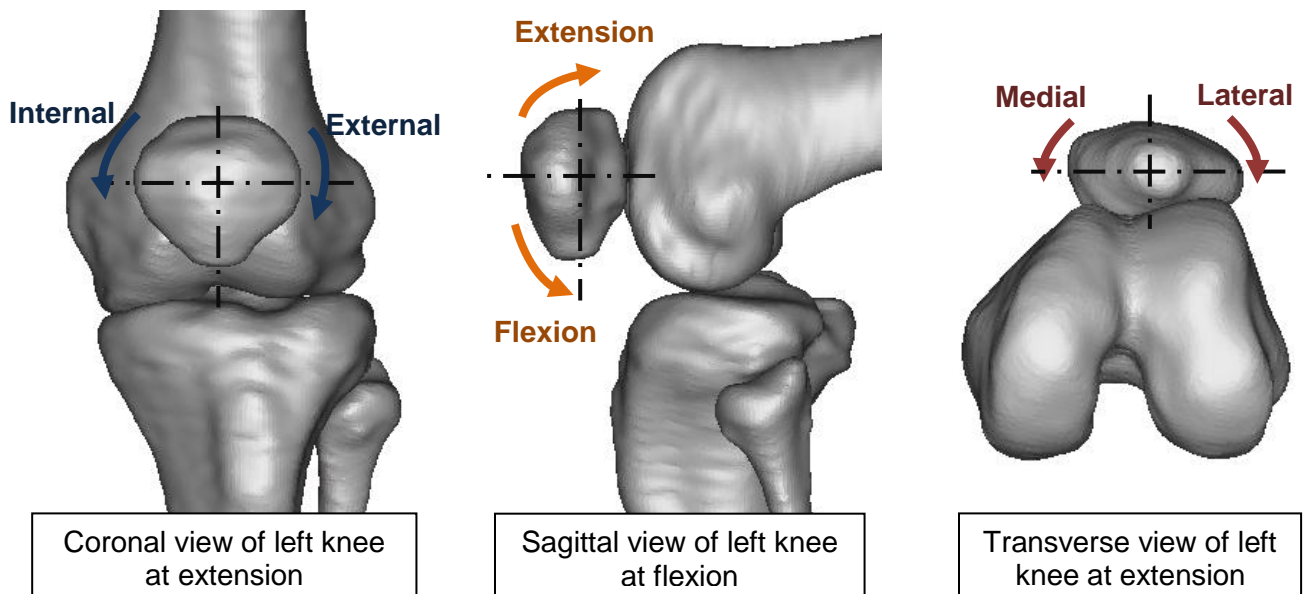


Figure 2.2: Illustration of the movement of the patellofemoral joint

2.1.2 Referencing axes on the femur

Knee alignment influences stability of the joint, patellar tracking and the long-term effects of reconstruction surgeries (Balcarek et al., 2010; Luo, 2004). Some studies have shown that poor outcomes after total knee arthroplasty (TKA) are due to the misalignment in rotation (Miller et al., 2001; Sikorski, 2008). This highlights the importance of using correctly defined reference axes during surgery (Lustig et al., 2008).

The rotational alignment of the femur is described around the epicondylar axes or the posterior condylar axis. There are two epicondylar axes: the surgical and the clinical. These axes are defined by the connection to the attachment sites of the lateral collateral ligament (LCL) and the medial collateral ligament (MCL) (Berger et al., 1993). The clinical epicondylar axis is the line connecting the prominence of the medial epicondyle (labelled MP in Figure 2.3) and the lateral epicondylar prominence (labelled LP in Figure 2.3). The surgical epicondylar axis is the line connecting the sulcus of the medial epicondyle (labelled MS in Figure 2.3) and the lateral epicondylar prominence. The posterior condylar axis is defined as the tangential line to the most posterior points on the condyles (Asano et al., 2004) (Figure 2.3). Berger et al. (1993) showed that the surgical epicondylar axis is more reliable and reproducible than the clinical epicondylar axis, whereas the posterior condylar axis is more reproducible than the epicondylar axes for determining the rotational alignment of the femur (Victor et al., 2009).

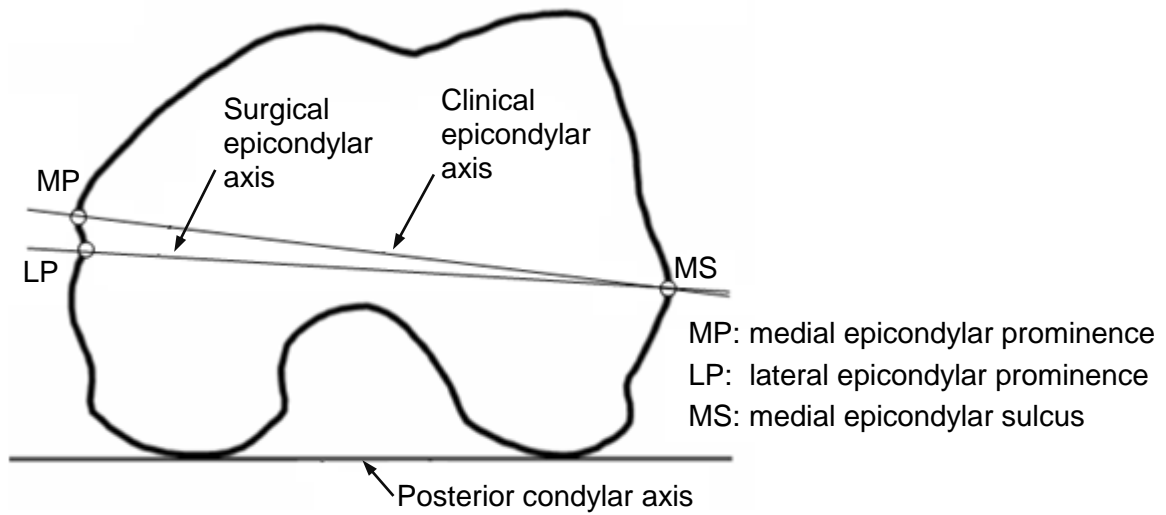


Figure 2.3: Anatomical landmarks and reference axes on the transverse view of distal femur edited from Asano et al. (2004)

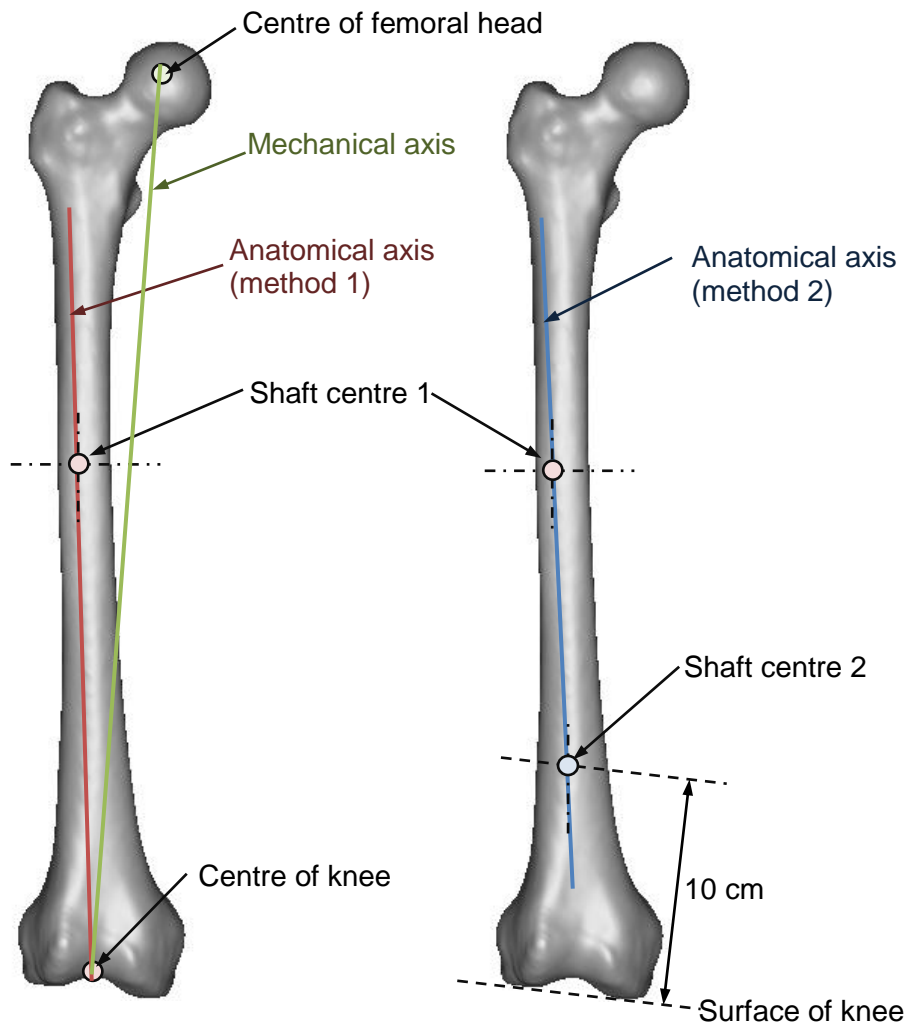


Figure 2.4: Defining anatomical axes (red and blue) and mechanical axis (green)

The anatomical axis of the femur describes the position of the shaft of the femur on the sagittal and the coronal planes. Luo (2004) presented two suitable methods for defining the anatomical axis. The first method relies on the line drawn from the centre of the knee to the shaft centre 1. The centre of the knee is the centre of the tibiofemoral joint and the femoral shaft centre 1 is the intersection point of the lines that bisect the femur in proximal-distal and medial-lateral directions (Figure 2.4). The second method relies on the line drawn from the centre of the femoral shaft 1 to the mid-point of the medial-lateral line drawn 10 cm above the surface of the knee (shaft centre 2 in Figure 2.4). The second method is preferred since it produces an axis closer to the centre of the femoral shaft (Luo et al., 2001; Moreland et al., 1987). The mechanical axis is the line connecting the centre of the knee and the centre of the femoral head (Figure 2.4). It represents the load-bearing axis of the femur (Cooke et al., 2007; Luo, 2004).

2.2 The Factors Affecting Patellofemoral Joint Stability

The soft tissue and the osseous geometry of the femur are the main features that maintain patellofemoral joint stability. It has been illustrated that an unstable patella is associated with many patellofemoral disorders such as patellofemoral pain, patellofemoral osteoarthritis, and patellar dislocation. Stability of the patella can be restored with ligament reconstruction (e.g., medial patellofemoral ligament (MPFL) reconstruction), bony realignment (e.g., tibial tubercle osteotomy), and/or changing the shape of the trochlea (e.g., trochleoplasty). In order for a successful surgery, it is important to determine which anatomical factors are responsible for patellar instability before any surgical intervention. This section presents the anatomy of some key soft tissue stabilisers and their functions in stabilising the patella, as well as the osseous geometry of the trochlea and its functions.

2.2.1 Soft tissues and their functions

The cartilage covers the articulating surfaces of the femur, the patella, and the tibia, protecting the bones from direct contact with each other and providing a smooth surface. The menisci are thick semi-lunar shaped cartilaginous structures rested on the tibial cartilage and function as shock absorbers (Figure 2.5). The femur undergoes rotational and translational movements on the menisci during the knee flexion. The cartilage contributes to the joint stability by exerting reactive forces onto the articulating surfaces.

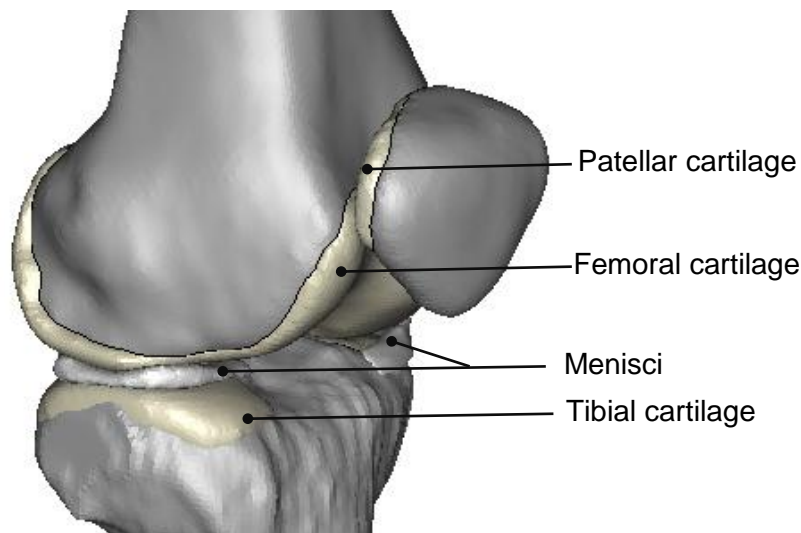


Figure 2.5: Cartilage on the knee joint and the menisci

The patella is anchored to the knee by the active and passive soft tissue stabilisers. The active contraction of the quadriceps muscle provides stability to the patella. The quadriceps muscle splits into six different components and exert pulling forces on the patella in the proximal and side directions: vastus lateralis longus (VLL), vastus lateralis obliquus (VLO), vastus medialis longus (VML), vastus medialis obliquus (VMO), rectus femoris (RF) and vastus intermedius (VI). Weakened quadriceps components may contribute to patellar instability (Farahmand et al., 1998).

In addition to the active muscle tensions, the ligaments play an important role as passive stabilisers of the patella. Medial patellofemoral ligament (MPFL in Figure 2.6) has been shown to be one of the key features that prevent the patella from dislocating laterally at the full extension of the knee. Patellar dislocation occurs most commonly at full extension and the MPFL tension is at its greatest at this position (Amis et al., 2003). If the MPFL does not provide enough tension, MPFL reconstruction is performed to ensure patellar stability.

The lateral retinaculum (LR in Figure 2.7) is the fibrous tissue that holds the patella to the femur on the lateral side of the knee. Although it is not common, an over tightened LR can contribute to lateral patellar instability, and, lateral retinacular release (LRR) can be considered to reduce the tension on the lateral side (Henry et al., 1986). However an isolated LRR has only a little role in stabilising the patella (Christoforakis et al., 2006; Lattermann et al., 2007).

The quadriceps tendon (QT in Figure 2.6) attaches the patella to the quadriceps muscle and the patella tendon (PT in Figure 2.6) connects the patella to the tibia. In this way the patella is stabilised in proximal and distal direction. Lateral patellar dislocation can occur

if the attachment site of the patella tendon on the tibia (tibial tubercle) is lateralised and the patella is pulled outwards towards a lateral direction. In a case like this, tibial tubercle osteotomy can be performed to change the direction of the pulling force applied on the patella by the extensor mechanism.

The medial collateral ligament (MCL in Figure 2.6) and the lateral collateral ligament (LCL) make connections between the femur and the tibia. The attachment sites of these ligaments on the femur are used as morphological landmarks to define epicondylar axes (Griffin et al., 2000).

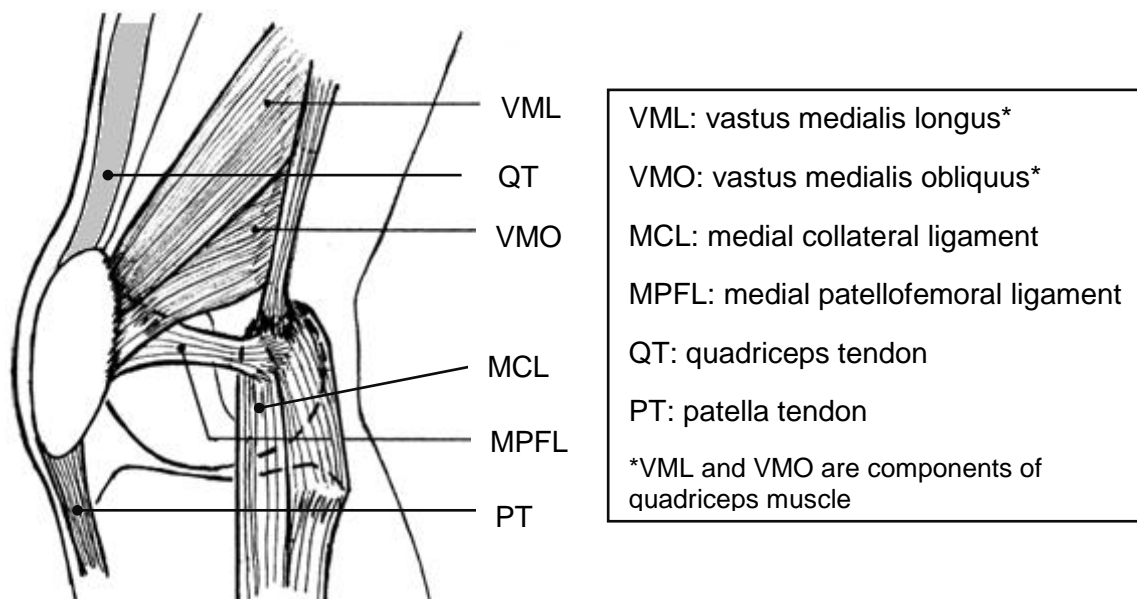


Figure 2.6: Medial anatomy of the patella stabilisers edited from Amis et al. (2003)

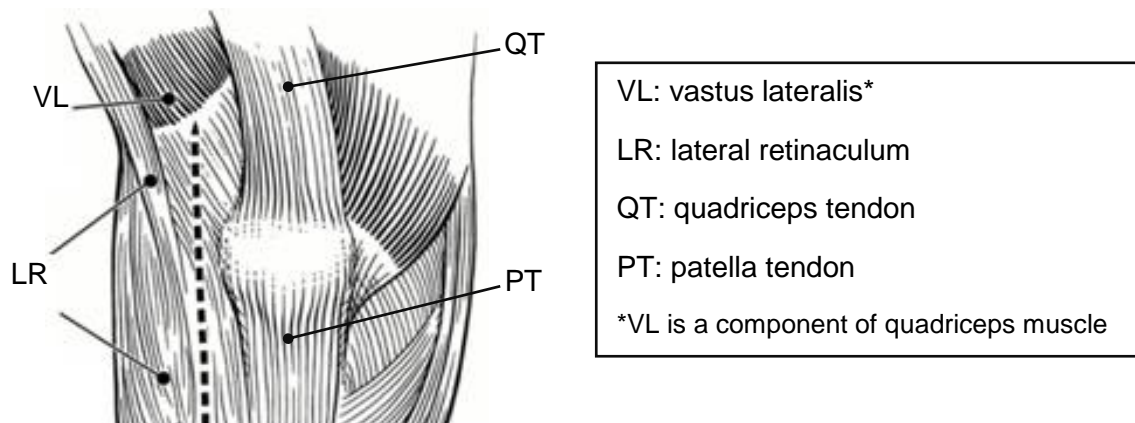


Figure 2.7: Anterior view of the soft tissue stabilisers edited from O'Neil (1997)

2.2.2 Shape of the trochlea

The trochlea has a complex three-dimensional shape and its orientation, length, and curvature varies amongst individuals (Feller et al., 2007). This makes it difficult to define the normal trochlear geometry. However, it is generally agreed that normal knees have deeper trochlear grooves than abnormal knees, with higher trochlear facets on the lateral side than the medial side (Figure 2.8). As a result of the normal alignment of the lower extremity and the origins of the extensor mechanism, the patella experiences greater force towards the lateral than the medial direction, and the prominence of the lateral facet and the depth of the trochlea prevents the patella from dislocating laterally (). The role of the groove in stabilising the patella was demonstrated by Jafaril et al. (2008), who showed that a shallower trochlear groove makes the patella unstable and shifts it laterally while the geometry of the patella is unchanged. Senavongse et al. (2005) showed that the flattened anterior lateral facet affects patellar stability more than the VMO and the MPFL at full extension of the knee. This implies that if the degree of trochlear dysplasia (abnormality of the trochlea shape) is severe, performing a soft tissue reinforcement (e.g., MPFL reconstruction) and a bony realignment (e.g., tibial tubercle osteotomy) may not be effective enough to restore the patellar stability. In these cases it might be indicated to also change the trochlear geometry (i.e., perform a trochleoplasty).

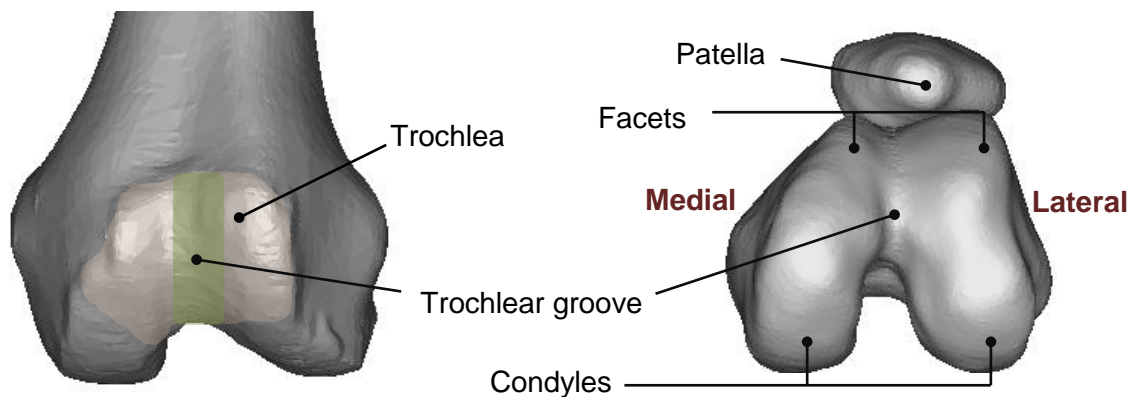


Figure 2.8: Anatomy of the trochlea

Trochleoplasty can be performed in a severe degree of trochlear dysplasia with no cartilaginous damage. Trochleoplasty reshapes the osseous geometry of the trochlea, thus it is more invasive than soft tissue reconstructions, or bony realignments. The published outcomes were satisfactory in terms of preventing the re-dislocation and the satisfaction index (Beaufils et al., 2012). If isolated patellofemoral arthritis presents, patellofemoral arthroplasty (PFA) can be considered to provide a smooth articulating surface and to change the bone geometry to a more normal shape (Figure 2.9).

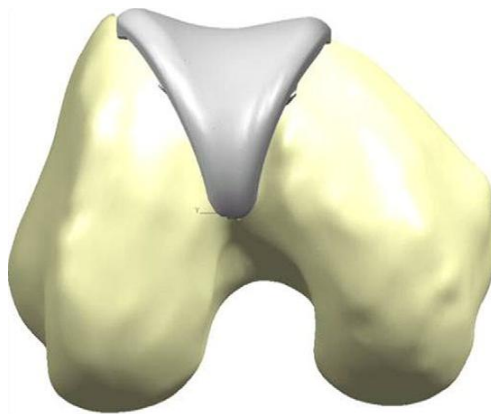


Figure 2.9: Illustration of patellofemoral arthroplasty (PFA) adapted from Farr et al. (2008)

2.3 Identification of Trochlear Dysplasia

Identifying and classifying the severity of trochlear dysplasia is important for surgeons when selecting the surgical methods to restore the normal patellofemoral joint function. Conventionally, X-rays were used for examining the knees, but computed tomography (CT) and magnetic resonance (MR) images are now also widely used. Although some studies (Biedert et al., 2011; Iranpour et al., 2010b; Muller et al., 2010) used three-dimensional computer models created from CT or MR scans to analyse the geometry of the femurs, it is not used widely in the clinical context. Trochlear dysplasia can be identified by either qualitative or quantitative methods. The qualitative method is dependent on the surgeon's decision, is made by identifying certain indicative features. The quantitative method is applied when certain morphologies are measured quantitatively and trochlear dysplasia is identified with the thresholds of the measurements. This section lists some key qualitative and quantitative methods that were established by various researchers.

2.3.1 Qualitative methods for identifying trochlear dysplasia

H. Dejour et al. (1990) established a qualitative definition of the trochlear dysplasia based on the "crossing sign" (encircled in Figure 2.10), using the true lateral view of the x-rays. The crossing sign appears when the two condylar outlines cross the outline of the trochlear floor. The trochlear dysplasia was classified into three categories, based on the severity of the dysplasia: type I indicates minor dysplasia and type III indicates major dysplasia (Figure 2.10). The crossing sign is present in 96 % of patients with patellar dislocation (1994).

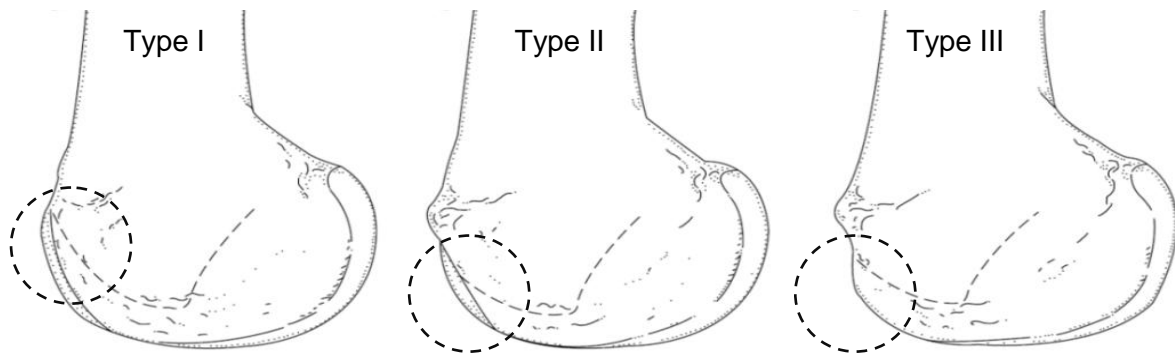


Figure 2.10: Classification of trochlear dysplasia developed by H. Dejour et al. (1990) adapted from Zaffagnini et al. (2010)

Based on the findings of H. Dejour (1990), D. Dejour et al. (2007) defined the four grades of trochlear dysplasia: type A, B, C and D (Figure 2.11). D. Dejour’s classification includes the “supra-trochlear spur” which represents the global prominence of the trochlea and the “double contour” sign (Zaffagnini et al., 2010). The supra-trochlear spur makes the patella “ski jump” when it engages the femur, and the double contour sign indicates that the medial facet is too low.

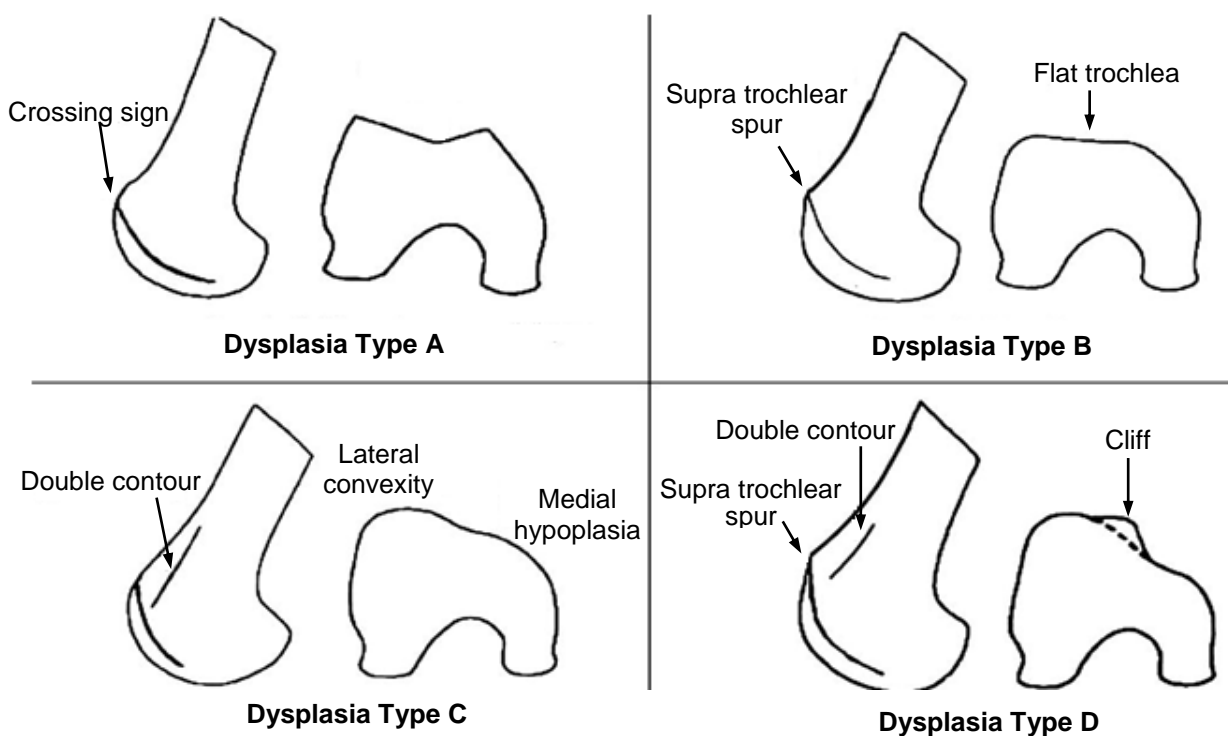


Figure 2.11: Trochlear dysplasia classification reproduced from D. Dejour et al. (2007)

Biedert et al. (2011) created three-dimensional computer models, segmenting the bones and cartilage of the distal femurs from the MR images slice by slice to compare the trochlear geometry between normal and dysplastic trochleas. Normal trochleas showed that

their lateral trochlear facets were higher than the medial trochlear facets, separated by the central trochlear groove. Biedert et al. (2011) proposed two types of trochlear dysplasia: proximal (Figure 2.12a) and distal (Figure 2.12b). Proximal trochlear dysplasia is characterised by a trochlear bump, flat or too short trochlea. Distal trochlear dysplasia is characterised by abnormal length of the distal lateral condyle, but depth of the trochlea is within normal range. However, “proximal trochlear dysplasia” and “distal trochlear dysplasia” are not widely used terms and “trochlear dysplasia” usually refers to proximal trochlear dysplasia in general. The identification method for distal trochlear dysplasia is not yet well researched and its influence on patellofemoral function is still unknown (Biedert et al., 2011).

(a) Proximal trochlear dysplasia **(b) Distal trochlear dysplasia**

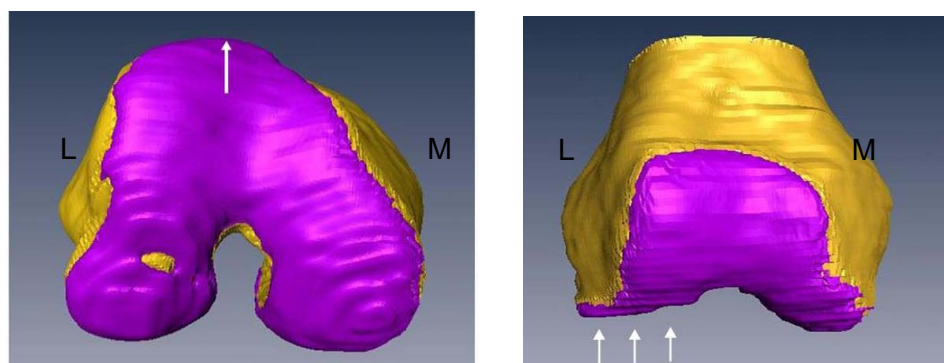


Figure 2.12: Three-dimensional model of the distal femur adapted from Biedert et al. (2011)

2.3.2 Quantitative methods for identifying trochlear dysplasia

Trochlear dysplasia is characterised by the flattened trochlea and its flatness is identified by quantitative measurements of the depth of the trochlea and the sulcus angle. The flatness of the lateral facet is identified by the lateral trochlear inclination (LTI) and the trochlear facet asymmetry (TFA) shows the medial-lateral location of the groove. These parameters are measured on CT or MR images and their threshold values have been determined in previous research (Dejour et al., 1994; Fucentese et al., 2007; Pfirrmann et al., 2000). However, researchers do not agree on the threshold values, mainly because: 1) different measurement methods were applied; and 2) the selection of the measurement slice is not standardised. This makes it difficult to compare and use the results obtained from previous studies. The following section describes the key femoral parameters measurement methods implemented by various researchers for identifying trochlear dysplasia.

- **Measurement planes**

The values of the measurements vary significantly with the selection of the measurement plane. Teichtahl et al. (2007) measured the sulcus angle on two different measurement planes (distal and proximal), showing that there is considerable difference in the sulcus angle value depending on the selection of the measurement plane (Figure 2.13). Fucentese et al. (2007) measured the sulcus angle on two different measurement planes, and the difference in mean sulcus angles measured from different measurement planes was 30.2°.

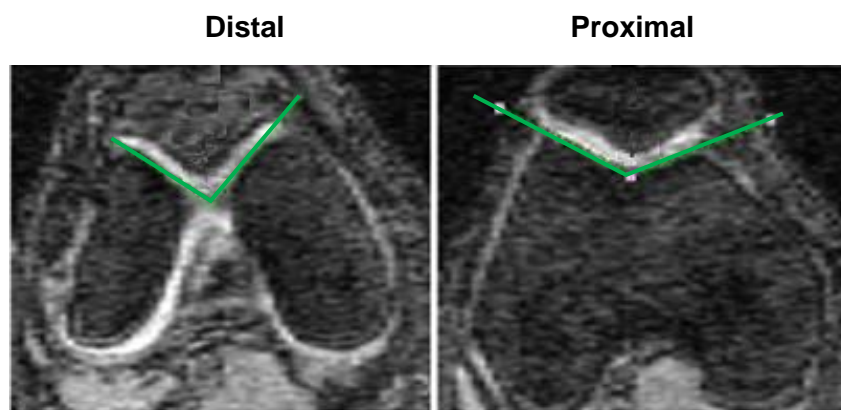
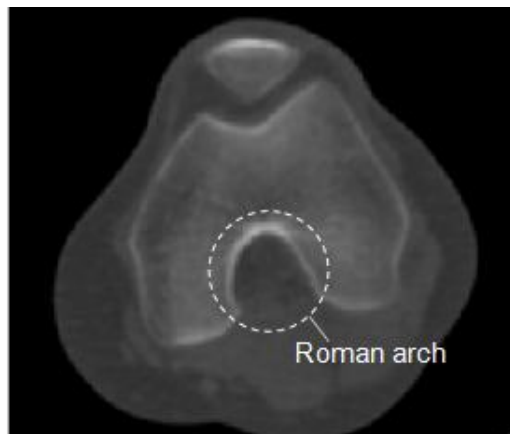


Figure 2.13: MR image of trochlear groove on distal and proximal plane adapted from Teichtahl et al. (2007)

Pfarrmann et al. (2000) measured the trochlear depth (TD) using MR images on the transverse planes 1 cm, 2 cm, and 3 cm above the tibiofemoral joint. It was demonstrated that the measurement taken on the 3 cm above the tibiofemoral joint (measurement plane 1) showed the most relevant difference between the dysplastic group and the control group. On the other hand, Escala et al. (2006), also using MR images, measured the trochlear depth on two different measurement planes: one that goes through the most anterior point of the trochlear groove (measurement plane 4), and the one that the intercondylar tunnel (Figure 2.14) is visualised with the semi circumferential shape of the roman arch (measurement plane 2). A statistical analysis indicated that the trochlear depth measurement showed higher sensitivity and specificity on measurement plane 2 for discriminating the dysplastic knees from the non-dysplastic ones. Carrillon et al. (2000) measured the lateral trochlear inclination (LTI) on the axial plane (on which trochlea is initially completely covered with cartilage) to identify the trochlear dysplasia (measurement plane 3). Four different measurement planes have been described, measurement plane 1, 2, 3 and 4 (Table 2.1).

Table 2.1: Transverse measurement planes

measurement plane	description	reference
measurement plane 1	3 cm above the tibiofemoral joint	Pfirschmann et al. (2000)
measurement plane 2	first proximal slice that intercondylar tunnel is visualised with the semi circumferential shape of roman arch	Escala et al. (2006)
measurement plane 3	first proximal slice on which trochlea is initially completely covered with cartilage	Carrillon et al. (2000)
measurement plane 4	slice that goes through the most ventral point of the trochlear groove	Escala et al. (2006)

**Figure 2.14: The roman arch is visible on the transverse slice**

The results are however contradictory: Pfirschmann et al. (2000) showed that the TD measured on measurement plane 1 has higher specificity than on the distal planes in identifying trochlear dysplasia, while Escala et al. (2006) noted different results. When these four planes were regenerated on MR slices using a three-dimensional model, it showed that the measurement planes 1, 3 and 4 were closely located to one another while the measurement plane 2 was positioned significantly distally from the other three measurement planes (Figure 2.15). This example highlights the possibility that the variability may be introduced by the alignment or flexion of the knee during scanning, demonstrating that there is a need for standardisation of the measurement procedure.

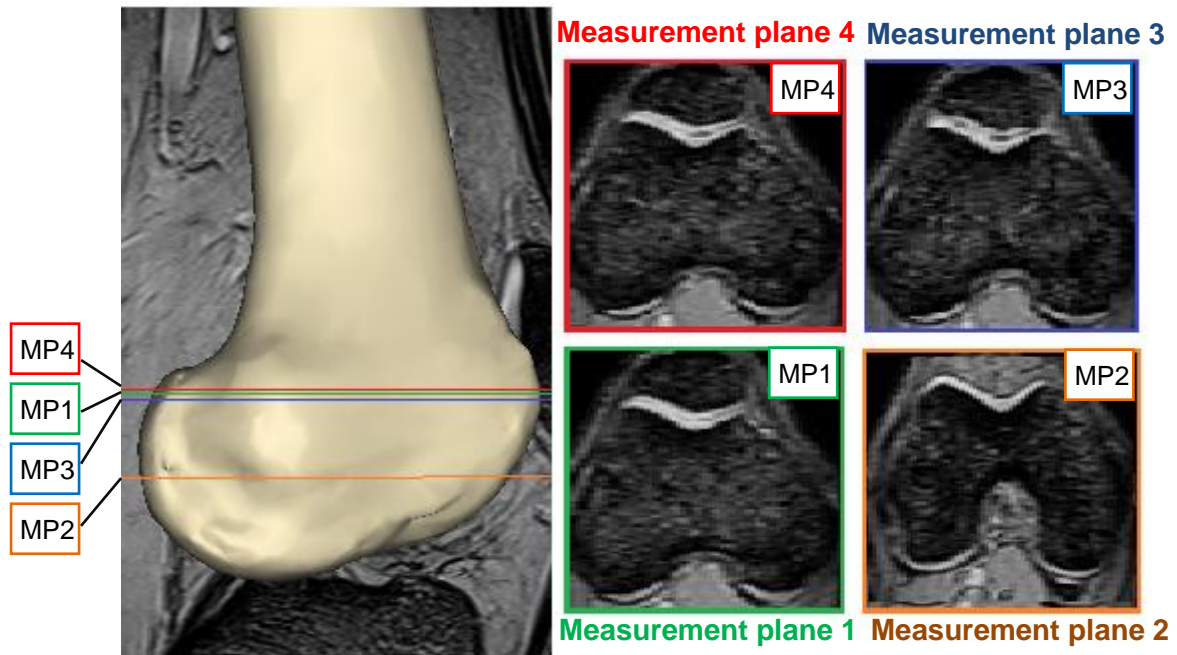


Figure 2.15: MR image of measurement planes of the same femur

- **Trochlear depth (TD)**

Trochlear depth (TD) is the parameter that quantifies the flatness of the trochlear groove. A deeper groove may indicate a stable patella. The measurement method, as well as the measurement plane selection method, varies. The TD (line OH in Figure 2.16a) is either measured as the shortest distance between the deepest point of the trochlear groove (point O in Figure 2.16a) and the line drawn from the most anterior point of the lateral condyle to the most anterior point of the medial condyle (line AB in Figure 2.16a) (Martino et al., 1998) or using anterior-posterior (AP) distances (Figure 2.16b).

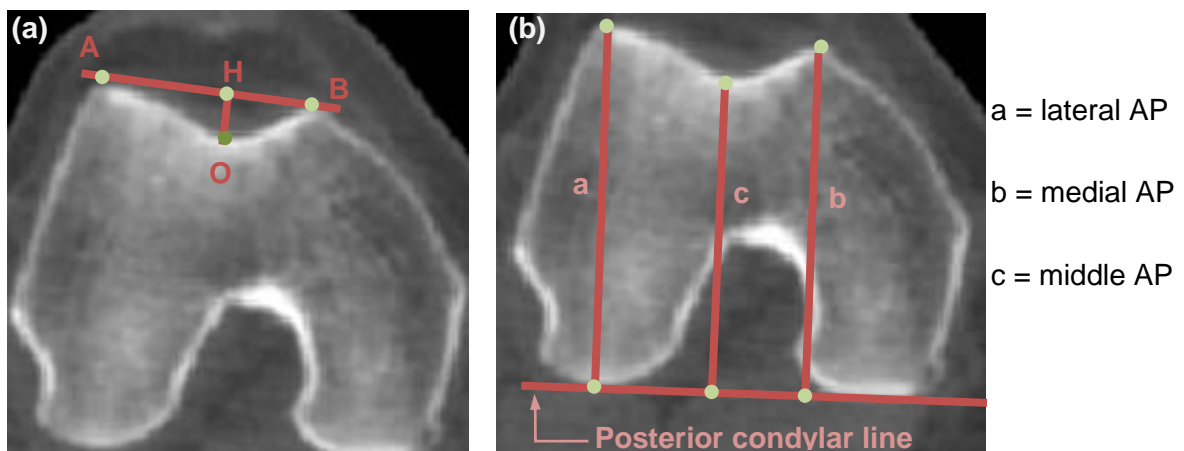


Figure 2.16: (a) Trochlear depth (b) Anterior-posterior (AP) distances on a transverse slice

Three AP distances can be measured on the trochlea: the lateral AP distance, the middle AP distance and the medial AP distance. The lateral and the medial AP distances are measured from the posterior condylar line to the most anterior points of the lateral and the medial facets (line a and b in Figure 2.16b) respectively. The middle AP distance is measured from the posterior condylar line to the deepest point of the trochlear groove (line c in Figure 2.16b). Using these AP distances, the trochlear depth can be defined as the difference between the lateral AP and the middle AP distances (Martinez et al., 1983), or from the following equation (Balcarek et al., 2010):

$$TD = \frac{a + b}{2} - c \quad (1)$$

where, a is the lateral AP distance, b is the medial AP distance, and c is the middle AP distance.

Since the trochlear depth is measured differently by various researchers, the suggested cut-off values did not agree. The summary of the trochlear depth measurement performed by various researchers is provided as follows (Table 2.2):

Table 2.2: Trochlear depth measurement on dysplastic knees by different researchers

measurement plane	scan method	sample size [patient]	age [years]	range [mm]	mean [mm]	threshold [mm]	reference
measurement plane 1	MR	101	14–40	0.9–6.0	0.9	–	Balcarek et al. (2010)
	MR	16	16–59	-6.5–2.7	-0.6	< 3	Pfirschmann (2000)
measurement plane 2	MR	59	16–45	1.2–13.3	4.2	< 5	Escala et al. (2006)
measurement plane 4	MR	59	16–45	-1.6–8.3	3.3	< 4	Escala et al. (2006)

- **Sulcus angle**

The sulcus angle represents the depression of the trochlear groove relative to the femoral condyles, and is typically measured from the two tangential lines of each trochlear facet (Balcarek et al., 2010). The sulcus angle is measured from the skyline view of radiographs (Teichtahl et al., 2007) or it is measured on a transverse measurement plane when CT or MR scanning is used (Figure 2.17).

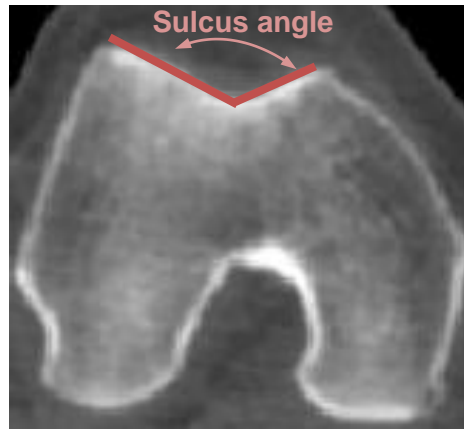


Figure 2.17: Sulcus angle measurement on a transverse slice

An increased sulcus angle indicates the existence of trochlear dysplasia. Insall et al. (1983) showed that a sulcus angle between 140° and 150° causes patellar pain and that a sulcus angle between 150° and 160° causes patellar instability, whereas Martino et al. (1998) suggested the normal range of 125° and 143° . Dejour et al. (1994) recommended the cut off value of greater than 145° for identifying trochlear dysplasia (Table 2.3).

Table 2.3: Summary of sulcus angle measurements on dysplastic knees from various studies

measurement plane	scan method	sample size [patient]	age [years]	range [°]	mean [°]	threshold [°]	reference
skyline view	x-ray	49	14–51	–	144	> 145	Dejour et al. (1994)
measurement plane 1	MR	101	14–40	138–166	152	–	Balcarek et al. (2010)
measurement plane 3	MR	25	14–49	146–167	156	–	Salzmann et al. (2010)

- **Lateral trochlear facet inclination (LTI)**

The lateral trochlear inclination (LTI) quantifies the flatness of the lateral trochlear facet by measuring the angle between the posterior condylar line and the tangential line to the lateral facet of the trochlea (Figure 2.18) (Keser et al., 2008). Carrillon et al. (2000) demonstrated that a low LTI value (lower than 11°) indicates the existence of patellar instability and anterior knee pain. However, researchers do not agree on the suggested cut-off values for the LTI (Table 2.4).

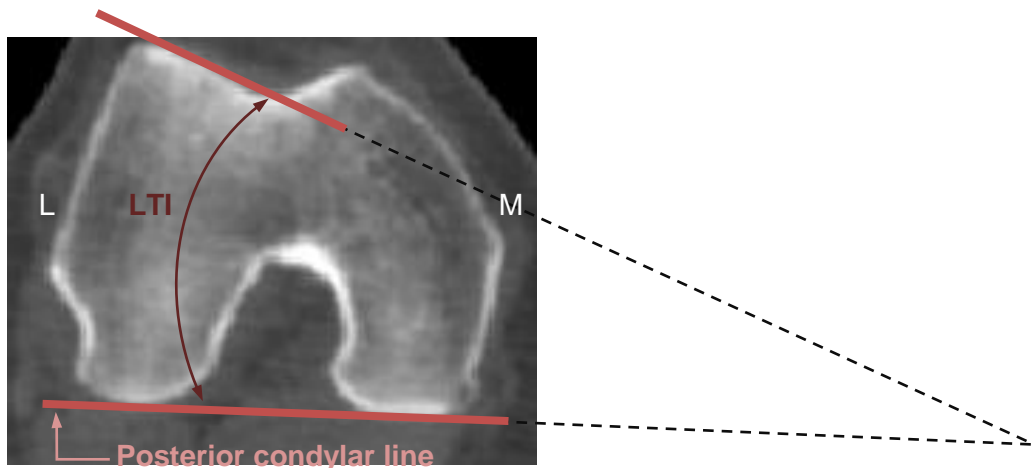


Figure 2.18: Lateral trochlear facet inclination (LTI) measurement

Table 2.4: Lateral trochlear inclination (LTI) measurement on dysplastic knees by different researchers

measurement plane	scan method	sample size [patient]	age [years]	range [°]	mean [°]	threshold [°]	reference
measurement plane 2	MR	59	16–45	1–23	12.5	< 14	Escala et al. (2006)
measurement plane 3	MR	30	15–42	–	6.17	< 11	Carrillon et al. (2000)
	MR	25	14–49	–	11.63	–	Salzmann et al. (2010)
measurement plane 4	MR	59	16–45	0–23	9.6	< 12	Escala et al. (2006)

- **Trochlear facet asymmetry ratio (TFA)**

Trochlear facet asymmetry (TFA) shows the relative position of the trochlear groove in a medial-lateral direction. It is the ratio of the medial trochlear facet length (line *a* in Figure 2.19) to the lateral facet length (line *b* in Figure 2.19) and is calculated with the following equation (Balcarek et al., 2010):

$$TFA = (a/b) \times 100 \quad (2)$$

where, *a* is the medial trochlear facet distance and *b* is the lateral trochlear facet distance.

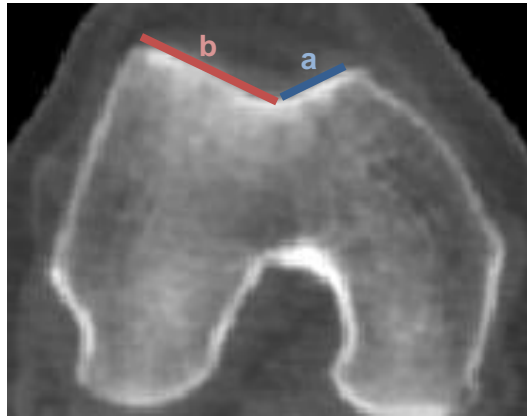


Figure 2.19: Measurement of lateral and medial trochlear facet lengths

Pfirschmann et al. (2000) showed that there is a significant increase in asymmetry in dysplastic knees and suggested a cut-off value of 40 % (Table 2.5). This threshold had 100 % sensitivity and 96 % specificity for discriminating trochlear dysplasia.

Table 2.5: Trochlear facet asymmetry measurement on dysplastic knees by different researchers

measurement plane	scan method	sample size [patient]	age [years]	range [%]	mean [%]	threshold [%]	reference
measurement plane 1	MR	101	14–40	11.4–57.4	34.9	–	Balcarek et al. (2010)
	MR	16	16–59	0.0–40.0	12.0	< 40.0	Pfirschmann et al. (2000)
measurement plane 3	MR	25	14–49	–	57.14	–	Salzmann et al. (2010)

- **Anterior-posterior to medial-lateral ratio (AP/ML)**

Biedert et al. (2009) measured the AP distances (Figure 2.16b) on the first transverse slice on which the cartilage covers the entire width of the trochlea beginning proximally (measurement plane 3). The medial to lateral (ML) distance of the femur was measured from the measurement slice. No statistical significance of the lateral AP/ML between normal and dysplastic femurs was found, whereas the medial and middle AP/ML increased significantly in the dysplastic group (Table 2.6). This finding suggests that the raised centre of the groove and the medial facet results in a flattening of the groove rather than decreased lateral trochlear height. This study also demonstrates the importance of investigating the AP distances of the femur because an appropriate type of trochleoplasty can be selected if the pathologic feature is correctly identified.

Table 2.6: Anterior-posterior to medial-lateral ratio results from Biedert et al. (2009)

	normal femur [%]	dysplastic femur [%]	student's t-test p value
lateral AP/ML	73–90	73–89	0.082
middle AP/ML	66–84	69–85	< 0.001
medial AP/ML	67–88	70–85	< 0.001

- **Ventral trochlear prominence (VTP)**

The ventral trochlear prominence (VTP) indicates the distance between the most ventral (anterior) point of the trochlear floor and the tangential line to the anterior cortex of the femur. It quantitatively indicates the existence of the supra-trochlear spur (Figure 2.20), a bump on the anterior trochlea which makes the patellar “ski jump”, thus causing patellar instability (Zaffagnini et al., 2010).

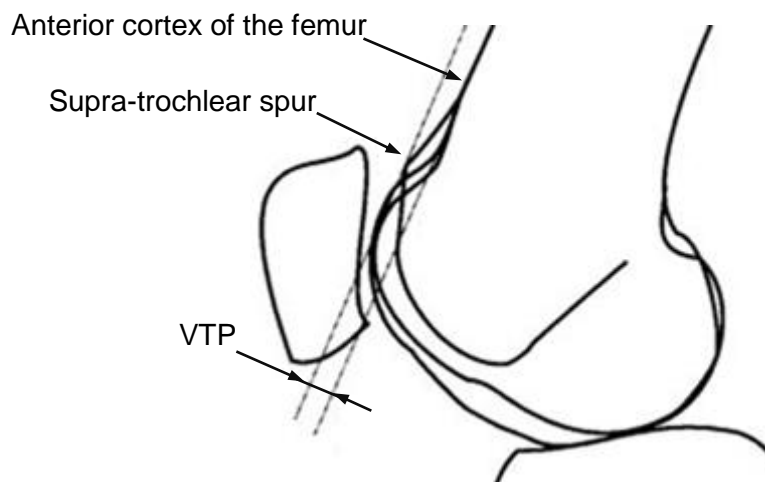


Figure 2.20: Ventral trochlear prominence (VTP) measurement edited from Pfirrmann et al. (2000)

The VTP is measured from the true lateral view of radiographs (Dejour et al., 1994) or on the mid-sagittal plane (which goes through the deepest point on the trochlear groove) when measured on CT or MR images (Pfirrmann et al., 2000). Dejour et al. (1990) suggested that a VTP value greater than 3 mm indicates trochlear dysplasia, but different threshold values were suggested for the MR images (Table 2.7).

Table 2.7: Summary of ventral trochlear prominence measurements on dysplastic knees from various studies

scan method	sample size [patients]	age [years]	range [mm]	mean [mm]	threshold [mm]	reference
x-ray	49	14–51	0.8–5.6	3.2	> 3	Dejour et al. (1994)
MR	16	16–59	6.9–15.5	9.3	> 8	Pfirschmann et al. (2000)
MR	59	16–45	0.8–8.9	4.8	> 4	Escala et al. (2006)

3 THREE-DIMENSIONAL MODEL GENERATION AND FEMORAL PARAMETER MEASUREMENTS

This chapter describes the segmentation methods for three-dimensional femur models from CT images. The accuracy of the segmentation technique, as well as the effects of the smoothing tool on the change in volume of the segmented femur model (used to produce a smooth surface) was evaluated. A repeatability and reproducibility (R&R) test was conducted to validate the measurement system accuracy. The reference framework and the coordinate system, in which the femoral parameters were measured, were defined. Finally, the measurement procedure and the results are presented.

3.1 Ethical Approval and Study Population

For the purpose of this thesis, existing CT images of the lower human body (taken during a research study performed by the Department of Mechanical and Mechatronic Engineering of Stellenbosch University, entitled “Investigating patellofemoral behaviour: An experimental and theoretical approach” (project number, NO8/02/029/2008)), were used. The ethical approval for this project was granted by the Committee for Human Research, Faculty of Health Sciences, Stellenbosch University in 2008 in accordance with the Declaration of Helsinki. 18 volunteers (7 males and 11 females between the ages of 19 and 65) were imaged with a computed tomography (CT) scanner (using a Siemens Emotion 16; 130 kV) after obtaining informed consent. None of the volunteers complained of knee pain or had any prior surgery performed on their knees. All scan data was made anonymous and it was impossible to identify individuals.

3.2 Validation of the Three-dimensional model Generation and Measurement Systems

3.2.1 Segmentation techniques from CT Scans

The volunteers' femurs and patellas were segmented from the CT images (Figure 3.1) using an automated segmentation algorithm for skeletal bones and then refined with a manual procedure that included the use of single and multi-slice edit tools (*Mimics*, Materialise, Leuven, Belgium). This segmentation technique has been described previously by Muller et al. (2010). The segmentation from CT has been benchmarked against laser scanning in a previous study (Van Schalkwyk, 2010) and the spatial accuracy was found to

be 99.7 %. These three-dimensional models developed in *Mimics* were imported into *3-matic* (Materialise, Leuven, Belgium) to take measurements.

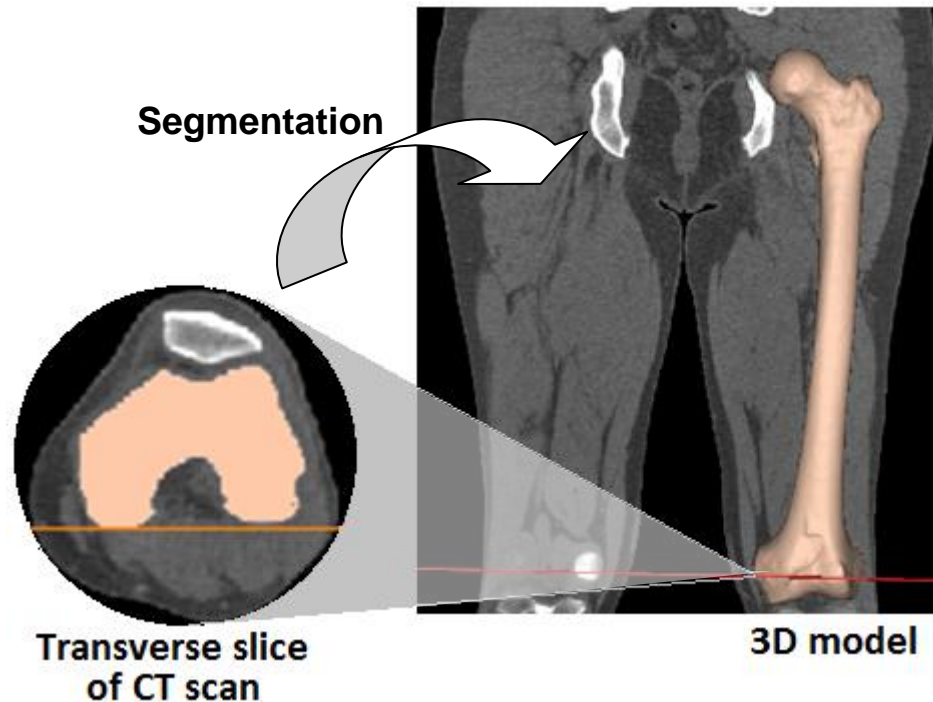


Figure 3.1: Three-dimensional model was generated by segmenting CT scans

3.2.2 Testing the effect of the smoothing tool on the accuracy of the model

The smoothing tool of *Mimics* was used to generate a smooth surface and to eliminate the rough surface introduced during the manual segmentation procedure. However, there was a risk of changing the shape of some important features. Therefore, it was necessary to examine the shape changes of the femur models in terms of their volume and dimensions. The smoothing effect was examined for seven randomly selected three-dimensional femur models by means of comparing the volume and measurements of the femur models before and after smoothing.

First, the volume difference before and after smoothing was measured. The average volume reduction was 0.25 % of the original femur model (Table 3.1). The 0.25 % reduction of the volume cause a 0.02 mm decrease in the radius of the cylinder with $500\,000\text{ mm}^3$ volume and 500 mm length when only a change in the radial direction is considered (illustrated in Figure 3.2) (the average volume of a femur is approximately $500\,000\text{ mm}^3$). Therefore, the radial distance change due to the volume reduction was considered negligible because it is less than the required accuracy of 1 mm, which is the level of the accuracy given by the surgical tools.

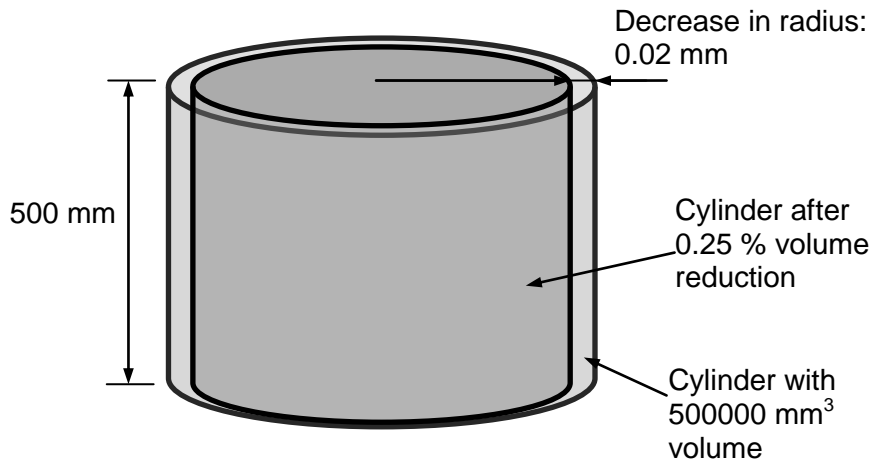


Figure 3.2: The assumptions made to estimate the effect of the change in volume due to the smoothing effect on the model features

Secondly, two surface curves were generated on the measurement plane, one from the femur before smoothing and the one after smoothing. On the measurement plane, the sulcus angles and the maximum distance between the two surface curves were measured (Figure 3.3). The average sulcus angle difference was 0.32° with a maximum of 1.03° . The mean value of the maximum distances between the two curves was 0.3 mm, with the maximum value of 0.41 mm. The change of these measurements was considered acceptable since they were comparable to the required accuracy for surgeries that are 1 mm and 1° . The methods used to create the measurement plane and to measure the sulcus angle are described in the following sections.

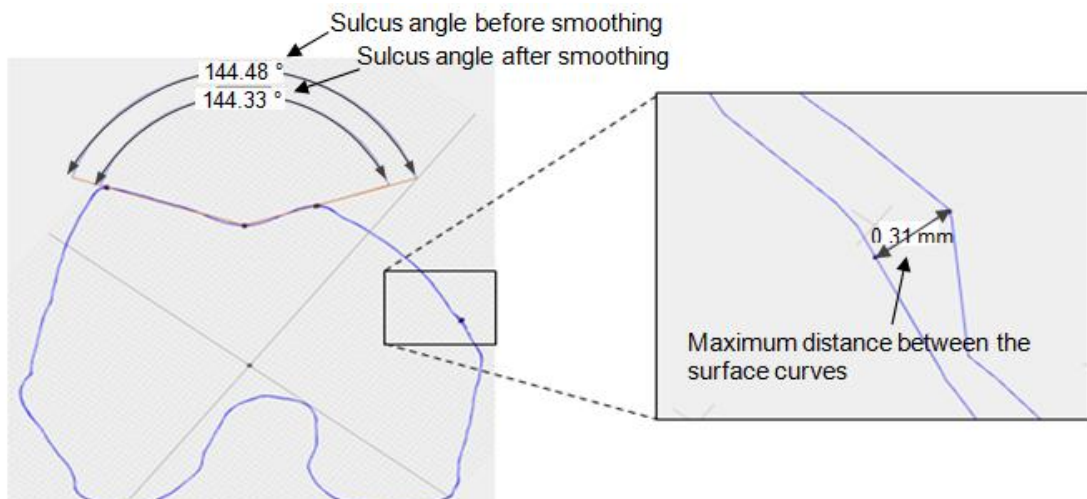


Figure 3.3: Measurement of the sulcus angles and maximum distance between the surface curves

Table 3.1: The parameters of the model before and after smoothing effect

model no.	volume before smoothing	volume after smoothing	volume reduction	sulcus angle before smoothing	sulcus angle after smoothing	sulcus angle difference	maximum distance between curves before and after smoothing
	[mm ³]	[mm ³]	[%]	[°]	[°]	[°]	[mm]
B012L	475195	473719	0.31	144.36	145.22	0.86	0.41
B013L	760889	759446	0.19	138.30	138.33	0.03	0.35
B014L	399728	398521	0.30	139.15	140.18	1.03	0.41
B015L	469951	468784	0.25	145.15	145.44	0.29	0.13
B016L	680621	679180	0.21	144.48	144.33	0.15	0.31
B017L	512190	510864	0.26	153.00	153.38	0.38	0.17
B021L	459446	458360	0.24	150.87	150.64	0.23	0.33
average	536860	535553	0.25	145.04	145.36	0.32	0.30

3.2.1 Validation of the measurement system with repeatability and reproducibility (R&R) test

The reliability of the measurement system and the inter-observer variability was tested by performing a repeatability and reproducibility (R&R) test (using the range and average method (Barrentine, 2002)). The repeatability represents the variability within the measurement system, while the reproducibility reflects on the variability introduced by different observers. Thirty measurements were taken by each observer, having 15 parts, two trials and two observers. The reference system reproducibility relies on the selection of the cylinder and the sphere fitting regions to generate the anatomical and the mechanical axes. Since the establishment of the reference framework is based on these axes, they determine the reliability of the coordinate system. Therefore the variability of generating these axes and the relative location to each other was tested by measuring the angle between them. In this way, the measurement system reliability can be tested in cases where it is considered acceptable if the R&R variability is less than 20 % (according to the guideline provided by Barrentine (2002)) (Table 3.2). The anatomical and the mechanical axes generation method is described in the following sections.

Table 3.2: Guideline for acceptance of the measurement system repeatability and reproducibility

R&R variability in %	acceptability
10 % or less	excellent
11 % to 20 %	adequate
21 % to 30 %	marginally acceptable
over 30 %	unacceptable

The percentage of the R&R variability was calculated to be 5.30 %. This measurement system showed to have an excellent acceptability by having a R&R variability of less than 10 % (Table 3.3). The R&R variability and the part variability do not add to 100 % because the calculations were made in a vector form. For example, a vector addition was used to add repeatability variability and reproducibility variability to attain R&R variability.

Table 3.3: Result for repeatability and reproducibility (R&R) test

variability type	% of the total variability
repeatability	3.61
reproducibility	3.88
R&R	5.30
part variability	99.86
total variability	100.00

3.3 Femoral Parameter Measurements and the Findings

The techniques for establishing the reference framework and the summary of the methods and femoral parameters measurements are provided in this section.

3.3.1 Reference and coordinate system

A cylinder was fitted to the femoral shaft to approximate the anatomical axis. This was achieved by selecting the region between the lesser trochanter and the section where the condyles of the distal femur start (Figure 3.4). The axis of this cylinder represents the anatomical axis. Thereafter the spherical portion of the femoral head was selected to approximate the hip centre (Figure 3.5). A line was connected from the intersection point between the anatomical axis and the distal femur to the centre of this sphere to define the mechanical axis (Figure 3.6).

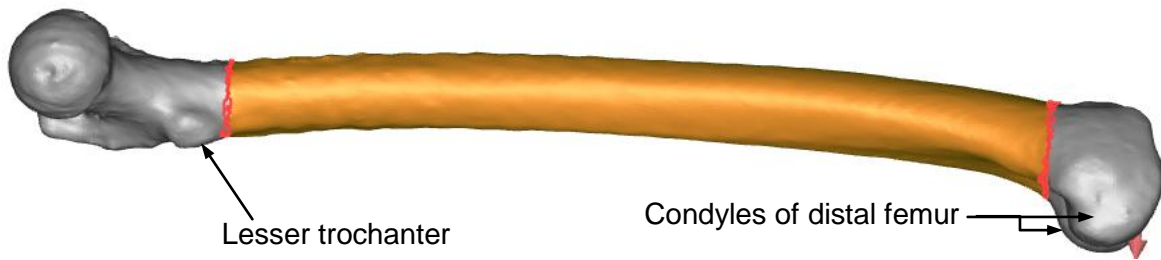


Figure 3.4: Highlighted region of the femoral shaft

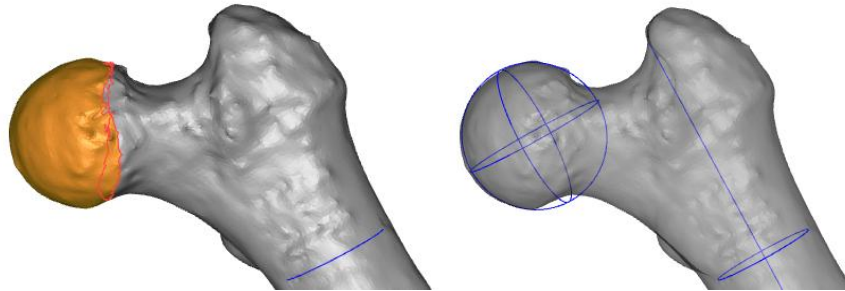


Figure 3.5: Generation of the best fit sphere to the highlighted surface of the femoral head

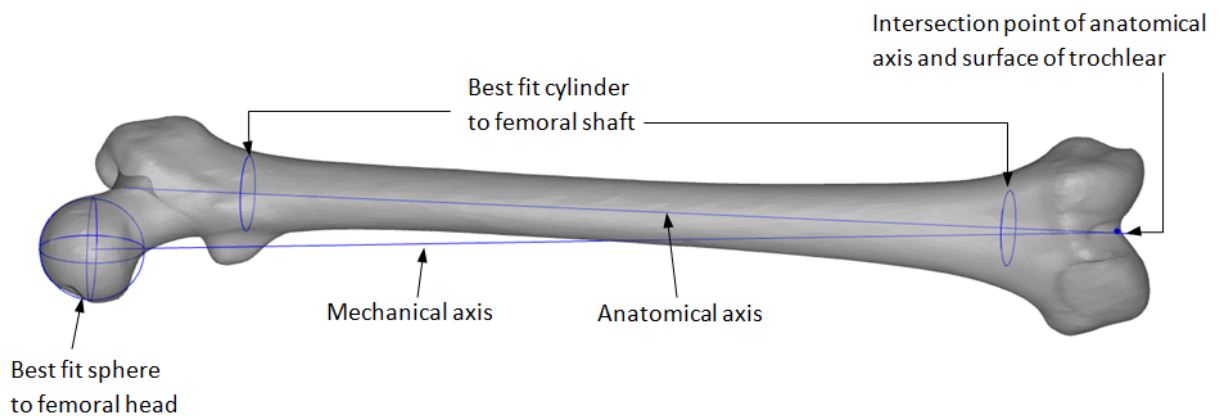


Figure 3.6: Generation of the anatomical and mechanical axes

Once the femoral axes (anatomical and mechanical) were constructed, the posterior condylar plane was defined on the three-dimensional model as the first referencing plane (Figure 3.7). The collaborating orthopaedic surgeon suggested that the posterior condylar axis is typically used as a reference during the patellofemoral surgery since it is easier to define than the epicondylar axes. Posterior condylar axis is the line joining the most posterior points of the lateral and the medial condyles. The posterior condylar plane, which contains the posterior condylar axis and is parallel to the mechanical axis, is then generated.

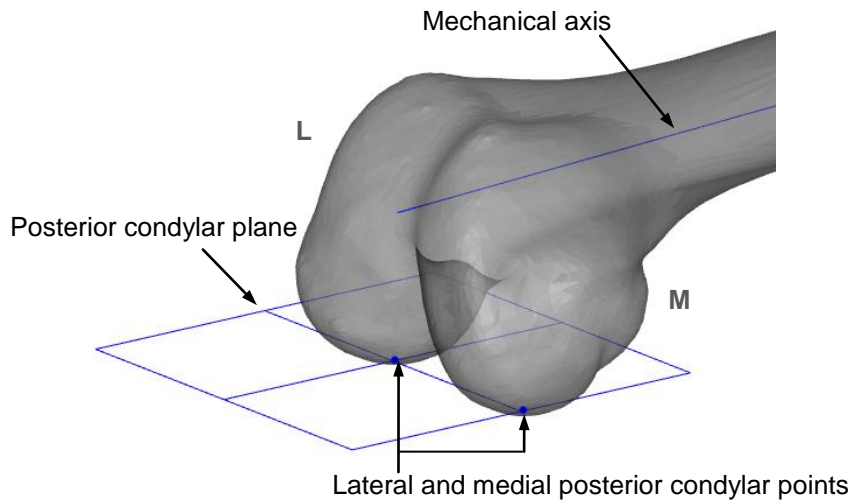


Figure 3.7: Construction of the posterior condylar plane

The distal plane was defined next: it went through the most distal points of both condyles and was perpendicular to the posterior condylar plane. The most distal points were determined by viewing the femur in a position perpendicular to the posterior condylar plane (Figure 3.8).

At the most posterior point of the lateral condyle, the measurement plane (Figure 3.8) was generated to be parallel to the distal plane. The distance between the distal plane and the measurement plane is approximately 2 cm (Table A1 and A2, Appendix A). Considering the thickness of the cartilages on the femur and the tibia, this distance is comparable to measurement plane 1 (Table 2.1), which is located approximately 3 cm above the tibiofemoral joint. Pfirrmann et al. (2000) noted the most significant difference between the normal and dysplastic groups when the parameters are measured on measurement plane 1, when compared with measurements on planes 1 cm and 2 cm above the tibiofemoral joint. The measurement plane does not go through the most posterior points of both the condyles, but only touches the lateral condyle. The trochlear depths, the sulcus angles, lateral trochlear inclination (LTI), trochlear facet asymmetry (TFA) and the AP distances were measured on the measurement plane.

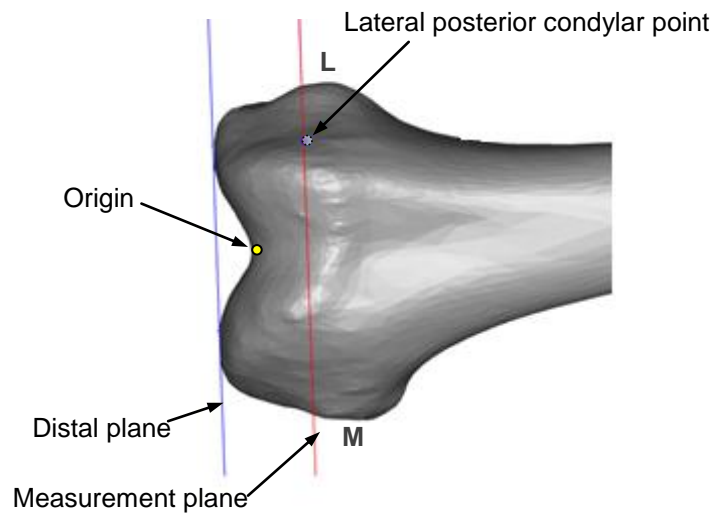


Figure 3.8: Illustration of the distal and measurement planes

The origin of the coordinate system was defined on the same view that the distal plane and measurement plane generated (Figure 3.8). The origin lies on the trochlear groove, giving the greatest orthogonal distance to the distal plane when the femur is viewed from the anterior side, perpendicular to the posterior condylar plane. Positive X was defined as the anterior to posterior direction perpendicular to the posterior condylar plane; positive Y as the distal to proximal direction parallel to the mechanical femoral axis and positive Z from lateral to medial direction of the line orthogonal to the XY plane (Figure 3.9). A defined coordinate system is useful for analysing curves with *Matlab* (MathWorks Inc, Massachusetts, USA) to which coordinates of the points on the curves were imported. The analysis of the curve is described in Chapter 5.

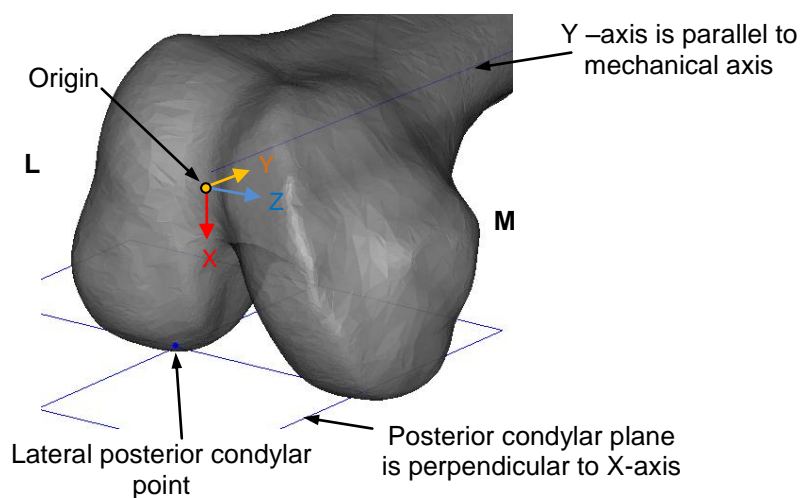


Figure 3.9: The coordinate system for the femur model

3.3.2 Femoral parameter measurement techniques

- **Trochlear depth**

The trochlear depth was measured on the intersection curve between the surface of the distal femur and the measurement plane following the method described by Martino et al. (1998). The shortest distance from the deepest point of the trochlear groove to the line joining the most anterior point of the lateral facet and the most anterior point of the medial facet was measured (Figure 3.10). The most anterior points were determined using the posterior condylar plane as the reference.

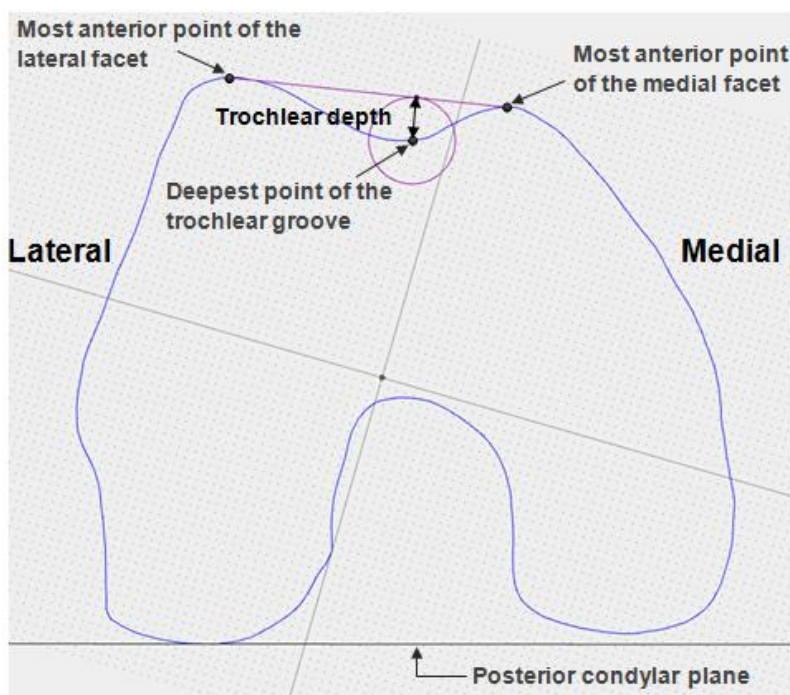


Figure 3.10: Measurement of the trochlear depth

- **Sulcus angle**

The sulcus angle is the angle between the tangent lines of the lateral and medial facets. However, the facets are often curved and variability is introduced when the observer defines the tangential lines of the facets. Therefore the most anterior points of the lateral and the medial facets were defined first, using the posterior condylar plane as a reference. Then the deepest point of the trochlear groove was selected using the same reference. The sulcus angle connecting these three points was then measured (Figure 3.11).

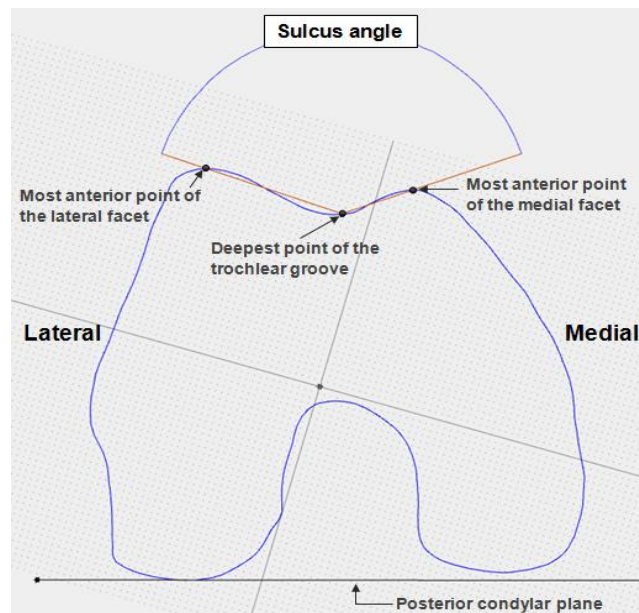


Figure 3.11: Measurement of the sulcus angle

- **Lateral trochlear facet inclination (LTI)**

The LTI is the angle between the tangential line to the lateral facet and the posterior condylar line (Fucentese et al., 2007). However, the LTI varies, depending on the point where the tangent is defined on the lateral facet. Therefore, to reduce the variability, the angle between the posterior condylar plane and the line joining the most anterior point of the lateral trochlear facet and the deepest point of the trochlear groove on the measurement plane was measured (Figure 3.12). These points were selected using the posterior condylar plane as a reference.

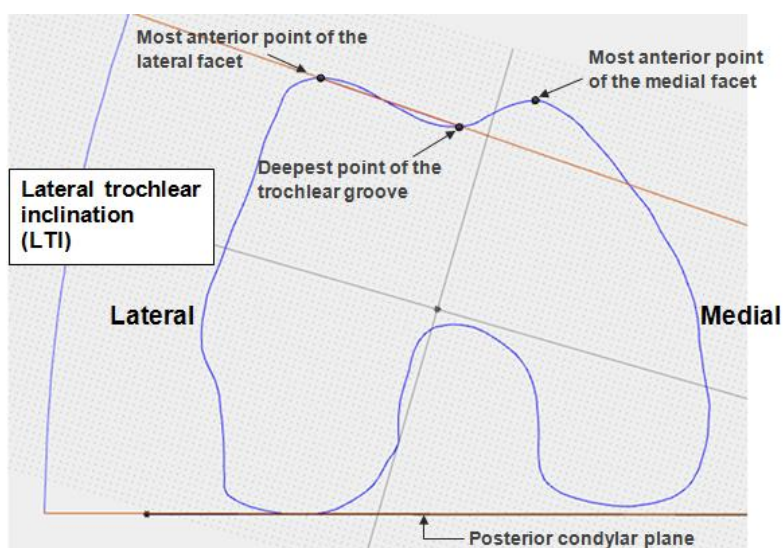


Figure 3.12: Measurement of lateral trochlear inclination (LTI)

- **Trochlear facet asymmetry (TFA) ratio**

The trochlear facet asymmetry (TFA) was calculated with a slight modification of equation (2) (refer to Section 2.3.2), and the equation is as follows:

$$\text{TFA} = (a/b) \times 100 \quad (3)$$

where, a is the line joining the most anterior point of the medial facet and the deepest point of the trochlear groove and b is the line joining the most anterior point of the lateral facet and the deepest point of the trochlear groove (Figure 3.13). All of these points were identified on the measurement plane, using the most posterior condylar plane as a reference.

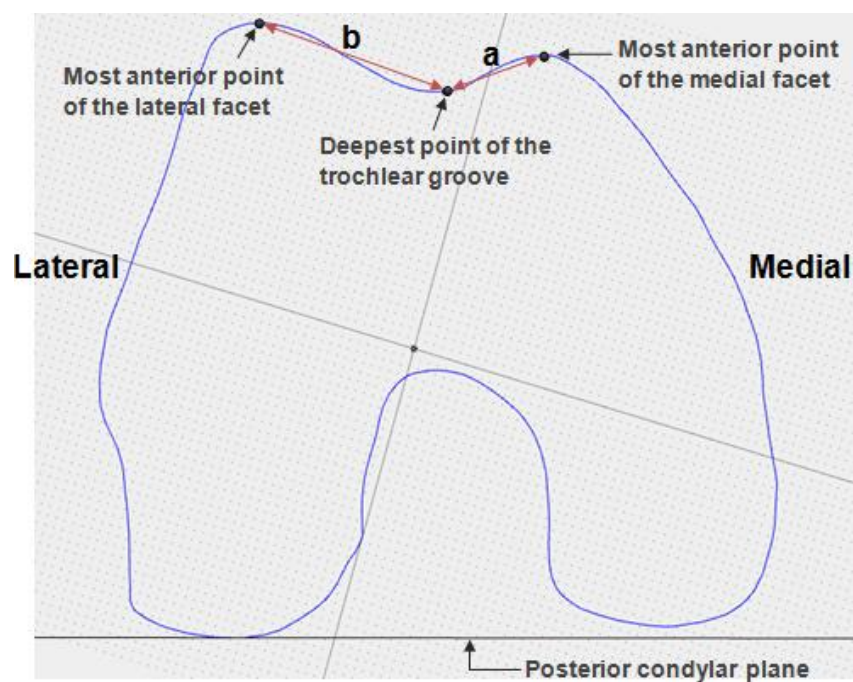


Figure 3.13: Illustration of the trochlear asymmetry ratio measurement method

- **Anterior-posterior (AP) distances**

The lateral anterior posterior (AP) distance was defined as the distance between the most anterior point of the lateral facet and the posterior condylar plane. The middle AP was then defined to be the distance between the posterior condylar plane and the deepest point of the trochlear groove. Finally, the medial AP medial distance was measured from the most anterior point of the medial facet to the posterior condylar plane (Figure 3.14).

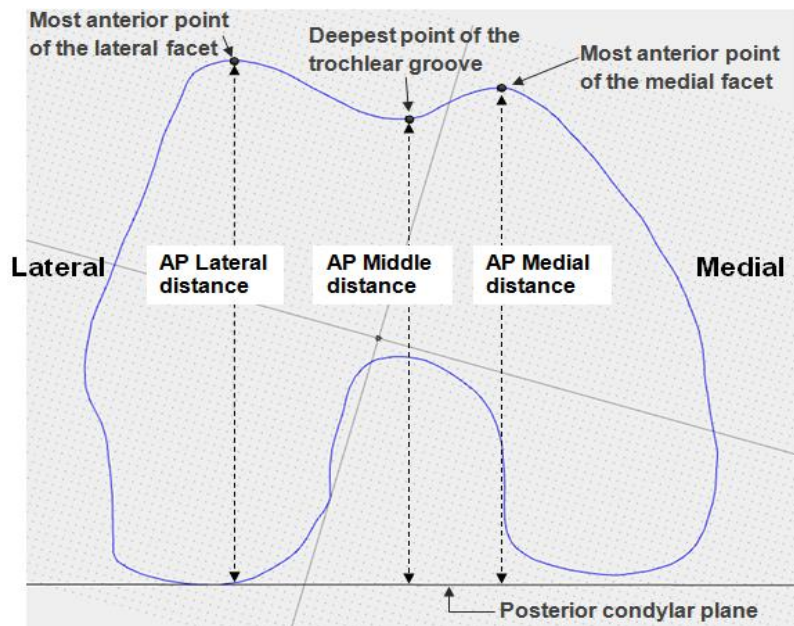


Figure 3.14: Measurement of the anterior-posterior (AP) distances

- **Medial-lateral (ML) distance**

The medial-lateral (ML) distance of the femur was measured on the three-dimensional femur model. On the most medial and the most lateral points of the femur, planes were generated to be in parallel with the anatomical axis and perpendicular to the posterior condylar plane (Figure 3.15).

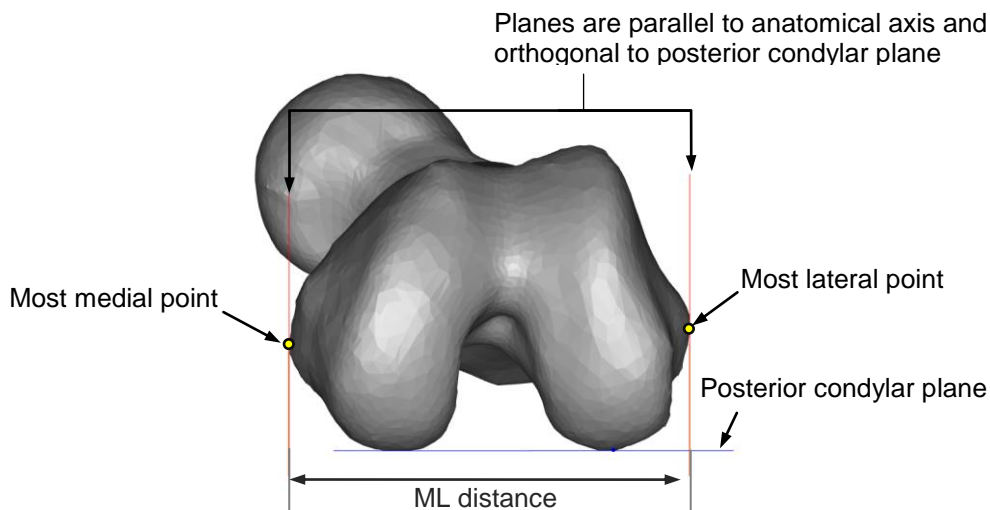


Figure 3.15: Medial-lateral (ML) distance measurement

- **Ventral trochlear prominence (VTP)**

The ventral trochlear prominence (VTP) is typically measured on the true lateral view of X-rays or on the mid-sagittal slice of CT or MR images. The mid-sagittal slice was generated at the origin of the three-dimensional models to be parallel to the mechanical axis

and perpendicular to the posterior condylar plane (Figure 3.16). This plane is now named the mechanical middle plane and will be used for the curvature analysis in the later sections.

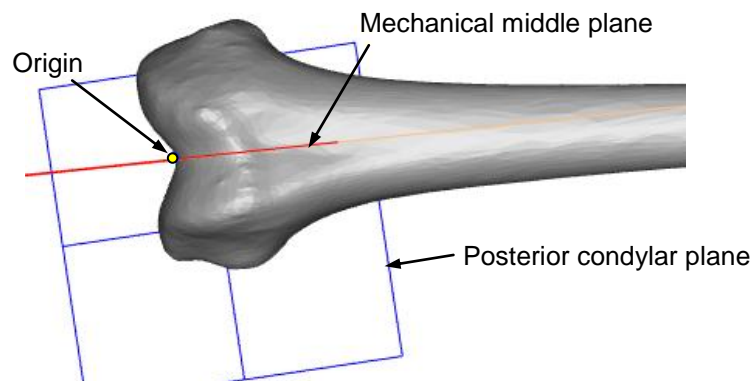


Figure 3.16: Schematic of the mechanical middle and posterior condylar planes

On the mechanical middle plane, the most anterior point can be selected using the posterior condylar plane as a reference. Then a tangential line was drawn to the ventral cortical surface of the distal femur. The shortest distance from the most anterior point to this tangential line was measured to define the VTP (Figure 3.17).

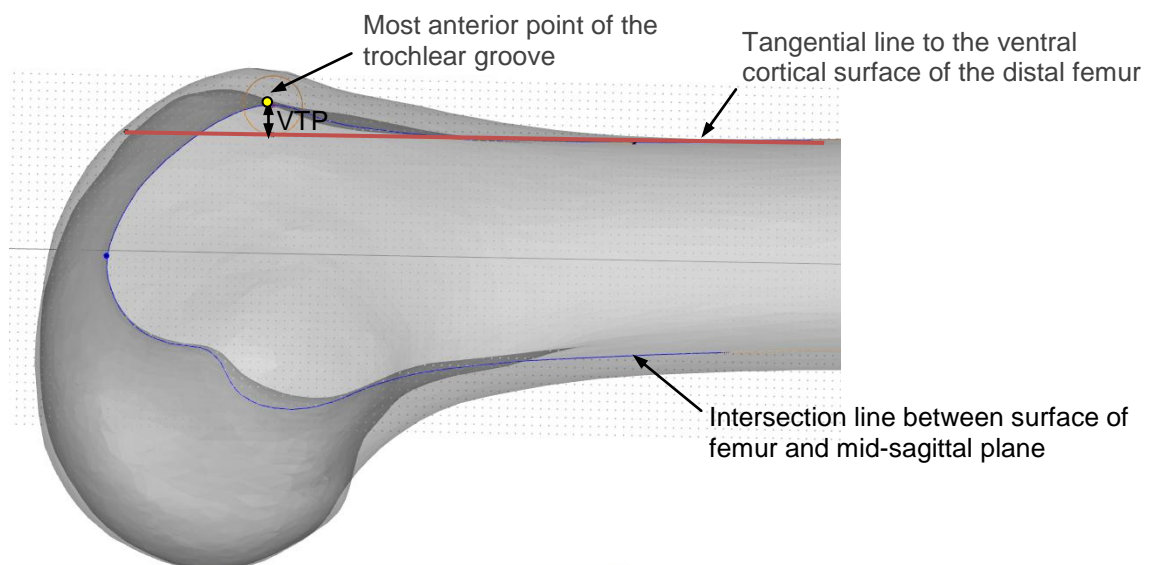


Figure 3.17: Lateral view for defining ventral trochlear prominence (VTP)

3.3.3 Findings from the femoral parameter measurements

Besides the trochlear facet asymmetry (TFA in Table 3.4), no statistically significant difference was found between the femoral parameters of the left and the right knees. However, no knees were classified as abnormal according to the TFA, as detailed in

Appendix B (Table B1 and B2). More left knees than right knees were dysplastic and this might have been reflected in the data, not necessarily illustrating the morphological difference due to the side of the femur.

The male and female femurs were then compared and it showed that there was a significant difference in trochlear depth, trochlear facet asymmetry and middle AP/ML ratio (Figure 3.5). This statistical difference according to gender could be due to having more female knee samples that were classified as dysplastic (Table B1 and B2). Another contributing factor to this difference could be the size difference (the female femurs is usually smaller than that of males). The values of all the femoral parameters measured are listed in the Appendix A (Table A1 and A2).

Table 3.4: Comparison between right and left femurs

parameters	right femur		left femur		student's t-test p value
	mean	standard deviation	mean	standard deviation	
trochlear depth [mm]	5.77	1.79	5.32	1.67	0.2215
LTI [°]	20.53	5.12	18.48	3.38	0.0830
sulcus angle [°]	141.40	8.81	142.74	7.62	0.3141
TFA [%]	67.77	10.30	60.67	9.85	0.0210
VTP [mm]	2.58	1.15	2.59	0.97	0.4881
AP (medial) / ML	0.75	0.02	0.76	0.02	0.0728
AP (middle) / ML	0.69	0.04	0.71	0.04	0.0751
AP (lateral) / ML	0.78	0.03	0.79	0.04	0.0902
angle between anatomical axis and mechanical axis [°]	5.15	0.53	5.24	0.64	0.3229
angle between anatomical plane and mechanical plane [°]	5.03	0.53	5.03	0.75	0.5000
angle between mechanical plane and distal plane [°]	94.43	1.66	94.25	1.50	0.3659

Table 3.5: Comparison between male and female groups

parameters	male group		female group		student's t-test p value
	mean	standard deviation	mean	standard deviation	
trochlear depth [mm]	6.65	1.39	4.84	1.36	0.0007
LTI [°]	20.04	3.80	19.16	4.80	0.2816
sulcus angle [°]	139.38	7.84	143.77	8.05	0.0584
TFA [%]	68.70	5.60	61.37	12.03	0.0203
VTP [mm]	2.63	1.05	2.56	1.07	0.4245
AP (medial) / ML	0.75	0.02	0.76	0.03	0.1444
AP (middle) / ML	0.68	0.03	0.71	0.04	0.0253
AP (lateral) / ML	0.77	0.03	0.79	0.04	0.0623
angle between anatomical axis and mechanical axis [°]	5.19	0.66	5.19	0.55	0.4982
angle between anatomical plane and mechanical plane [°]	5.08	0.65	5.00	0.64	0.3528
angle between mechanical plane and distal plane [°]	94.60	1.63	94.17	1.52	0.2125

3.4 Discussion

Smooth, three-dimensional models were generated from CT scans and their measurements were taken with an accuracy level of 1 mm and 1°. The reliability of the measurement method was examined using the repeatability and reproducibility (R&R) test and it was shown to be acceptable. The standardised methods for femoral parameter measurement were established to be performed on the three-dimensional models, eliminating the error due to the misalignment scanning.

The femoral parameters measurements showed that there were more morphological differences due to the gender than could be attributed to the particular side of the femur. Due to the limited sample size, it was, however, assumed in this study that the side of the knee and the gender do not influence the classification of the knee as normal or dysplastic. The measured femoral parameters will then be used to classify the femurs as either normal or abnormal, depending on the existence of trochlear dysplasia, as presented in the next chapter.

4 CLINICAL CLASSIFICATION OF NORMAL AND ABNORMAL KNEES

This chapter provides the procedures followed to identify the femurs with trochlear dysplasia by means of three different approaches. First, the femurs were classified quantitatively, using only the femoral parameters. Then the qualitative classification was done by experienced orthopaedic surgeons. Lastly, artificial neural networks (ANN) were used to match the femoral parameters to the qualitative classification. These three different classification methods were compared and then a set of normal knees were selected for the normal geometry analysis.

4.1 Quantitative Classification with Femoral Parameters

The cut-off values of the femoral parameters for identifying trochlear dysplasia were defined from literature (Table 4.1). The knees were classified according to these parameters: trochlear depth, sulcus angle, ventral trochlear prominence (VTP), trochlear facet asymmetry (TFA), and lateral trochlear inclination (LTI). The “overall quantitative classification” was made by following the classification that three or more parameters indicated abnormality. This was then compared with the surgeons’ “overall qualitative classification” and to the classification made by an artificial neural network (ANN).

Table 4.1: Cut-off values for identification of trochlear dysplasia for different femoral measurements

femoral measurements	the knee is dysplastic if:	reference
trochlear depth	< 5 mm	Escala et al. (2006)
sulcus angle	> 145°	Dejour et al. (1994)
TFA	< 40 %	Pfarrmann et al. (2000)
LTI	< 14°	Escala et al. (2006)
VTP	> 3 mm	Dejour et al. (1994)

The classification made by the parameters agreed on 14 out of 36 knees only (38.9 % agreement) and they were all normal knees. This was because the TFA classified all the knees as normal. The trochlear depth and the sulcus angle showed high agreement on the classification (88.9 %). The classification result for each femur is given in Appendix B.

4.2 Qualitative Classification by Surgeons

The knees were qualitatively classified using Dejour’s (2007) classification method for trochlear dysplasia as the guideline. Three experienced orthopaedic surgeons (Erasmus,

Stellenbosch medi-clinic; Dejour, Lyon-Ortho-Clinic; Arendt, University of Minnesota) examined the lateral view of the three-dimensional femoral models and the first transverse CT slice on which the “roman arch” was visible when examined from the distal to proximal side (Figure 4.1). The surgeons identified the signs of trochlear dysplasia from these two images of each femur model and classified them into either normal or abnormal. The “overall surgeons’ classification” was made by following the categorisation that two or more surgeons agreed on.

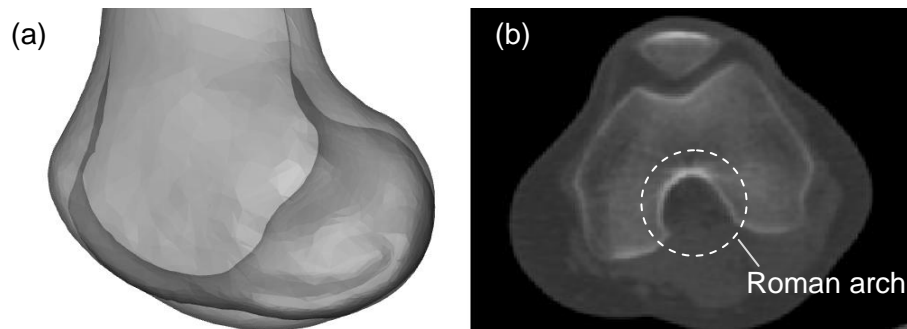


Figure 4.1: (a) Lateral view of the distal femur, (b) First transverse CT slice on which the roman arch is visible when examined from the distal side.

All three surgeons classified 25 knees (69.4 % agreement) into the same category, with a greater agreement than the agreement between the femoral parameters (38.9 %). The agreement between the “overall quantitative classification” and the “overall surgeons’ classification” was 75 %. These results show that there is a correlation between the surgeons’ qualitative classification and the quantitative classification using the femoral parameters, although it is not clearly visible. The artificial neural network (ANN) was used to take both the qualitative and quantitative nature of the classification into account.

4.3 Classification with Artificial Neural Networks Pattern Recognition Tool

An artificial neural network (ANN) has advantages over the traditional statistical procedures like the Bayesian decision theory (Duda and Hart, 1973), the latter which works well only with sufficient understanding of the target value and the underlying probability of the model. On the other hand an ANN is a data-driven self-adaptive mathematical modelling method which enables the data to adjust itself through a number of hidden-layer neurons. There is no need for probability assumption for this model. Another advantage of ANN is that complex parameter space is used to identify its inter-relationship for a classification (Baxt, 1990), although this means that the performance of ANN has to be tested to find the optimal number of hidden-layer neurons and the number of parameters. However, because of these

advantages of the ANN, it is suitable for classification of the dysplastic femur (which is dependent on the complex and nonlinear relationship between the femoral parameters). The combined effect of the femoral parameters can be compared to the surgeon's classification and be interpreted in a simpler way.

4.3.1 Overview of the procedure

The input parameters (Table 4.2) of the database of the 36 femurs were trained with the pattern recognition function within the ANN toolbox provided by *Matlab R2010b* (MathWorks Inc, Massachusetts, USA). The parameters of the femurs with the matching output and the ones without matching output were input to train the data: the parameters with matching output (18 normal and 7 dysplastic femurs) gave information for the ones without matching output (11 unclassified femurs), which enabled the data to group itself in a self-adaptive way (Figure 4.2). The matching output is the known answer to the input; the classification that all three surgeons agreed upon in this case. The training based on the Levenberg-Marquardt optimisation was used for updating the weights of the multiple layered feed-forward neural networks. The femurs were classified as either normal or abnormal as a result of the training. The output (classification) would not necessarily be the same as the "matched output" because the output relied more on the pattern of the data than the given answer. Some of the knees were classified as abnormal by the ANN even though all surgeons classified them as normal.

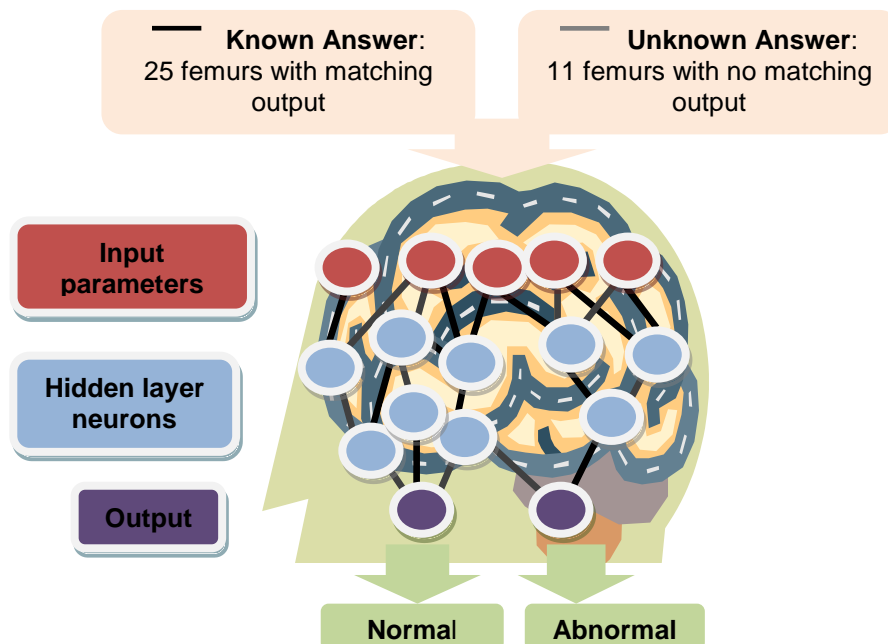


Figure 4.2: Classification method using pattern recognition function of artificial neural networks (ANN)

4.3.2 Selection of optimum number of input parameters and number of hidden layer neurons

There are two factors that influence the classification of the ANN: the number of the input parameters, and the number of the hidden-layer neurons. The various combinations of these factors were tested to find the optimal condition to maximise the agreement between the surgeons' overall classification and the classification made by the ANN. First, the statistical overlap factor (SOF) of each parameter was calculated in order to examine the separation between the distributions of the normal and abnormal femurs. This was done to select the possible input parameters. The knees on which all the surgeons were in agreement were used in this phase. The SOF was proposed by Mdlazi et al. (2007) as represented in the equation below:

$$SOF = \left| \frac{\bar{x}_1 - \bar{x}_2}{(\sigma_1 + \sigma_2)/2} \right| \quad (4)$$

where \bar{x}_1 and \bar{x}_2 are the averages of the distributions, σ_1 and σ_2 are their respective standard deviations. The higher SOF value indicates the greater separation between the normal and abnormal values of the parameters.

The number of the input parameters was varied between the four and 10 parameters with the highest SOF values, while the number of hidden-layer neurons was varied between $2n-3$ to $2n+3$, where n is the number of the input parameters. This gives 49 possible combinations of different number of input parameters and number of hidden-layer neurons. The average agreement between the ANN and the surgeons' overall classifications over 15 identical runs was recorded for the each combination. The average goal function was recorded as well: it indicates the error between the estimation.

Table 4.2: Selected parameters for network training and their statistical overlap factor

Input parameters	SOF
trochlear depth	1.29
AP middle / ML	1.21
LTI	1.14
sulcus angle	1.12
AP medial / ML	0.78
AP lateral / ML	0.54
TFA	0.53
angle between anatomical and mechanical axes	0.21
angle between anatomical and mechanical planes	0.17
angle between mechanical and distal planes	0.13

The maximum average agreement over the 15 runs was 80.6 % (minimum agreement: 63.6 %) when the number of input femoral parameters was eight (with 19 hidden-layer neurons with the standard deviation of 0.136 %) (Table C1 and C2, Appendix C). The average goal function was 0.164 (Table C3) with the standard deviation of 0.154 (Table C4). At this optimum combination of the number of parameters and hidden-layer neurons, the ANN classified 17 knees as normal and 19 knees as abnormal.

The following table (Table 4.3) outlines the extent of agreement between the ANN and the quantitative and qualitative classifications. The trochlear depth showed the highest agreement with the ANN amongst all the femoral parameters (75 %) which suggests that it may be used for identification of trochlear dysplasia. The details of the comparison amongst the different classification methods are provided in Appendix B.

Table 4.3: Agreement between ANN and other classification methods

agreement between femoral parameters' quantitative classification and ANN [%]						agreement between surgeons' qualitative classification and ANN [%]			
trochlear depth	VTP	sulcus angle	TFA	LTI	overall quantitative classification	Erasmus	Dejour	Arendt	overall surgeons' classification
75.0	69.4	69.4	47.2	55.6	66.7	77.8	41.7	83.3	80.6

4.4 Analysis of Classification Methods

The student's t-test was conducted for the normal and abnormal femur groups classified by the ANN to identify parameters that are suitable indicators of trochlear dysplasia. The trochlear depth, sulcus angle and middle AP/ML had a p value less than 0.001, achieving 99.9 % confidence level. The new cut- off values for these three parameters was suggested with the use of the box-whisker plots (Figure 4.3 and Table 4.4).

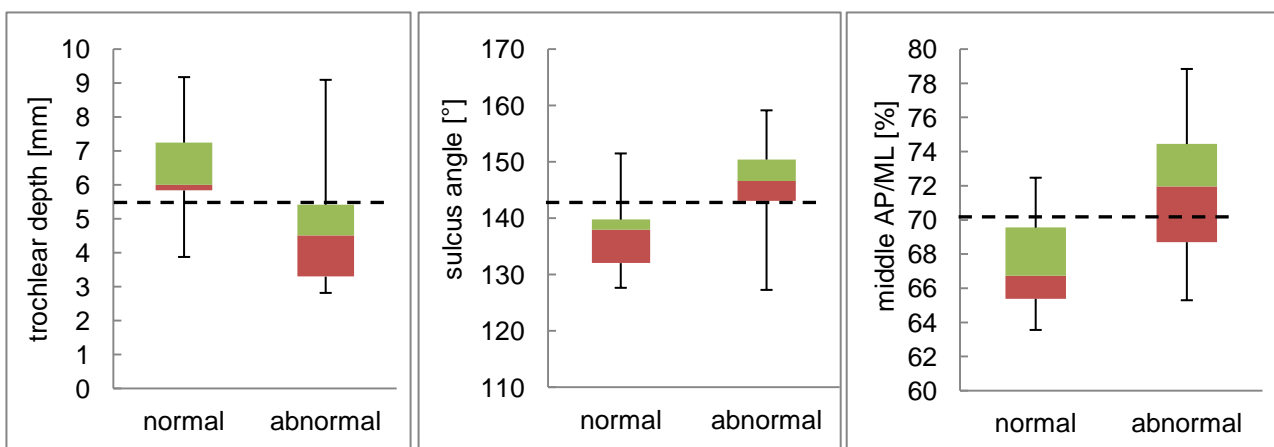


Figure 4.3: Box-whisker plot for trochlear depth, sulcus angle and middle AP/ML

Table 4.4: The mean and standard deviation of the input parameters for the normal and dysplastic groups

parameters	normal group		dysplastic group		student's t-test p value	new cut-off value
	mean	standard deviation	mean	standard deviation		
trochlear depth [mm]	6.46	1.39	4.73	1.60	0.0007	5.4
LTI [°]	21.60	3.96	17.63	3.98	0.0026	–
sulcus angle [°]	137.73	6.09	145.94	7.91	0.0007	142
TFA [%]	67.52	8.88	61.28	11.29	0.0382	–
VTP [mm]	2.14	1.02	2.98	0.93	0.0072	–
AP (medial) / ML	0.74	0.02	0.76	0.03	0.0093	–
AP (middle) / ML	0.67	0.03	0.72	0.04	0.0001	0.7
AP (lateral) / ML	0.77	0.03	0.80	0.03	0.0038	–
angle between anatomical axis and mechanical axis [°]	5.19	0.41	5.19	0.72	0.4865	–
angle between anatomical plane and mechanical plane [°]	5.05	0.50	5.02	0.75	0.4507	–
angle between mechanical plane and distal plane [°]	94.60	1.82	94.10	1.28	0.1749	–

The sensitivity and specificity test for identifying the trochlear dysplasia was conducted on the old and new cut-off values of these three parameters. The sensitivity and specificity was improved with the new cut-off values (Table 4.5). With the new trochlear depth cut-off value and the measuring method proposed by this study, it yielded higher sensitivity and specificity than a study by Escala et al. (2006) who presented sensitivity of 0.86 and specificity of 0.72.

Table 4.5: Sensitivity and specificity for identifying trochlear dysplasia

parameter	trochlear depth		sulcus angle		middle AP/ML
	new: 5.4 mm	old: 5.0 mm	new: 142°	old: 145°	new: 0.7
sensitivity	0.88	0.87	0.84	0.80	0.81
specificity	0.76	0.71	0.82	0.67	0.70

4.5 Discussion

Thirty six femurs were classified using three different methods: 1) widely used femoral parameters for identifying trochlear dysplasia; 2) experienced orthopaedic surgeons

using CT scans; and 3) artificial neural networks (ANN) which incorporates the femoral parameters and the surgeons' classification. For the ANN, an optimal running condition was tested to be eight input parameters, with 19 hidden-layer neurons. The input parameters were: trochlear depth, sulcus angle, TFA, LTI, AP/ML, angle between anatomical and mechanical axes.

A 80.6 % agreement between the ANN and the surgeons' classification was achieved, compared to the 69.4 % agreement amongst the surgeons. The ANN classification was made by matching and identifying the pattern between the parameter values and the surgeons' decisions. The minimum agreement between the qualitative and ANN classification was 41.7 % which indicates that the surgeon's classification may not always match the quantitative data. This motivates the added consultation of a quantitative guideline.

The classification by ANN showed a 66.7 % agreement with the femoral parameters, compared to the 38.9 % agreement amongst the femoral parameters. The low agreement amongst the femoral parameters is because no femur was classified as dysplastic according to the cut-off value suggested for TFA (40°). This showed that some femoral parameters were not suitable for discriminating trochlear dysplasia, or new cut-off value had to be determined.

A student's t-test was therefore conducted for all the femoral parameters. Three parameters showed a statistically significant difference between the normal and abnormal group within 99.9 % confidence level with the newly suggested cut-off values: trochlear depth (5.4 mm), sulcus angle (142°), and middle AP/ML (0.7). The sensitivity and specificity was improved with the new thresholds in classifying trochlear dysplasia. The trochlear depth showed the highest sensitivity (88 %) and the sulcus angle showed the highest specificity (82 %).

As the result of the ANN classification, 17 femurs were classified as normal and nineteen femurs as abnormal. However, there were two of the normal femurs that exhibited a ventral prominence (VTP) higher than 3 mm and a bump was identified on the trochlea. In collaboration with an experienced orthopaedic surgeon (Erasmus, Stellenbosch medi-clinic), it was decided that these two knees should be taken out of the normal knee database to ensure an accurate geometry analysis. Therefore, 15 normal knees were identified in this chapter which will be used for the analysis and prediction of the normal trochlea as presented in the next chapter.

5 ANALYSES FOR NORMAL TROCHLEA PREDICTION

This chapter describes the investigation of the trochlea geometry of the 15 normal knees which were identified in the previous chapter. Using the least squares theorem, the sagittal shape of the trochlear groove was approximated by B-spline and constant radii curves. Based on these analyses, the method for normal trochlea prediction by means of the self-organising maps (SOM) was validated by examining the error between the predicted values from SOM and the measured parameters of the normal knees.

5.1 Sagittal Surface Curve Analysis

5.1.1 Sagittal surface curve generation and selection methods

Four medial and four lateral duplicate planes were created by sequentially moving the mechanical middle plane medially and laterally, creating nine slicing planes with 3 mm spacing (Figure 5.1). Intersection curves between the femoral surface and the nine slicing planes were then generated using the generating curves tool in *3-Matics* software. The coordinates of these curves were exported to *Matlab* for further analysis.

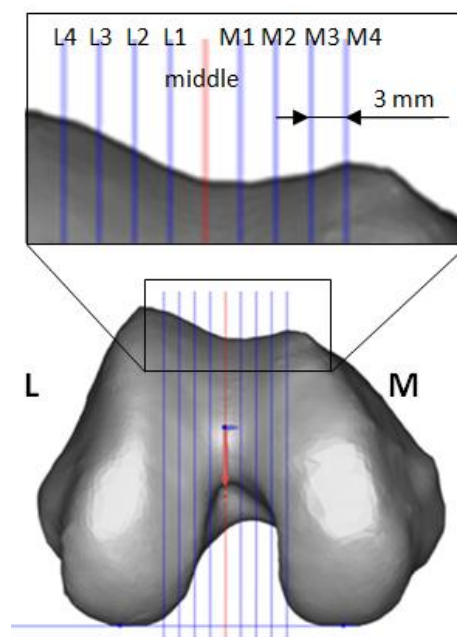


Figure 5.1: Mechanical middle plane (red) and other sagittal slicing planes (blue)

Since only the articulating surface on the trochlea was the subject of interest, the following portions of the surface curves were selected: the curve between the most anterior point and the sulcus terminalis (seen in Figure 5.2a), which indicates the distal termination of

the trochlear groove. In the cases where the sulcus terminalis were invisible, the section of the curve between the most anterior point and the most distal point was selected (Figure 5.2b).

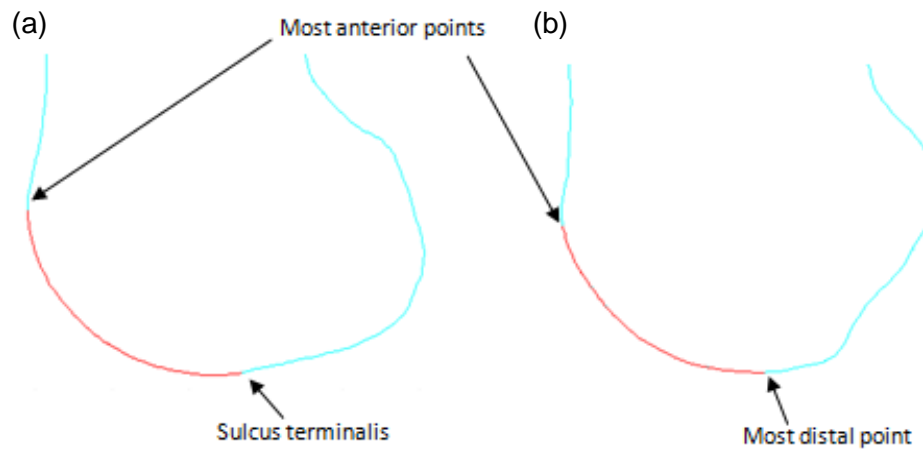


Figure 5.2: Selection of the portion of the curve to be analysed (red) a) on a lateral slice (L3) and b) medial slice (M1)

5.1.2 Generation of B-spline curves and finding the centres of the curvatures

The shape of the curves was examined by fitting a B-spline curve on the trochlea in the sagittal direction in each slice. The centre of curvature of each curve was then plotted. A 3rd order B-spline curve was fit to the data points by following a similar procedure described by Kosel et al. (2010). The B-spline curve was mathematically approximated with the least squares method (Piegl, 1997) to produce a smooth curve, thereby eliminating noise in the data (refer to Appendix D for calculations). The number of the control points was set to be five. However, if the maximum error between the data points and the B-spline exceeded the limit of 0.3 mm, then the number of control points was increased until the maximum error became smaller than the limit. The distance between the adjacent points on the B-spline curve was set to be 0.1 mm.

After generating the B-splines, the centre of the curvature was estimated using the three consecutive points (points P1, P2, and P3 on Figure 5.3) on the B-spline curve (curve AB on Figure 5.3) by fitting a circle that goes through these three points. If a line is drawn from the centre to a chord of a circle, the line meets the chord at its midpoint with the angle of 90°. Using this property, the centre point of curvature can be estimated, assuming that the three consequent points are on a circle. Perpendicular lines are drawn from the midpoints of the chords (M1 and M2 on Figure 5.3) and the intersection point (C1 on Figure 5.3) is the centre point of the curvature. This procedure was repeated for all the points on the B-spline

to plot a distribution of the estimated centre of the changing curvatures (estimated centres are seen in Figure 5.4).

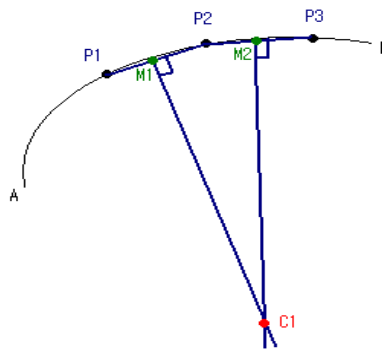


Figure 5.3: Centre of curvature estimation method

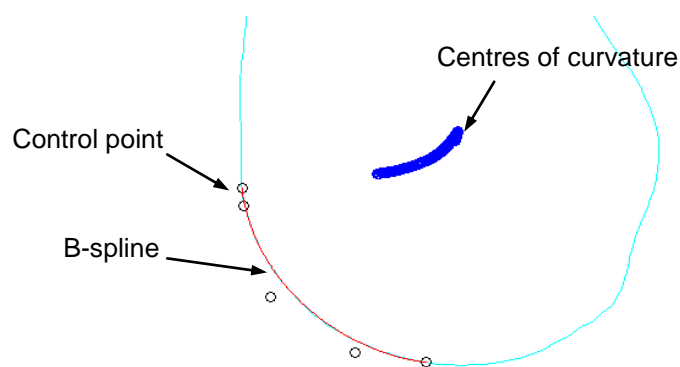


Figure 5.4: Centres of the curvatures for the points on B-spline curve fit to a sagittal surface curve (M2)

5.1.3 Circular arc fitting using least squares theorem

Iranpour et al. (2010a) showed in their study that a circle could be fit to the middle of the trochlea and its lateral and medial sections within a tolerance of 0.3 mm. However, the distribution of the centre of the curvature obtained by the B-spline fitting showed that the selected region cannot be estimated with a single centred circular arc (Figure 5.5a). Since it has been shown previously that the trochlea can be considered circular in the sagittal plane, the B-spline and a circular arc were both fitted onto the same data points to identify the circular region. The data point of the curve was then removed from the distal side until the centre of the B-spline's curvature and the centre of the circle was in close proximity (Figure 5.5b), since the centres estimated with the B-splines will coincide with the centres of the circular arc for the curve to be circular. The maximum error between the data points and the circular arc was defined to be 0.5 mm (Table E1, Appendix E). The average distance between the centre points from the two methods (B-spline and least squares) were also measured.

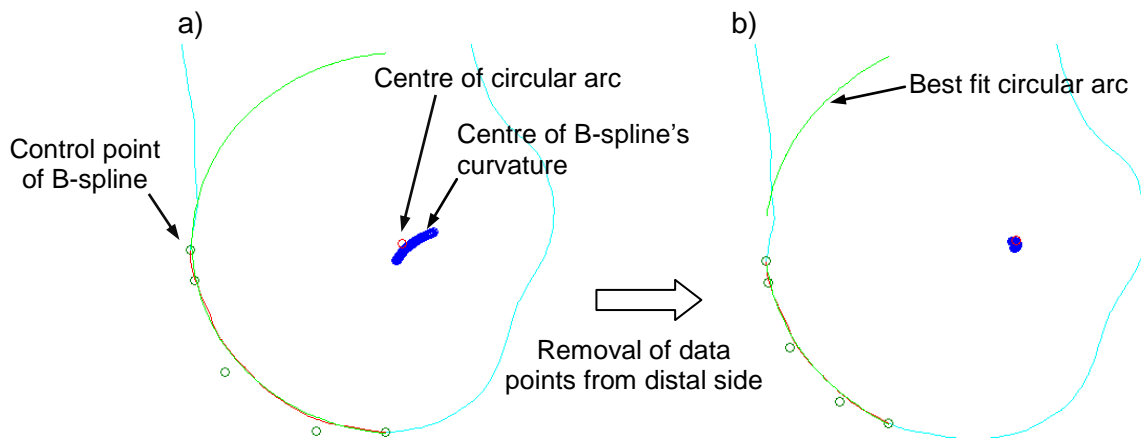


Figure 5.5: Selecting the circular portion of a sagittal surface curve (M2)

The trochlear flexion angle and the radius of the circular arc were then measured to describe the circular region. The trochlear flexion angle is measured from the centre point of the circular arc and it indicates the circular region of the sagittal curves (Figure 5.6a). The distances between the centre point and the data point were plotted against the trochlear flexion angle to illustrate the region represented with a single radius (Figure 5.6b). As the position of the centre point is known, the radius and trochlear flexion angle of the circular arc and the circular portion of the trochlea could be replicated on any sagittal slice.

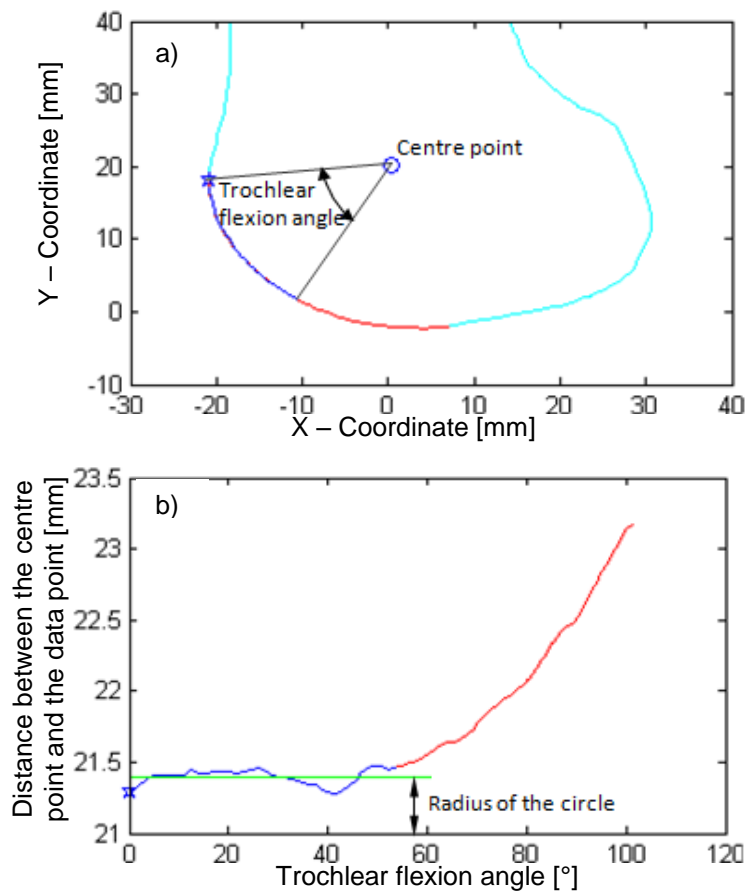


Figure 5.6: (a) Trochlear flexion angle and (b) radius for the circular region (blue line)

5.1.4 Results of the curve analysis

This study reconfirmed that the trochlear groove can be considered circular in the sagittal view parallel to the mechanical axis, with at least 40° and at most 90° of trochlear flexion angle, with an average of 56.3°. The average distance between the centre points of the sagittal curve plots was 2.9 mm (Table 5.1). This distance resulted from imperfect arcs of the B-spline curves, although it effectively found the circular regions. The selected circular region had a minimum tolerance of 0.03 mm, the maximum of 0.5 mm and the mean of 0.2 mm between the data points and the estimated circular arcs. The radius of the circular arc as well as the AP distance for each slice was measured. These parameters are used to predict the normal geometry using self-organising maps (SOM) as described in the following sections. The details of the measurements are provided in the Appendix E.

Table 5.1: Results of curve analysis

		slice plane									
		L1	L2	L3	L4	M1	M2	M3	M4	middle	mean
average distance between B-splines and least squares centre points	[mm]	2.7	2.8	3.8	3.9	3.0	2.8	2.5	1.8	2.4	2.9
average radius of the circular arc	[mm]	24.7	24.7	24.9	24.8	22.1	20.4	20.3	20.6	22.8	22.8
average trochlear flexion angle	[°]	50.0	52.7	60.7	62.3	60.0	59.7	55.3	56.3	50.0	56.3

5.1.5 Plane fitting to the centre points of the least squares circular arcs

Once the circular region of the surface curve was defined by fitting the circular arcs, it was observed that the centre points of these arcs were lying on a plane, even though they were not collinear. The best fit plane was defined through the centre points from each of the nine sagittal slices using the least squares method, thereby forming the centre plane. Then the position of this centre plane was described by measuring the rotation around the X-axis and Z-axis and then by the translation in the Y direction when using the X-Z plane at the origin as the reference (Figure 5.7).

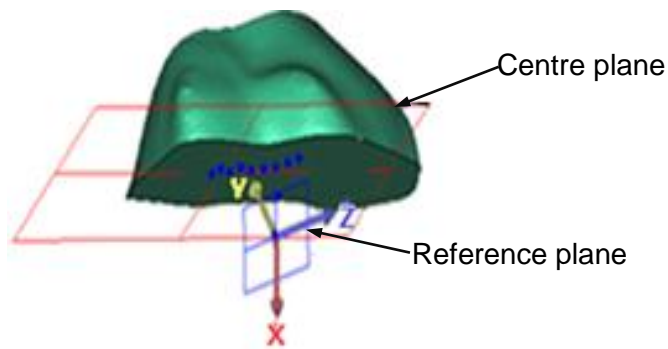


Figure 5.7: Centre plane position

The orthogonal distances between the centre points and the centre plane were measured and the tolerance was found to be 1 mm, while the mean value of the average error over the 9 slices was 0.42 mm (Table 5.2). The measurement for each femur model is provided in Appendix E (Table E5).

The above finding is significant because if the centre plane can be accurately positioned, the centre points of the circular arcs can be estimated. Thus the geometry of the anterior trochlea can be estimated. The intersection between the centre plane and the slice would be present as a line on the slice plane on which the centre lies. The centre point of the circular arc can be positioned using the AP height and the radius. However, the X-rotation showed a high variability with a standard deviation of about 50 % of the mean value. Also, no obvious and visible trend between the position of the centre plane and other femoral parameters were observed. These challenges lead to the validation of the geometry prediction method using the centre plane as one of the parameters. In the following section, the validation method and result for predicting the position of the circular arcs, using a type of artificial neural networks, is discussed.

Table 5.2: Summary of centre plane fitting result

	X-rotation [°]	Z-rotation [°]	Y-translation [mm]	average error between centre points and centre plane [mm]
mean	-10.52	-132.46	18.99	0.42
standard deviation	5.50	29.51	2.88	0.26

5.2 Validation for Normal Trochlea Geometry Prediction Method: Self-Organizing Maps (SOM)

5.2.1 Introduction

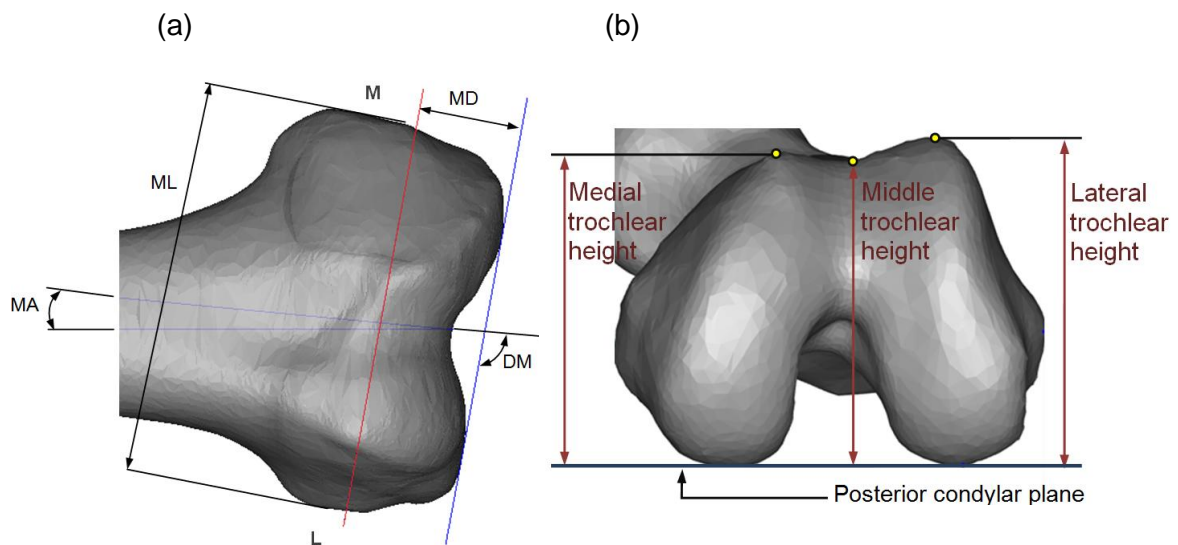
Self-organising maps (SOM) is a type of artificial neural network (ANN) (developed by Kohonen (1997)) which identifies the hidden relationship between high dimensional data by mapping it onto a regular low-dimensional grid. One of advantages of the SOM is that missing data can be predicted based on the other data provided within the database. Using this property of the SOM, the values of the parameters for the normal femurs can be predicted. Like other ANN tools, the SOM also required the testing for the optimal conditions; the optimal grid size of the SOM had to be decided. This section therefore provides the method and results for testing the accuracy of the SOM application on normal knee parameter prediction. The optimal grid size was determined during the process so that the prediction best matched the actual values.

5.2.2 Materials and methods

Using the SOM toolbox developed for *Matlab*, the network was trained and then a prediction, with 28 input variable sets of the 15 normal femurs, was made. There are two types of input variables, namely dysplasia independent and dysplasia dependent variables. Dysplasia independent variables are parameters that did not show a statistically significant difference between the normal and abnormal groups (Table 5.3, Figure 5.8a), therefore, used as the input signal to search for appropriate values for dysplasia dependent variables. Dysplasia dependent variables are parameters affected by trochlear dysplasia; hence they were used to predict the normal geometry. The dysplasia independent variables were the medial-lateral (ML) distance, the distance between the measurement and the distal planes (MD), the angle between the distal and mechanical planes (DM) and the angle between the mechanical and anatomical planes (MA). The dysplasia dependent parameters were the radius and the anterior-posterior (AP) distance of the 9 slices, the centre plane location parameters (X-rotation, Z-rotation and Y-translation) and finally, the trochlear heights (lateral, middle, medial). The trochlear heights (Figure 5.8b) were measured to find out what caused the trochlear dysplasia: whether the trochlear is flattened due to the raised groove or the decreased facet heights.

Table 5.3: Statistical difference between normal and dysplastic groups

dysplasia independent parameter	student's t-test p value
measurement plane-distal plane distance (MD)	0.47
medial-lateral distance (ML)	0.27
angle between mechanical and anatomical axes (MA)	0.45
angle between distal and mechanical planes (DM)	0.36

**Figure 5.8: a) Trochlear dysplasia independent parameters b) Trochlear heights**

To test for the optimal grid size of the SOM, four dysplasia independent parameters and 24 dysplasia dependent parameters of 14 normal knees were used for training. Then, only the dysplasia independent parameters of the 15th normal knee were input to the SOM as the “test sample” to predict its values of the dysplasia dependent parameters. The prediction was made by comparing the input data with the best matching unit (BMU) of the trained dataset. The procedure was repeated to test all 15 knees, and the difference between the prediction and the actual data was recorded. This procedure (Figure 5.9) was repeated for the SOM grid size between 6x6 and 10x10.

The accuracy increased when the prediction was made separately for each of the four types of the dysplasia dependent parameters (location of the centre plane, radius, AP distance, and trochlear height) rather than predicting all the parameters together. Therefore the optimal grid size testing was done separately.

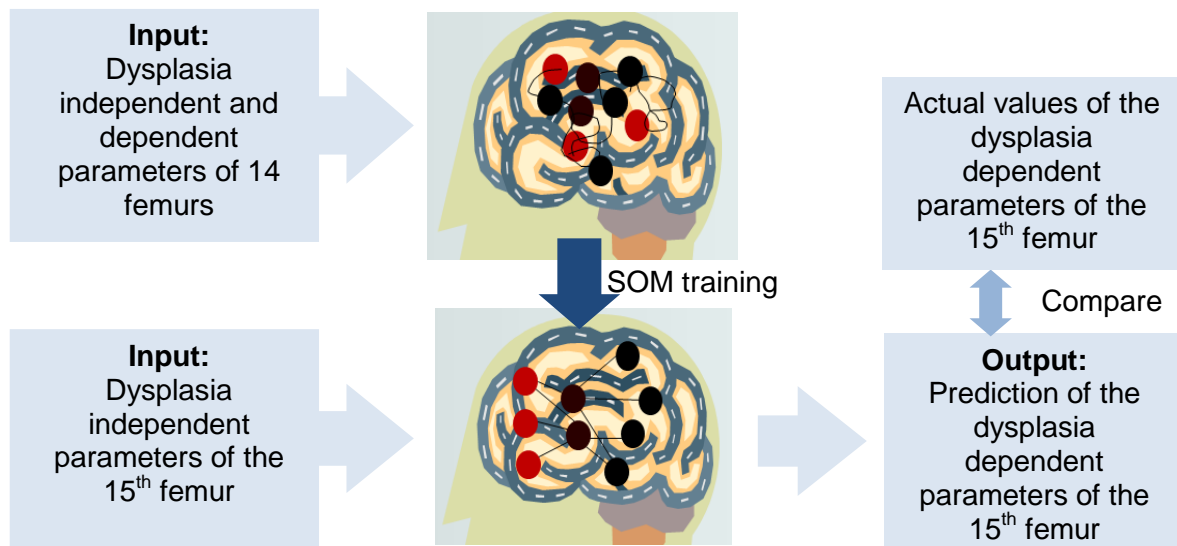


Figure 5.9: Schematic of testing normal geometry prediction method using Self-Organising Maps (SOM) for one sample

5.2.3 Results and discussion

The radius of the circular arcs and the AP distance were predicted with an average agreement of 88.4 % and 97.8 % at its given optimal grid size (Table 5.4). The average errors were 2.8 mm and 1.4 mm for the radius and AP distance respectively. The agreement between the predicted and the actual values of the plane location parameters and the trochlear heights was higher than 94.0 %, except for the X-rotation (46.5 % agreement Table 5.5). The error of the X-rotation prediction was 5°. This error changes the Y-coordinate of the centre points the most significantly on the sagittal slices lying furthest from the origin, i.e. L4 and M4 planes. The effect on the Y-coordinate was estimated with the length of an arc with a 12 mm radius and the angle of 5°, resulting 1.1 mm position change. The low agreement of the X-rotation can be due to the nature of the sample, which also showed a high variability, since its standard deviation was about 50 % of the mean value. With the grid size of 7x10, the X-rotation had a minimum agreement of 18.0 % showing that the prediction is greatly influenced by the selection of the SOM grid size (Table 5.5).

Table 5.4: Average % agreement between the measured and predicted values of radius and AP distance

parameter	grid size	slice plane									
		L1	L2	L3	L4	M1	M2	M3	M4	middle	mean
radius	max at 9x8	88.0	91.0	88.2	88.3	83.9	91.6	91.1	88.4	85.0	88.4
	min at 7x8	83.9	91.7	87.7	88.8	80.6	88.6	90.0	86.4	84.9	87.0
AP distance	max at 8x6	97.8	97.8	98.0	98.1	97.6	97.6	97.6	97.6	97.6	97.8
	min at 10x10	97.1	97.1	97.4	97.6	97.0	97.2	97.3	97.2	96.8	97.2

Table 5.5: Average % agreement between the measured and predicted values of location of plane and trochlear heights

location of the plane				trochlear heights			
grid size	X-rotation	Z-rotation	Y-translation	grid size	lateral	middle	medial
max at 10x6	46.5	95.6	94.2	max at 10x9	97.6	98.0	97.3
min at 7x10	18.0	95.0	94.1	min at 9x8	96.9	97.1	96.7

The pattern of the medial-lateral distance (ML) shows similar patterns to the AP distances (Figure 5.10) and the trochlear heights (Figure 5.11). This suggests a linear relationship, since the AP distances and the trochlear heights increase with an increase in the ML distance.

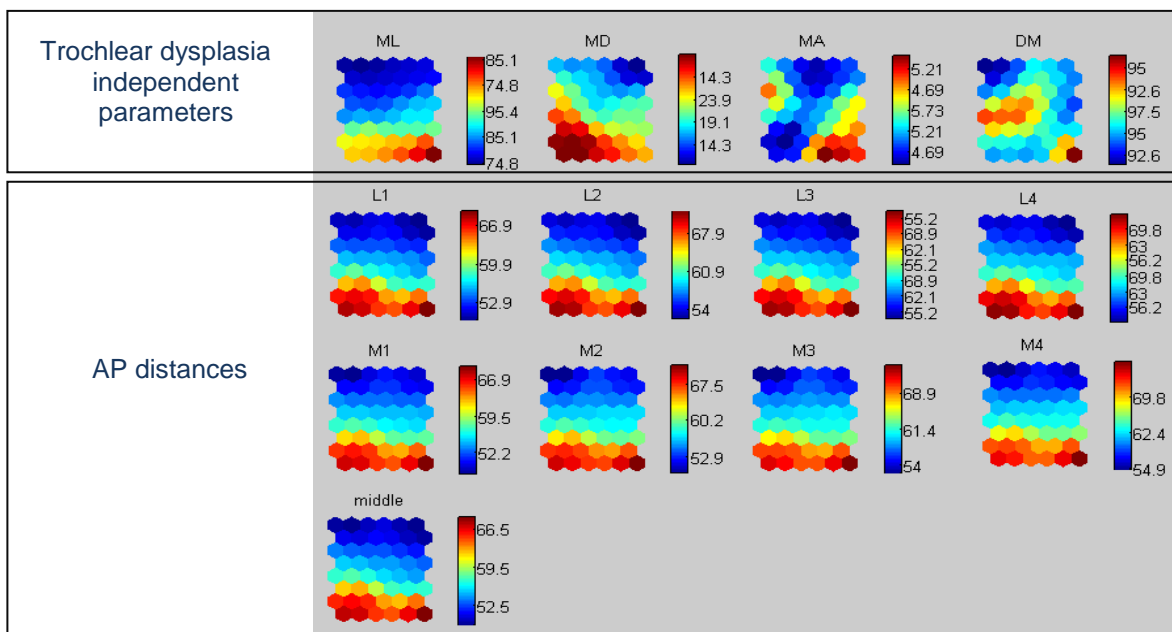


Figure 5.10: SOM pattern of the trochlear dysplasia independent parameters and anterior-posterior (AP) distances

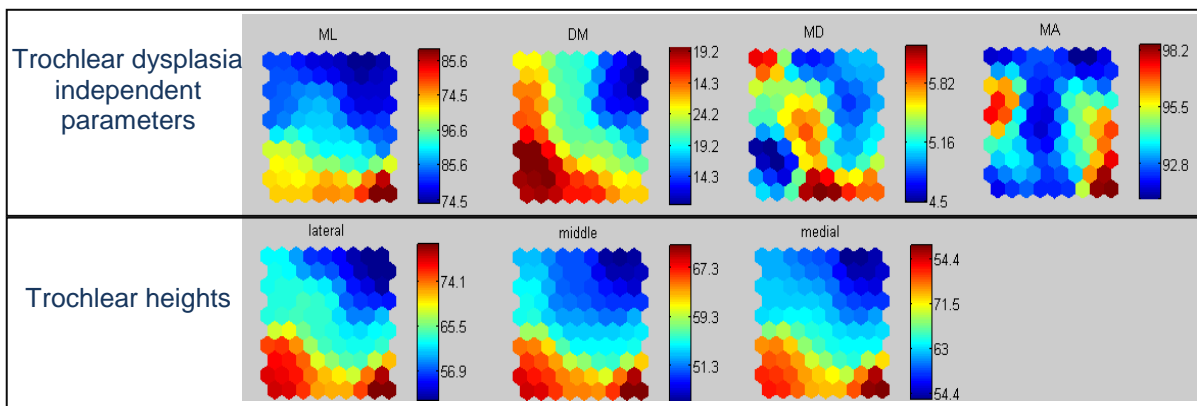


Figure 5.11: SOM pattern of the trochlear dysplasia independent parameters and the trochlear heights

The AP distances and the trochlear heights were shown to be the most reliably predicted parameters, having an average agreement higher than 97 %. These parameters determine the anterior shape of the trochlear groove. On the other hand, the radii and the location of the plane determine the distal shape of the trochlea and these parameters were predicted with less agreement (47 % – 96 %). This sums up that the proposed prediction method predicts the proximal geometry of the trochlear groove more accurately than the distal shape. This could be due to the variability in the distal shape of the normal femur models used for this research. The trochlear dysplasia classification was dependent on Dejour's method (2007) and it only identifies the high VTP or flattened trochlea which refers to proximal dysplasia, whereas Biedert et al. (2009) showed the existence of distal trochlear dysplasia which was characterised by a flat distal lateral condyle. This normal geometry prediction method using SOM can therefore only be used for predicting the normal geometry of the proximal trochlea.

With the resulted accuracy of the prediction tool in this validation, it was shown that the SOM can predict the anterior heights of the trochlea within an agreement level of 97 %. Although the prediction accuracy exceeded the required accuracy of 1 mm and 1°, it can still be used to predict the normal geometry for dysplastic knees to serve as a guideline for knee surgery planning. For example, this proposed method would be able to suggest that the sulcus needs to be deepened for a flat trochlea and indicate the approximate position of the normal sulcus, but would not be able to give an accurate number for it. As much as the numeric guideline could be useful to achieve an optimum result in knee surgeries, the surgeons usually have an estimation of the normal geometry while performing the surgery. Therefore a number may not be as necessary if a qualitative guideline (for example that the groove has to be deepened or the facet has to be elevated) is given. The accuracy of the prediction may be increased with an increased number of the samples in the database of the SOM.

5.3 Overview of the Normal Trochlear Geometry Analyses and Prediction

In this chapter, the sagittal shape of the anterior part of the 15 normal knees were analysed and it was reconfirmed that they were circular within 0.5 mm tolerance. The centre points of a femur were shown to be co-planar within the tolerance of 1 mm and this plane was defined as the centre plane. This observation led to a possibility that the centre points could be positioned using the location of the centre plane and the radius and AP distance of each sagittal slice. However, the rotation around the X-axis showed the highest variation,

having a standard deviation of 52 % of the mean value. Therefore, SOM was used to test the relationship between the parameters to determine whether training the SOM with the data of the normal knees would lead to a prediction of the values for the dysplastic knees.

The SOM prediction and the original data had the highest average agreement of 98.0 % (AP distance and trochlear height) and the lowest was 46 % (X-rotation of the centre plane) on their optimal grid size. The low agreement for the X-rotation could be ascribed to the high variability of distal geometry within the samples. This suggests that this proposed method for predicting the normal trochlea can be used as a guideline for the surgical treatment of proximal dysplasia, although an accurate quantification may be limited.

6 CASE STUDY: RECONSTRUCTION OF THE TROCHLEAR GROOVE OF THE DYSPLASTIC KNEES USING NEURAL NETWORKS

This chapter presents a case study of four femurs with varying degrees of trochlear dysplasia. These dysplastic knees were remodelled by means of the parameters predicted with self-organising maps (SOM) which utilised the database of the femoral parameter of the 15 normal knees. After the surfaces were remodelled, an appropriate type of trochleoplasty was suggested based on the femoral parameters and the changes to the geometry.

Three trochleoplasty procedures were considered in this case study: a lateral facet elevation, a sulcus deepening trochleoplasty and a sulcus depression trochleoplasty. A lateral facet elevation is less invasive and surgically less demanding, but it may result in an excessive trochlear prominence which increases the compression force between the patella and the femur (Dejour and Le Coultre, 2007). On the other hand, a sulcus deepening trochleoplasty results in proximal realignment without elevation although it might affect the congruency between the patella and trochlea. Also, the sulcus deepening procedure is more invasive and technically demanding than a lateral facet elevation. A depression trochleoplasty, with a retro trochlear wedge resection, can be performed on the knees with an excessive anterior trochlear prominence (supra trochlear spur) to decrease the instability of the patella (Goutallier et al., 2002). This procedure is technically less demanding and less invasive than a sulcus deepening trochleoplasty, while the congruency of the patella and femur is unaltered. It only decreases the prominence of the proximal trochlea and the sulcus angle is not changed.

6.1 Materials and Methods

Four dysplastic knees were remodelled (type A, B, C and D dysplasia according to the method proposed by Dejour et al. (2007)). The SOM was trained with the database of the parameters from the 15 normal knees. The dysplasia independent variables were then input to the trained SOM to predict the normal values of the dysplasia dependent variables of the dysplastic knees. Using the predicted values, the centre plane was created and it appeared as a line on the sagittal slices. The centre point of the circular arc was positioned on the centre plane using the AP distance and the radius. The predicted surface curve (the circular arc) was then drawn from the centre point, joining the rest of the surface curve (Figure 6.1). This procedure was done for all nine sagittal slices.

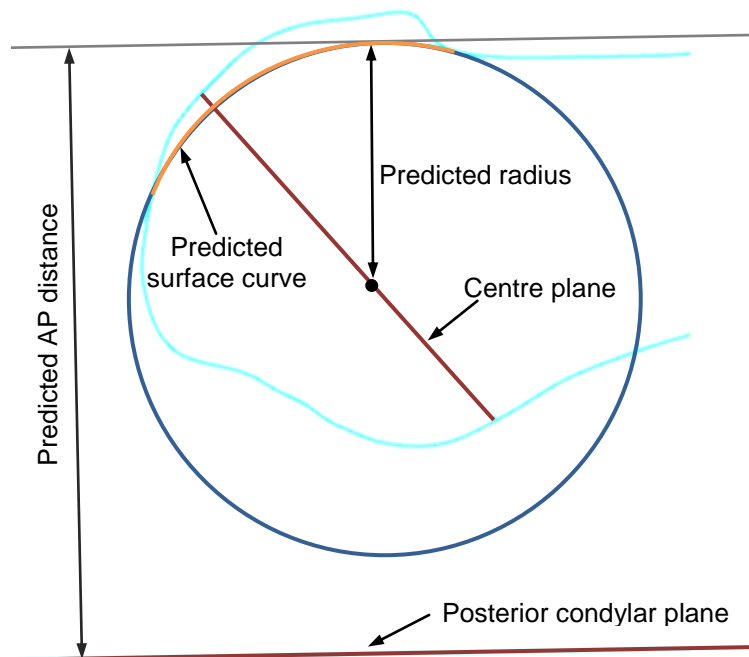


Figure 6.1: Sketch on a medial sagittal plane (M2) showing the prediction of the anterior portion using SOM estimation

The surface of the dysplastic femur was morphed to the nine predicted surface curves with the circular arcs on their anterior region to remodel the anterior femoral surface by using the morphing tool and smooth tool of *3-Matic*. The trochlear depth, VTP, sulcus angle, TFA, LTI and AP/ML ratios were measured before and after the remodelling procedure. The most appropriate trochleoplasty, i.e., a sulcus deepening, a facet elevation, or a retro-trochlear wedge procedure, was then identified.

6.2 Results and discussion of the Surface Prediction and Remodelling

After the trochlear groove remodelling, the femoral parameter measurements indicated that the trochlear geometry was restored to normal (Table 6.1). The mean trochlear depth was 5.5 mm (normal range > 5.4 mm) compared to the mean trochlear depth of 2.9 mm before the remodelling. The ventral trochlear prominence (VTP) was also corrected from an average value of 4.1 mm to a value of 0.0 mm (normal range < 3 mm), and the mean sulcus angle was corrected from 154° to 138° (normal range < 142°). The average LTI changed from 12.6° to 21.5°. The mean value of the trochlear facet asymmetry (TFA) was corrected from 55.1 % to 60.1 % (normal range > 40 %). Although no femur was classified as abnormal according to TFA with the given threshold (Section 2.3.1), it still showed a significant increase of 5 %.

The medial and the middle AP distances decreased after the trochlea surface was remodelled by 2.0 % and 4.4 % on average respectively, whereas the average change in lateral AP/ML was only 0.5 %. This result was consistent with Biedert et al. (2009) who showed a statistically significant difference in the middle and the medial AP/ML between the normal and abnormal groups, while no significant difference was shown for the lateral AP/ML. This illustrates that the raised groove and the medial facet is a more common cause of trochlear dysplasia rather than the lowered lateral trochlear facet.

Table 6.1: Key femoral parameters for dysplastic femurs before and after virtual surface reconstruction

type of femur	trochlear depth [mm]	VTP [mm]	sulcus angle [°]	TFA [%]	LTI [°]	lateral AP/ML [%]	middle AP/ML [%]	medial AP/ML [%]
dysplasia type A	2.5	1.8	155.2	39.0	13.7	80.5	73.5	75.8
corrected	4.7	0.0	140.2	59.1	19.6	80.1	71.5	76.8
dysplasia type B	4.1	3.2	148.0	69.9	10.6	81.4	76.9	83.2
corrected	5.6	0.0	139.0	65.9	20.5	81.4	71.6	77.9
dysplasia type C	2.7	5.4	150.7	35.1	14.5	80.7	73.6	76.3
corrected	6.3	0.0	132.9	58.1	26.6	80.2	67.4	73.3
dysplasia type D	2.2	5.9	163.4	76.2	11.7	77.7	72.5	73.8
corrected	5.5	0.0	140.5	57.1	19.5	76.6	68.2	73.1
mean(dysplastic)	2.9	4.1	154.3	55.1	12.6	80.1	74.1	77.3
mean(corrected)	5.5	0.0	138.1	60.1	21.5	79.6	69.7	75.3

The trochlear heights of all four dysplastic knees were measured and then compared to the values predicted by SOM. This was done to examine whether the height of the lateral trochlear facet should be changed as well, since the peak of the lateral facet was not included within the remodelled region (the remodelled region is highlighted in Figure 6.2).

The result indicated that the middle trochlear height had to be deepened by at least 3 mm in most cases, which is consistent with the middle AP/ML measurements. The medial trochlear height indicated that a decrease greater than 3 mm is needed for one femur and that the remodelling region covers the full medial facet. The peak of the lateral facet was not included in the remodelling region but the suggested changes based on the prediction were less than 1 mm for all four femurs, which can be considered as not significant (Table 6.2).

Table 6.2: Trochlear height difference between the measurement and the prediction

dysplasia type	the predicted trochlear height value is smaller than the original measurement by		
	x: less than 1 mm	-: between 1mm and 3 mm	- -: greater than 3 mm
	lateral	middle	medial
type A	x	-	x
type B	x	--	--
type C	x	--	x
type D	x	--	x

The anterior view of the dysplastic femur before and after the surface morphing was captured (Figure 6.2). The femurs had deeper grooves after the remodelling with decreased VTP and the groove orientation of the type B femur was also corrected from being more externally rotated than normal femurs. This shows that results from the SOM and the trochlear surface remodelling method can be used to predict and visualise the normal geometry of the dysplastic knees. Surgeons can use this to visualise the outcome of the surgery during the planning step.

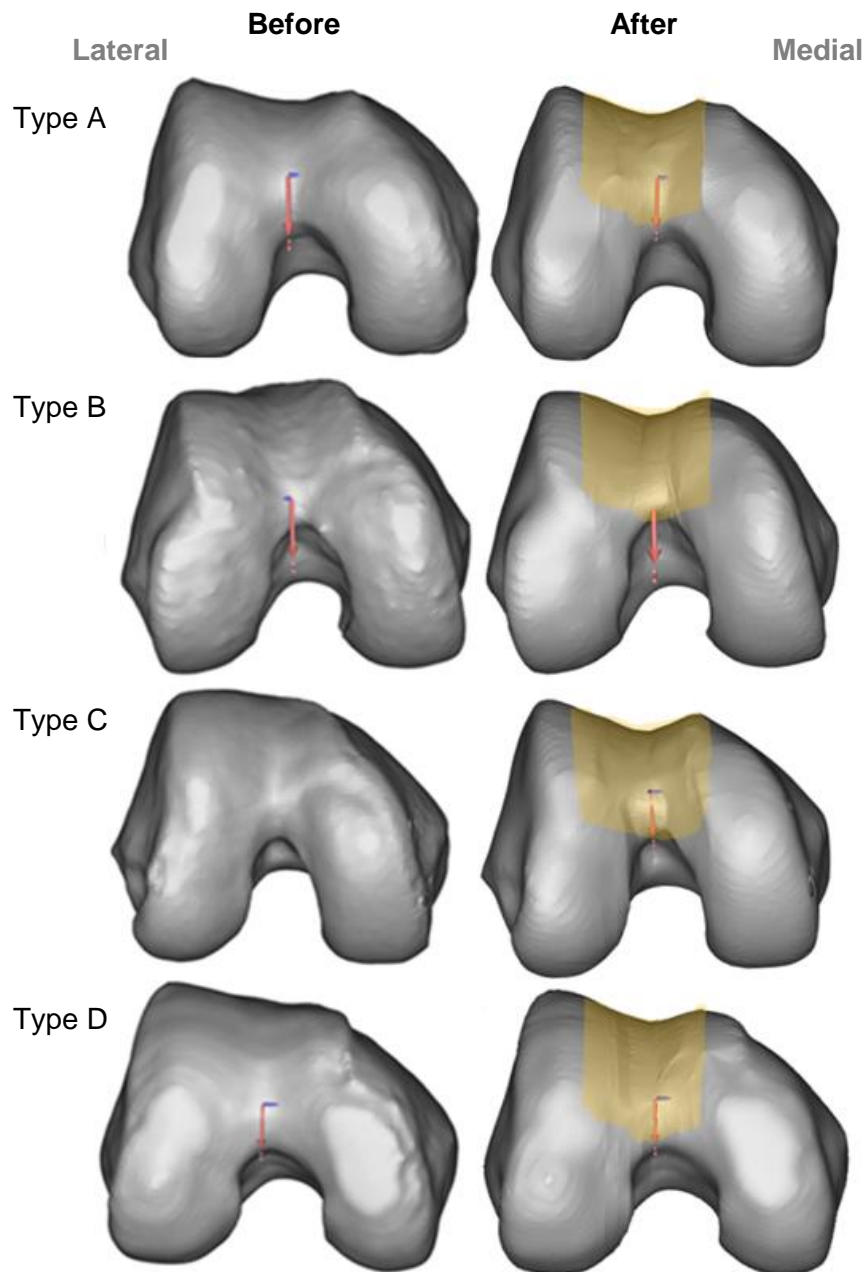


Figure 6.2: Anterior view of dysplastic femurs before and after surface remodelling

6.3 Clinical Suggestions and Trochleoplasty Selection

The four considered cases suggested that either a sulcus deepening or a sulcus depression trochleoplasty would be an appropriate option. The lowered lateral facet was not identified as the cause of trochlear dysplasia in this case study, but the raised groove and the medial facet were the key factors. This was demonstrated in the previous chapter (Section 6.2) by comparing the measured and the predicted values of the trochlear heights, which suggested less than 1 mm change on the lateral trochlear height. This result was consistent with the findings that lateral AP/ML ratio change was significantly less than the decrease in medial and the middle AP/ML ratios after the surface remodelling. To summarise, a lateral facet elevation was not suggested because the prediction indicated that the lateral trochlear height should not be raised, but the groove should rather be deepened. An elevation of the lateral facet is not advised as it will induce excessive pressure between the femur and the patella.

For the type A femur, trochleoplasty was considered to be not appropriate since its ventral trochlea prominence (VTP) was within the normal range. The geometrical change of this femur was not significant when the anterior view before and after the remodelling was observed (Figure 6.2), in spite of the trochlear depth (2.5 mm) and the sulcus angle (155.2°). Trochleoplasty was therefore not a suitable treatment for this type because of its invasive nature. A medial patellofemoral ligament (MPFL) reconstruction with or without tibial tubercle osteotomy may be a more suitable and effective treatment strategy, depending on the patellar alignment and the laxity of the MPFL. Suggesting a soft tissue realignment procedure is, however, outside the scope of this study.

The type B femur had TFA within the normal range (69.9 %) but the sulcus angle (148°) and the trochlear depth (4.1 mm) values were within abnormal range. However it had the deepest groove depth and the smallest sulcus angle amongst the four dysplastic knees. Also, the type B femur is the only one with the medial trochlear height higher than the lateral height. This can be corrected by taking out a wedge which is thicker on its medial side than the lateral side, performing a depression trochleoplasty. The VTP and LTI and the orientation of the groove can also be restored as a result, while keeping the sulcus angle and the trochlear depth unaltered. Although depression trochleoplasty would result in decreased AP distances, this procedure is less invasive than the sulcus deepening.

All the parameters were within the abnormal range for the type C and D femurs, except for the LTI (14.5°) of the type C femur and the TFA (76.2 %) of the type D femur.

These knees had lower trochlear depth (< 3 mm) and higher sulcus angle (> 150°) than the type B femur. The VTP values of the type C and D femurs are higher than that of the type B femur - these femurs could therefore be suitable candidates for depression trochleoplasty if the groove geometry was less flattened. Hence a sulcus deepening was suggested for both type C and D since the trochlear depth and the sulcus angle cannot be changed with a depression trochleoplasty. Although a sulcus deepening is a more invasive procedure than a depression method, a sulcus deepening can reshape the femoral trochlea to match the predicted normal AP distances, whereas depression trochleoplasty results in decreased AP distances (Table 6.3).

The effect of a trochlear depression procedure on the femur with a severe degree of dysplasia (type D) was examined by performing a virtual depression trochleoplasty. The AP distances were decreased (light blue lines in Figure 6.3 show the predicted surface) as a result of the depression trochleoplasty but it effectively corrected the proximal shape of the femur by correcting the VTP (Figure 6.3). If the absolute AP distances of a femur are not important, this procedure is suitable for knees with a severe degree of dysplasia, because it is technically less demanding and a less invasive method than deepening trochleoplasty. However, the relationship between the function of the patellofemoral joint and its AP distances were not studied sufficiently enough to draw a conclusion at the current stage. Nevertheless, it is important to note that Biedert et al. (2009) have previously shown the significance of the AP/ML ratio, which was reconfirmed by the findings of this study (Section 5.2). This illustrates a possibility for having a normal range of the trochlear heights or the AP distances for the given ML distance, i.e. size of the knee.

Table 6.3: Femoral parameters before and after the virtual depression trochleoplasty

type of femur	trochlear depth [mm]	VTP [mm]	sulcus angle [°]	TFA [%]	LTI [°]	medial AP/ML [%]	middle AP/ML [%]	lateral AP/ML [%]
dysplasia type D	2.2	5.9	163.4	76.2	11.7	73.8	72.5	77.7
corrected with depression trochleoplasty	2.5	0.0	161.5	70.8	10.9	71.2	69.3	73.3

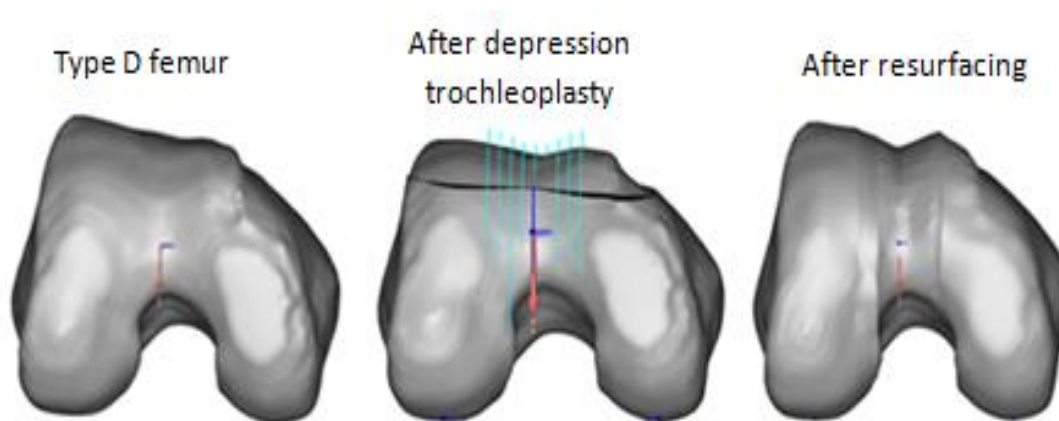


Figure 6.3: The anterior view of type D dysplastic femur before and after virtual trochleoplasty (the light blue lines show the guidelines for the surface morphing)

Another drawback of a depression trochleoplasty is that it does not change the sulcus angle and trochlear depth (Table 6.3), the latter which was shown to be the most appropriate parameter for identifying trochlear dysplasia, followed by the sulcus angle (Chapter 4). Therefore, a depression trochleoplasty would be the most appropriate procedure for knees with a congruent patella and femur with the normal values of the trochlear depth and sulcus angle with the supra trochlear spur. On the other hand the sulcus deepening can correct the alignment and congruency of the patella and the femur, and is therefore more appropriate for the femurs with a higher degree of dysplasia and with an incongruent patella and femur set. Jafaril et al. (2008) demonstrated that deepened trochlear grooves make the patella more stable and medialise the patella even when the geometry of the patella is unchanged. This finding supports the theory that a change in the geometry of the trochlear groove (while the geometry of the patella is unaltered), strengthens its role in stabilising the patella.

6.4 Overview of the Case Study

This case study demonstrated that the normal geometry of knees with trochlear dysplasia could be predicted by using the database of SOM consisting of the femoral parameters of the normal knees. The predicted normal geometry was reconstructed on the four dysplastic femur models. Appropriate surgical methods were recommended for each type of dysplasia by comparing the femoral parameter measurements on the original and the remodelled femurs, as well as visually examining them.

A virtual depression trochleoplasty was performed to demonstrate an application of the three-dimensional model modifications. This enables the surgeons to postulate the result of knee surgeries. The visualisation of the result prior to surgery decreases the chance that

an inappropriate surgical procedure is chosen by a surgeon, and therefore the possibility of serious complications and surgical revision are limited.

7 CONCLUSIONS

This chapter lists the major findings and the conclusions of this study. It then focuses on the clinical aspect of this study, which is followed by the limitations and the future work for further improvements.

7.1 Summary of Methods in Context of the Literature Study

7.1.1 Three-dimensional model generation

For the purpose of this thesis three-dimensional computer models were generated from CT scans using the same technique described by Muller et al. (2010). The same commercial software packages (*Mimics*, Materialise, Leuven, Belgium) were also used.

7.1.2 Reference framework

Iranapour et al. (2010b) aligned the femur with the reference plane, generated by connecting the sphere centres that were fit to the medial and lateral condyles, and the femoral head. They defined the trochlear axis as the line joining the centres of two spheres fit to the each side of the articulating surfaces on the trochlea. Iranapour et al. (2010a; 2010b) showed that the circular path of the trochlear groove is aligned with the trochlear axis. The mechanical axis is also aligned closely with the trochlear groove on the coronal plane. The alignment between the trochlear axis and the posterior condylar axis was not examined. Eckhoff et al. (2001) showed that the groove is positioned between anatomical and mechanical axes on the coronal plane and it is perpendicular to the posterior condylar axis. This also confirms that the groove is circular when viewed on the sagittal plane. Both authors investigated the osseous geometry only.

Considering the results obtained by both authors, this study analysed the sagittal shape of the trochlear groove, aligned with the mechanical axis and perpendicular to the posterior condylar axis. The femur was aligned using the anatomical axis which was generated by fitting a cylinder to the femoral shaft. The trochlear axis was not used because the sphere fitting is dependent on selecting the fitting region on the facets of the trochlea, which do not have a full spherical shape. This means that the procedure cannot not be easily standardised.

An advantage of the framework used for this thesis is that a coordinate system was developed. Another advantage is that identification of the posterior condyles and the femoral

shaft is relatively easier than defining the trochlear axis by identifying the spherical region of the distal trochlea. Afore mentioned studies analysed only the deepest path of the groove whereas this study generated multiple sagittal slices to analyse the shape of the medial and lateral facets of the trochlea as well.

7.1.3 Parameter measurement

The measurement planes are defined on the CT or MR scans and the four different selection methods are commonly used amongst the previous studies (refer to section 2.3). This study uses three-dimensional computer models to generate the measurement plane once it is properly aligned. This method is more repeatable than taking measurements on CT and MR images because the measurement is not affected by the alignment and knee flexion of the femur during the scanning.

7.1.4 Sagittal curve analysis method

The sagittal curves were analysed using B-splines. A method similar to the one of Kosel et al. (2010), who analysed the curvature of the distal femoral condyles, was used. This study fixed the number of the control points to five and this simplified the analysis. The tolerance level was set at 0.3 mm. Kosel et al. (2010) plotted the centres of the curvature of the B-splines to show that the condyles are not circular in shape. This study used the centre of the curvatures, by comparing it to the centre of the circles fit to the original data points, to identify the circular region.

7.1.5 Artificial neural networks (ANN)

Cloete (2009) classified the normal and abnormal gait using artificial neural networks (ANN). Three different training functions based on Levenberg-Marquardt optimization, the back propagation method and variable learning rate gradient decent algorithm were tested for their accuracy where after the Levenberg-Marquardt method was selected. Using the same methods, this study identified the femurs with trochlear dysplasia and the normal knees by training the network with the Levenberg-Marquardt optimisation function.

ANN can also be applied to the selection of the correct size of a prosthesis by feeding the size of the patient's knee into a self-organising maps (SOM) (a type of ANN) in order to predict the normal size (Van den Heever et al., 2011; Van Schalkwyk, 2010). Van Schalkwyk (2010) used a 10x10 grid size with a database of 12 parameters of 24 healthy knees whereas Van den Heever et al. (2011) used a 35x9 grid size which corresponds to 35

samples and 9 parameters. None of these researchers tested the accuracy of the different grid sizes because it is not critical for selecting the prosthesis size. However, the effect of the grid size had to be tested in this study of which the aim is to predict the normal geometry as accurately as possible.

7.2 Summary of Outcomes and Major Conclusions

7.2.1 Standardised three-dimensional model measurement system

A standardised femoral parameter measurement system on three-dimensional femoral models was established. By performing the measurements on three-dimensional models, the measured values can be measured and compared in a more repeatable manner since it is not affected by the alignment of the femur during the scanning as opposed to measuring on X-rays, CT and MR images. The standard deviation of the sulcus angle measurement on a CT scan was 2.25 times higher than the standard deviation of the sulcus angle measured on a three-dimensional model (Appendix G).

The accuracy of the segmentation technique from CT scans was 99.7 % for creating three-dimensional models. The level of the measurement accuracy was about 1 mm and 1°, which is comparable to the surgical equipment tolerance level. A repeatability and reproducibility (R&R) test showed that the established femoral parameter measurement system framework has an excellent reliability.

7.2.2 Trochlear dysplasia identification

An artificial neural network (ANN) was employed to match the qualitative classification made by surgeons and the qualitative femoral parameter measurements to identify the femurs with trochlear dysplasia and the normal femurs. The agreement between the ANN and the surgeons' classification was 80.6 % in comparison to the agreement within the surgeons' classification of 69.4 %, showing that ANN can be used as an objective tool which incorporated the surgeons' decisions and the numerical data.

Three femoral parameters which are appropriate for identifying trochlear dysplasia were suggested with the new threshold: trochlear depth (< 5.4 mm), sulcus angle (> 142°), and middle AP/ML (> 0.7). The mean sensitivity and the specificity were improved by 3 % and 12 % respectively.

7.2.3 Normal geometry

Nine sagittal slices were created on each femur and the sagittal shape of a normal trochlea was shown to be circular arcs with the maximum angle 40° and the maximum of 90° within a tolerance of 0.5 mm. The centre points of the circular arcs were shown to be not collinear but coplanar. The groove was aligned with the mechanical plane, which is parallel to the mechanical axis and perpendicular to the posterior condylar axis.

A linear relationship between the medial-lateral (ML) distance and the anterior-posterior (AP) distance was observed and was shown to be a reliable guide line for predicting the normal geometry with an agreement level higher than 97 %. The peak of the lateral facet (lateral trochlear height) was measured on four dysplastic knees and the normal values were predicted with self-organising maps (SOM) and the difference between the measurement and the prediction was less than 1 mm for all four knees. On the other hand, the predicted values were significantly lower than the measured values for the middle and the medial trochlear heights. This illustrates a possibility that trochlear dysplasia is caused by a raised groove rather than a lowered lateral facet.

7.3 Clinical Applications

7.3.1 Prosthesis design

A good patellofemoral arthroplasty (PFA) prosthesis design should replicate the normal geometry of the trochlea, and the findings of this study suggest it should have the following characteristics:

- a circular sagittal shape;
- asymmetrical in medial-lateral direction (trochlear facet asymmetry is not 100 % for normal knees);
- aligned in a way that the mechanical axis is parallel to the sagittal plane;
- the AP height is appropriately positioned with the corresponding ML distance (the suggested values for the medial AP/ML is 70 %);
- the lateral facet should be higher than the medial facet;
- the trochlear depth should be greater than 5.4 mm; and

- the lateral trochlear facet inclination (LTI) should be greater than 142° .

7.3.2 Surgical planning

On the four dysplastic knees, of which each represents each of the four trochlear dysplasia types, the normal trochlea geometry was predicted with the SOM. Then the surface of the trochlea was remodelled to the predicted normal geometry to visualise the normal shape. A type of trochleoplasty was selected for each femur by comparing the geometry of the trochlea before and after the remodelling. The remodelled surface could visualise the effect of the deepening trochleoplasty and can give a feel for the surgeons by how much the bone has to be removed and where. A lateral facet elevation trochleoplasty was not suggested for any of the four knees because the SOM prediction suggested that the peak of the lateral facet did not have to be increased, instead, it suggested that the height of the groove (middle trochlear height) had to be lowered. In order to decrease the height of the groove, either a deepening or a depression trochleoplasty was suggested.

Both a depression and a deepening trochleoplasty were performed on the type D femur and the result of the two different procedures was compared visually. It illustrated that the outcomes of different types of trochleoplasty can be visualised prior to the surgical intervention. This should help surgeons to select the most appropriate procedure and plan the knee surgery better.

7.4 Limitations and Future Work

7.4.1 Number of the samples

This study only had 36 samples, which included 15 normal femurs. The sample size was not big enough to examine the morphological difference between the age, sex, the severity and the type trochlear dysplasia, and therefore, only considered the presence of proximal dysplasia. With more of the samples categorised into type A, B, C and D trochlear dysplasia by surgeons due to its severity, the artificial neural network (ANN) can also classify the knees into different types of the dysplasia.

The presence of the distal dysplasia can be examined by the surgeons and it is anticipated that the angle between the mechanical and the distal planes (DM) should have significant difference between the groups with and without distal dysplasia. Again, this can potentially be identified with the ANN if more samples are provided and the same applies to

identification of the morphological differences according to the gender and the age. The accuracy of the SOM prediction can also be increased as a result of the sample size.

7.4.2 Cartilaginous geometry of the trochlea

This study segmented the femoral models from the CT scans, which visualise the osseous geometry well, but not the soft tissues. For this reason, the cartilaginous geometry could not be analysed which reflects the true articulating geometry. As a future study, the three-dimensional cartilaginous geometry can be analysed using models segmented from MR images, which visualise the soft tissues better than CT scans.

7.4.3 Relative patellar position and geometry to the femur

The congruency between the trochlea and the patella and the relative position of the patella to the femur for the normal and abnormal knees were not studied. The reason being that the position of the femur is sensitive to the flexion angle and quadriceps muscle activation, and this information was unavailable. Some studies (Grelsamer et al., 2008; Insall et al., 1983) however illustrated that the normal knees have more congruent patella and femur set than abnormal knees. Therefore, as a future study, patellofemoral parameters such as the patella tilt and the patella height can be added to the measurements set to examine the location of the patella at a known knee flexion angle with and without the muscle activation. This should provide the information regarding the role of the soft tissues and the muscles in their roles for stabilising the patella. With this information available, surgeons can decide which soft tissue realignment procedure is indicated. For example, if a type A dysplasia knee has a recurrent lateral patellar dislocation, a medial patellofemoral ligament (MPFL) reconstruction would be an appropriate procedure. Depending on the alignment and height of the patella, a tubercle osteotomy can also be considered. Therefore the relative position between the patella and the femur can be added to future studies.

7.4.4 Alignment of the lower limb

The relationship between the geometry of the patellofemoral joint and the alignment of the lower limb was not studied. The alignment is affected by the internal-external rotation of the knee and the foot and no data was available regarding the alignment and the position of the feet and the knee.

The relationship between the geometry of the patellofemoral joint and the alignment of the lower limb can be studied with the scans of the lower limb at a fixed position and

rotation of the feet and the knee. In this way, the mechanics of the lower body and the knee function and its geometry can be studied.

8 REFERENCES

- Amis, A. A., Firer, P., Mountney, J., Senavongse, W., Thomas, N. P., 2003. Anatomy and biomechanics of the medial patellofemoral ligament. *The Knee* 10, 215-220.
- Asano, T., Akagi, M., Nakamura, T., 2004. The functional flexion-extension axis of the knee corresponds to the surgical epicondylar axis, In vivo analysis using a biplanar image imagematching. *The Journal of Arthroplasty* 20, 1060 – 1067.
- Balcarek, P., Jung, K., Ammon, J., Walde, T. A., Frosch, S., Schuttrumpf, J. P., Sturmer, K. M., Frosch, K. H., 2010. Anatomy of lateral patellar instability: trochlear dysplasia and tibial tubercle-trochlear groove distance is more pronounced in women who dislocate the patella. *Am J Sports Med* 38, 2320-7.
- Balcarek, P., Walde, T. A., Frosch, S., Schuttrumpf, J. P., Wachowski, M. M., Sturmer, K. M., Frosch, K. H., 2011. Patellar dislocations in children, adolescents and adults: a comparative MRI study of medial patellofemoral ligament injury patterns and trochlear groove anatomy. *Eur J Radiol* 79, 415-20.
- Barrentine, L. B., 2002. Concepts for R&R studies. American Society for Quality, .
- Baxt, W. G., 1990. Use of an artificial neural network for data analysis in clinical decision-making: the diagnosis of acute coronary occlusion. *Neural Comput* 2, 480-489.
- Beaufils, P., Thauinat, M., Pujol, N., Scheffler, S., Rossi, R., Carmont, M., 2012. Trochleoplasty in major trochlear dysplasia: current concepts. *Sports Medicine, Arthroscopy, Rehabilitation, Therapy & Technology : SMARTT* 4, 7.
- Berger, R. A., Rubash, H. E., Seel, M. J., Thompson, W. H., Crossett, L. S., 1993. Determining the rotational alignment of the femoral component in total knee arthroplasty using the epicondylar axis. *Clinical Orthopaedics and Related Research* 286, 40-47.
- Biedert, R., Sigg, A., Gal, I., Gerber, H., 2011. 3D representation of the surface topography of normal and dysplastic trochlea using MRI. *The Knee* 18, 340-346.
- Biedert, R. M., Bachmann, M., 2009. Anterior-posterior trochlear measurements of normal and dysplastic trochlea by magnetic resonance imaging. *Knee Surgery and Sports Traumatol Arthroscopy* 17, 1225-1230.
- Birrer, R. B., O'Connor, F. G., 2004. Sports medicine for the primary care physician. CRC press.
- Carrillon, Y., Abidi, H., Dejour, D., Fantino, O., Moyon, B., Tran-Minh, V. A., 2000. Patellar instability: Assessment on MR Images by measuring the lateral trochlear inclination-initial experience. *Radiology* 216, 582-585.
- Christoforakis, J., Bull, A. M., Strachan, R. K., Shymkiw, R., Senavongse, W., Amis, A. A., 2006. Effects of lateral retinacular release on the lateral stability of the patella. *Knee Surgery, Sports Traumatology, Arthroscopy : Official Journal of the ESSKA* 14, 273-277.

- Cloete, T., 2009. Benchmarking full-body inertial motion capture for clinical gait analysis. MSc Thesis. University of Stellenbosch.
- Cooke, T. D., Sled, E. A., Scudamore, R. A., 2007. Frontal plane knee alignment: a call for standardized measurement. *The Journal of Rheumatology* 34, 1796-1801.
- Davies, A. P., Vince, A. S., Shepstone, L., Donell, S. T., Glasgow, M. M., 2002. The Radiologic Prevalence of Patellofemoral Osteoarthritis. *Clin Orthop* 402, 206-212.
- Dejour, D., Le Coultre, B., 2007. Osteotomies in patello-femoral instabilities. *Sports Medicine and Arthroscopy Review* 15, 39-46.
- Dejour, H., Walch, G., Neyret, P., Adeleine, P., 1990. Dysplasia of the femoral trochlea. *Revue De Chirurgie Orthopedique Et Reparatrice De l'Appareil Moteur* 76, 45-54.
- Dejour, H., Walch, G., Nove-Josserand, L., 1994. Factors of patellar instability: an anatomic radiographic study. *Knee Surg, Sports Traumatol, Arthroscopy* 2, 19-26.
- D'Lima, D. D., Chen, P. C., Kester, M. A., Colwell, C. W., 2003. Impact of patellofemoral design on patellofemoral forces and polyethylene stresses. *Journal of Bone and Joint Surgery*, 85-93.
- Donell, S. T., Glasgow, M. M. S., 2007. Isolated patellofemoral osteoarthritis. *The Knee* 14, 169-176.
- Duda, P. O., Hart, P. E., 1973. *Pattern classification and scene analysis*. Wiley, New York, .
- Eckhoff, D. G., Dwyer, T. F., Bach, J. M., Spitzer, V. M., Reinig, K. D., 2001. Three-dimensional morphology of the distal part of the femur viewed in virtual reality. *The Journal of Bone and Joint Surgery.American Volume* 83-A Suppl 2, 43-50.
- Enderle, J. D., Blanchard, S. M., Bronzino, J. D., 2005. *Introduction to biomedical engineering*. Elsevier Academic Press, California, USA.
- Escala, J. S., Mellado, J. M., Olona, J. M., Gine, M., Sauri, A., Neyret, P., 2006. Objective patellar instability: MR-based quantitative assessment of potentially associated anatomical features. *Knee Surg, Sports Traumatol, Arthroscopy* 14, 264-272.
- Farahmand, F., Senavongse, W., Amis, A. A., 1998. Quantitative study of the quadriceps muscles and trochlear groove geometry related to instability of the patellofemoral joint. *Journal of Orthopaedic Research : Official Publication of the Orthopaedic Research Society* 16, 136-143.
- Farr, J., 2nd, Barrett, D., 2008. Optimizing patellofemoral arthroplasty. *The Knee* 15, 339-347.
- Feller, J. A., Amis, A. A., Andrish, J. T., Arendt, E. A., Erasmus, P. J., Powers, C. M., 2007. Surgical biomechanics of the patellofemoral joint. *Arthroscopy : The Journal of Arthroscopic & Related Surgery : Official Publication of the Arthroscopy Association of North America and the International Arthroscopy Association* 23, 542-553.

Fucentese, S. F., Schottle, P. B., Pfirrmann, C. W., Romero, J., 2007. CT changes after trochleoplasty for symptomatic trochlear dysplasia. *Knee Surg Sports Traumatol Arthrosc* 15, 168-74.

Goutallier, D., Raou, D., Van Driessche, S., 2002. Retro-trochlear wedge reduction trochleoplasty for the treatment of painful patella syndrome with protruding trochleae. Technical note and early results. *Revue De Chirurgie Orthopedique Et Reparatrice De l'Appareil Moteur* 88, 678-685.

Grelsamer, R. P., Weinstein, C. H., Gould, J., Dubey, A., 2008. Patellar tilt: the physical examination correlates with MR imaging. *The Knee* 15, 3-8.

Griffin, F. M., Math, K., Scuderi, G. R., Insall, J. N., Poilvache, P. L., 2000. Anatomy of the epicondyles of the distal femur, MRI analysis of normal knees. *The Journal of Arthroplasty* 15, 354-359.

Henry, J. H., Goletz, T. H., Williamson, B., 1986. Lateral retinacular release in patellofemoral subluxation. Indications, results, and comparison to open patellofemoral reconstruction. *The American Journal of Sports Medicine* 14, 121-129.

Insall, J. N., Aglietti, P., Tria, A. J., Jr, 1983. Patellar pain and incongruence. II: Clinical application. *Clinical Orthopaedics and Related Research* (176), 225-232.

Iranpour, F., Merican, A. M., Baena, F. R., Cobb, J. P., Amis, A. A., 2010a. Patellofemoral joint kinematics: the circular path of the patella around the trochlear axis. *Journal of Orthopaedic Research : Official Publication of the Orthopaedic Research Society* 28, 589-594.

Iranpour, F., Merican, A., Dandachli, W., Amis, A. A., Cobb, J. P., 2010b. The Geometry of the Trochlear Groove. *Clinical Orthopaedics and Related Research* 468, 782-788.

Jafaril, A., Farahmand, F., Meghdari, A., 2008. The effects of trochlear groove geometry on patellofemoral joint stability--a computer model study. *Proceedings of the Institution of Mechanical Engineers. Part H, Journal of Engineering in Medicine* 222, 75-88.

Juhn, M. S. M., 1999. Patellofemoral pain syndrome: a review and guidelines for treatment. *American Family Physician* 60, 2012-2022.

Katchburian, M. V., Bull, A. M., Shih, Y. F., Heatley, F. W., Amis, A. A., 2003. Measurement of patellar tracking: assessment and analysis of the literature. *Clinical Orthopaedics and Related Research* (412), 241-259.

Keser, S., Savranlar, A., Bayar, A., Ege, A., Turhan, E., 2008. Is there a relationship between anterior knee pain and femoral trochlear dysplasia? Assessment of lateral trochlear inclination by magnetic resonance imaging. *Knee Surgery, Sports Traumatology, Arthroscopy* 16, 911-915.

Kohonen, T., 1997. *Self-Organizing Maps*.

Kosel, J., Giouroudi, I., Scheffer, C., Dillon, E., Erasmus, P., 2010. Anatomical study of the radius and center of curvature of the distal femoral condyle. *Journal of Biomechanical Engineering* 132, 091002.

- Kulkarni, S. K., Freeman, M. A. R., Poal-Manresa, J. C., Asencio, J. I., Rodriguez, J. J., 2000. The patellofemoral joint in total knee arthroplasty: Is the design of the trochlea the critical factor? *The Journal of Arthroplasty* 15, 424-429.
- Lattermann, C., Toth, J., Bach, B. R., Jr, 2007. The role of lateral retinacular release in the treatment of patellar instability. *Sports Medicine and Arthroscopy Review* 15, 57-60.
- Luo, C. F., Koshino, T., Takeuchi, R., Saito, T., 2001. Reliability of the transepicondylar line as a parameter of femoral axial alignment. *Journal of Orthopaedic Science : Official Journal of the Japanese Orthopaedic Association* 6, 373-377.
- Luo, C., 2004. Reference axis for reconstruction of the knee. 11, 251-257.
- Lustig, S., Lavoie, F., Selmi, T. A., Servien, E., Neyret, P., 2008. Relationship between the surgical epicondylar axis and the articular surface of the distal femur: an anatomic study. *Knee Surgery, Sports Traumatology, Arthroscopy : Official Journal of the ESSKA* 16, 674-682.
- Martinez, S., Korobkin, M., Fondren, F. B., Hedlund, L. W., Goldner, J. L., 1983. Computed tomography of the normal patellofemoral joint. *Investigative Radiology* 18, 249-253.
- Martino, F., De Serio, A., Macarini, L., Rizzo, A., Laforgia, R., Rotondo, A., Angelelli, G., 1998. Ultrasonography versus computed tomography in evaluation of the femoral trochlear groove morphology: a pilot study on healthy, young volunteers. *European Radiology* 8, 244-247.
- Mdlazi, L., Marwala, T., Stander, C. J., Scheffer, C., Heyns, P. S., 2007. Principal component analysis and automatic relevance determination in damage identification. *CoRR abs/0705.1672*.
- Merchant, A. C., 1988. Classification of patellofemoral disorders. *Arthroscopy: The Journal of Arthroscopic & Related Surgery* 4, 235-240.
- Miller, M. C., Berger, R. A., Petrella, A. J., Karmas, A., Rubash, H. E., 2001. Optimizing femoral component rotation in total knee arthroplasty. *Clinical Orthopaedics and Related Research* (392), 38-45.
- Moreland, J. R., Bassett, L. W., Hanker, G. J., 1987. Radiographic analysis of the axial alignment of the lower extremity. *The Journal of Bone and Joint Surgery.American Volume* 69, 745-749.
- Muller, J. H., Scheffer, C., Erasmus, P. J., Dillon, E. M., Elvin, A., 2010. Comparison of two commercial patellofemoral prostheses by means of computational modeling. *Conference Proceedings : ...Annual International Conference of the IEEE Engineering in Medicine and Biology Society.IEEE Engineering in Medicine and Biology Society.Conference 2010*, 5105-5108.
- O'Neill, D. B., 1997. Open Lateral Retinacular Lengthening Compared with Arthroscopic Release. A Prospective, Randomized Outcome Study*. *The Journal of Bone & Joint Surgery* 79, 1759-69.

Pfirschmann, C. W. A., Zanetti, M., Romero, J., Hodler, J., 2000. Femoral trochlear dysplasia: MR findings. *Radiology* 216, 858-864.

Piegl, L. A., 1997. *The NURBS book*. Springer, Berlin ; London, .

Salzmann, G. M., Weber, T. S., Spang, J. T., Imhoff, A. B., Schottle, P. B., 2010. Comparison of native axial radiographs with axial MR imaging for determination of the trochlear morphology in patients with trochlear dysplasia. *Archives of Orthopaedic and Trauma Surgery* 130, 335-340.

Senavongse, W., Amis, A. A., 2005. The effects of articular, retinacular, or muscular deficiencies on patellofemoral joint stability: a biomechanical study in vitro. *The Journal of Bone and Joint Surgery*. British Volume 87, 577-582.

Sikorski, J. M., 2008. Alignment in total knee replacement. *Journal of Bone Joint Surgery [Br]* 90b, 1121-1127.

Teichtahl, A. J., Parkins, K., Hanna, F., Wluka, A. E., Urquhart, D. M., English, D. R., Giles, G. G., Cicuttini, F. M., 2007. The relationship between the angle of the trochlear groove and patella cartilage and bone morphology--a cross-sectional study of healthy adults. *Osteoarthritis and Cartilage / OARS, Osteoarthritis Research Society* 15, 1158-1162.

Utting, M. R., Davies, G., Newman, J. H., 2005. Is anterior knee pain a predisposing factor to patellofemoral osteoarthritis? *The Knee* 12, 362-365.

Van den Heever, D., Scheffer, C., Erasmus, P., Dillon, E., 2011. Method for selection of femoral component in total knee arthroplasty (tka). *Australasian Physical & Engineering Sciences in Medicine / Supported by the Australasian College of Physical Scientists in Medicine and the Australasian Association of Physical Sciences in Medicine* 34, 23-30.

Van Schalkwyk, E. P., 2010. Determining femoral component goodness-of-fit using computer segmentation and numerical simulation. MSc. Thesis. University of Stellenbosch.

Varadarajan, K. M., Rubash, H. E., Li, G., 2011. Are Current Total Knee Arthroplasty Implants Designed to Restore Normal Trochlear Groove Anatomy? *The Journal of Arthroplasty* 26, 274-281.

Victor, J., Van Doninck, D., Labey, L., Van Glabbeek, F., Parizel, P., Bellemans, J., 2009. A common reference frame for describing rotation of the distal femur: a ct-based kinematic study using cadavers. *The Journal of Bone and Joint Surgery*. British Volume 91, 683-690.

Wilk, K. E., Davies, G. J., Mangine, R. E., Malone, T. R., 1998. Patellofemoral disorders: a classification system and clinical guidelines for nonoperative rehabilitation. *The Journal of Orthopaedic and Sports Physical Therapy* 28, 307-322.

Zaffagnini, S., Dejour, D., Arendt, E. A., 2010. *Patellofemoral pain, instability, and arthritis*. Springer-Verlag, Berlin, Germany.

APPENDIX A: MEASUREMENTS OF PATELLAR PARAMETERS

Table A1: Patellar parameters for right knees

femur model number	gender	angle between anatomical axis and mechanical axis	MA	DM	MD	trochlear depth	sulcus angle	LTI	VTP	ML	trochlear facet asymmetry			AP distance		
		[°]	[°]	[°]	[mm]	[mm]	[°]	[°]	[mm]	[mm]	FL [mm]	FM [mm]	ratio [%]	lateral [mm]	middle [mm]	medial [mm]
B002R	M	5.85	5.83	93.53	22.69	3.88	151.52	15.55	2.97	90.66	21.35	12.56	58.82	66.67	61.31	66.09
B003R	F	5.49	5.46	94.83	24.41	2.82	159.17	11.24	4.34	91.58	24.59	11.48	46.68	73.38	68.63	70.54
B004R	F	6.02	6.02	94.32	15.61	4.38	147.67	17.89	2.51	74.69	19.54	13.2	67.55	60.28	54.21	57.48
B005R	F	5.67	5.67	93.00	20.33	6.25	137.46	24.12	1.21	78.63	20.14	15.11	75.02	62.70	54.47	59.25
B006R	F	4.44	4.33	93.3	17.30	6.44	133.35	24.39	3.84	79.26	18.87	14.35	76.04	59.57	51.76	57.13
B007R	F	5.09	4.92	92.29	16.02	5.95	139.07	31.43	1.31	73.90	20.22	13.19	65.23	56.09	48.71	53.75
B008R	F	5.09	4.92	93.64	13.99	5.94	136.83	20.09	1.21	76.52	19.52	13.82	70.79	56.02	49.32	54.73
B009R	F	5.14	4.85	93.69	14.09	5.84	137.96	20.75	1.07	76.18	18.42	14.63	79.42	56.13	49.60	54.92
B010R	M	5.48	5.07	93.29	21.35	9.10	127.31	27.40	3.33	89.55	24.28	17.85	73.51	71.72	60.44	67.99
B011R	M	5.29	5.29	93.31	18.67	8.52	131.48	24.29	2.07	81.31	24.05	18.28	76.00	61.79	51.89	59.40
B012R	M	4.86	4.85	95.01	19.55	6.00	139.78	20.42	1.57	82.69	20.19	15.38	76.17	62.37	55.18	60.39
B013R	M	5.68	5.52	98.21	20.79	7.16	139.99	17.63	4.30	96.68	25.82	17.67	68.43	72.04	64.19	71.00
B014R	F	4.75	4.69	95.58	15.35	7.25	131.90	24.19	2.23	76.27	19.04	14.69	77.15	57.67	49.87	56.71
B015R	F	5.02	4.98	97.29	16.91	5.90	138.90	20.73	2.84	78.63	21.71	13.78	63.47	61.00	53.32	58.12
B016R	M	4.78	4.74	95.19	22.06	6.79	139.02	23.66	3.81	88.3	22.28	17.23	77.33	71.07	62.14	67.27
B017R	F	5.45	5.00	95.66	22.68	2.86	155.77	16.01	3.03	80.06	18.90	10.70	56.61	66.61	61.40	62.92
B020R	M	3.94	3.88	95.63	20.06	5.74	145.85	16.04	1.13	83.77	24.52	16.31	66.51	66.29	59.52	64.59
B021R	F	4.57	4.57	91.91	20.06	3.07	152.08	13.65	3.62	74.29	20.55	9.28	45.158	61.83	56.98	59.27
mean		5.15	5.03	94.43	19.00	5.77	141.40	20.53	2.58	81.83	21.33	14.42	67.77	63.51	56.27	61.20

Table A2: Patellar parameters for left knees

femur model number	gender	angle between anatomical axis and mechanical axis	MA	DM	MD	trochlear depth	sulcus angle	LTI	VTP	ML	trochlear facet asymmetry			AP distance		
		[°]	[°]	[°]	[mm]	[mm]	[°]	[°]	[mm]	[mm]	FL [mm]	FM [mm]	ratio [%]	lateral [mm]	middle [mm]	medial [mm]
B002L	M	6.13	6.05	93.20	22.78	5.31	143.93	18.63	3.02	89.36	20.95	14.54	69.40	68.06	61.37	65.73
B003L	F	5.91	5.89	93.69	21.79	3.06	156.92	13.91	3.09	93.43	24.74	11.11	44.90	72.17	66.20	68.00
B004L	F	5.93	5.90	94.33	15.68	4.51	146.62	16.12	2.08	75.10	23.00	11.99	52.13	60.43	54.04	57.59
B005L	F	5.67	5.66	92.22	16.13	4.99	142.6	19.47	2.71	77.39	21.38	12.31	57.57	64.40	57.24	61.03
B006L	F	3.91	3.45	92.28	18.64	5.50	137.96	20.18	3.59	77.26	18.24	13.29	72.86	58.28	51.99	56.94
B007L	F	5.44	5.05	93.79	18.70	4.16	147.25	16.88	3.24	72.82	19.98	11.75	58.80	59.48	53.68	56.89
B008L	F	4.68	4.43	94.47	16.38	4.36	144.78	16.74	1.57	75.99	17.13	12.49	72.91	57.16	52.23	56.18
B009L	F	4.75	3.91	93.58	20.91	6.70	132.06	27.11	2.15	80.44	25.42	12.42	48.85	68.13	56.54	60.96
B010L	M	5.37	5.02	93.12	23.56	8.25	129.30	24.70	1.94	89.43	24.16	16.15	66.84	72.27	62.20	69.29
B011L	M	5.71	5.66	92.98	18.65	9.18	127.68	21.16	2.51	81.98	25.95	17.51	67.47	61.46	52.11	61.18
B012L	M	5.29	5.29	93.14	19.68	5.34	143.55	16.77	1.92	83.45	21.82	14.08	64.52	62.54	56.24	60.98
B013L	M	5.66	5.56	96.50	25.26	7.63	137.99	19.59	4.48	96.87	25.73	18.21	70.77	73.01	64.34	71.25
B014L	F	4.82	4.65	93.81	18.42	5.13	139.31	18.52	1.31	76.07	17.66	12.69	71.85	58.07	53.07	57.86
B015L	F	5.09	5.09	97.60	22.10	4.97	145.02	17.20	1.53	79.13	24.86	12.49	50.24	63.35	55.99	59.81
B016L	M	4.46	4.39	95.00	24.45	5.35	145.23	19.64	1.71	87.86	23.64	14.48	61.25	71.63	63.68	67.46
B017L	F	5.70	5.30	95.83	21.72	3.35	152.17	16.23	3.17	79.7	20.07	10.74	53.51	65.71	60.09	62.25
B020L	M	4.16	4.03	96.29	20.01	4.78	148.79	15.15	1.99	83.45	22.64	14.67	64.79	66.03	60.11	64.17
B021L	F	5.57	5.26	94.58	19.56	3.25	148.10	14.63	4.57	72.15	19.66	8.55	43.48	61.85	56.89	59.43
mean		5.24	5.03	94.25	20.25	5.32	142.74	18.48	2.59	81.77	22.06	13.30	60.67	64.67	57.67	62.06

APPENDIX B: CLASSIFICATION RESULTS

Table B1: Quantitative and qualitative classification for trochlear dysplasia of right knees (A: dysplastic femur N: normal femur)

femur model number	gender	quantitative classification with femoral ratios						qualitative classification by surgeons				classification by ANN	
		trochlear depth	VTP	sulcus angle	TFA	LTl	overall	Erasmus	Dejour	Arendt	overall		
has trochlear dysplasia if:		< 5 mm	> 3 mm	> 145°	< 40 %	< 14°							
B002R	M	A	N	A	N	N	N	N	N	N	N	N	N
B003R	F	A	A	A	N	A	A	A	A	N	A	A	A
B004R	F	A	N	A	N	N	N	A	N	A	A	A	A
B005R	F	N	N	N	N	N	N	N	N	N	N	N	N
B006R	F	N	N	N	N	N	N	A	N	A	A	A	A
B007R	F	N	N	N	N	N	N	N	N	N	N	N	N
B008R	F	N	N	N	N	N	N	A	N	N	N	N	N
B009R	F	N	N	N	N	N	N	N	N	N	N	N	N
B010R	M	N	A	N	N	N	N	N	N	N	N	N	A
B011R	M	N	N	N	N	N	N	N	N	N	N	N	N
B012R	M	N	N	N	N	N	N	A	N	N	N	N	N
B013R	M	N	A	N	N	N	N	N	N	N	N	N	N
B014R	F	N	N	N	N	N	N	N	N	N	N	N	N
B015R	F	N	N	N	N	N	N	N	N	N	N	N	N
B016R	M	N	A	N	N	N	N	N	N	N	N	N	A
B017R	F	A	A	A	N	N	A	A	N	A	A	A	A
B020R	M	N	N	A	N	N	N	A	N	A	A	A	A
B021R	F	A	A	A	N	A	A	A	A	A	A	A	A

Table B2: Quantitative and qualitative classification for trochlear dysplasia of left knees (A: dysplastic femur N: normal femur)

femur model number	gender	quantitative classification with femoral ratios						qualitative classification by surgeons				classification by ANN
		trochlear depth	VTP	sulcus angle	TFA	LTI	overall	Erasmus	Dejour	Arendt	overall	
has trochlear dysplasia if:	< 5 mm	> 3 mm	> 145°	< 40 %	< 14°							
B002L	M	N	A	N	N	N	N	N	N	N	N	A
B003L	F	A	A	A	N	A	A	A	A	A	A	A
B004L	F	A	N	A	N	N	N	A	A	A	A	A
B005L	F	A	N	N	N	N	N	N	N	N	N	A
B006L	F	N	A	N	N	N	N	A	N	A	A	A
B007L	F	A	A	A	N	N	A	N	N	N	N	A
B008L	F	A	N	N	N	N	N	A	A	A	A	A
B009L	F	N	N	N	N	N	N	N	N	N	N	N
B010L	M	N	N	N	N	N	N	N	N	N	N	N
B011L	M	N	N	N	N	N	N	N	N	N	N	N
B012L	M	N	N	N	N	N	N	A	A	N	A	A
B013L	M	N	A	N	N	N	N	N	N	N	N	N
B014L	F	N	N	N	N	N	N	N	A	N	N	N
B015L	F	A	N	A	N	N	N	N	A	N	N	N
B016L	M	N	N	A	N	N	N	N	N	N	N	N
B017L	F	A	A	A	N	N	A	A	A	A	A	A
B020L	M	A	N	A	N	N	N	A	A	A	A	A
B021L	F	A	A	A	N	N	A	A	A	A	A	A

APPENDIX C: TESTING FOR OPTIMAL RUNNING CONDITION OF ARTIFICIAL NEURAL NETWORKS (ANN) PATTERN RECOGNITION

Table C1: Average agreement over 15 runs

number of input parameters (n)	number of hidden-layer neurons						
	2n - 3	2n - 2	2n - 1	2n	2n + 1	2n + 2	2n + 3
10	79.6	69.8	75.4	74.6	66.1	72.4	70.7
9	78.0	71.3	74.4	75.4	72.8	73.1	69.8
8	76.5	74.6	78.0	75.4	68.0	69.6	80.6
7	73.3	67.4	70.9	72.2	75.0	72.6	76.7
6	70.2	63.9	66.9	71.3	70.6	73.7	67.6
5	64.3	72.4	71.7	72.6	65.6	70.4	70.0
4	67.8	76.1	71.3	73.0	66.7	69.0	67.2

high agreement  low agreement

Table C2: Standard deviation of the agreement over 15 runs

number of input parameters (n)	number of hidden-layer neurons						
	2n - 3	2n - 2	2n - 1	2n	2n + 1	2n + 2	2n + 3
10	0.177	0.196	0.167	0.169	0.143	0.177	0.160
9	0.155	0.194	0.140	0.120	0.174	0.145	0.141
8	0.099	0.145	0.165	0.183	0.193	0.203	0.136
7	0.161	0.186	0.115	0.152	0.116	0.106	0.102
6	0.205	0.198	0.150	0.171	0.153	0.065	0.199
5	0.176	0.183	0.152	0.105	0.155	0.175	0.119
4	0.173	0.104	0.121	0.128	0.129	0.209	0.102

high agreement  low agreement

Table C3: Average goal function over 15 runs

number of input parameters (n)	number of hidden-layer neurons						
	2n - 3	2n - 2	2n - 1	2n	2n + 1	2n + 2	2n + 3
10	0.121	0.212	0.169	0.205	0.284	0.269	0.228
9	0.168	0.189	0.180	0.186	0.231	0.279	0.217
8	0.173	0.195	0.161	0.186	0.240	0.235	0.164
7	0.178	0.262	0.219	0.180	0.233	0.216	0.207
6	0.207	0.276	0.263	0.208	0.284	0.213	0.287
5	0.265	0.299	0.256	0.240	0.279	0.193	0.236
4	0.210	0.178	0.239	0.208	0.270	0.200	0.256

low error  high error

Table C4: Standard deviation of the goal function over 15 runs

number of input parameters (n)	number of hidden-layer neurons						
	$2n - 3$	$2n - 2$	$2n - 1$	$2n$	$2n + 1$	$2n + 2$	$2n + 3$
10	0.114	0.148	0.170	0.175	0.150	0.221	0.161
9	0.146	0.188	0.141	0.120	0.182	0.245	0.154
8	0.105	0.141	0.169	0.161	0.198	0.190	0.154
7	0.126	0.172	0.128	0.121	0.165	0.108	0.189
6	0.170	0.181	0.128	0.152	0.196	0.097	0.212
5	0.158	0.253	0.203	0.182	0.146	0.143	0.136
4	0.115	0.128	0.134	0.135	0.102	0.161	0.093

low error



high error

APPENDIX D: EQUATIONS FOR B-SPLINES

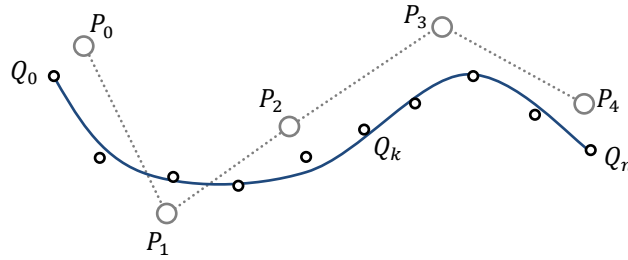


Figure D1: B-spline curve

The B-spline curve, $C(u)$ is defined as follows:

$$C(u) = \frac{\sum_{i=0}^n P_i N_{i,k}(u)}{\sum_{i=0}^n N_{i,k}(u)} \quad (5)$$

where P_i is a control point and $N_{i,k}$ is normalised B-spline basis function of degree k

For the given set of data points $\{Q_k\}$, $k = 0, \dots, n$, a p^{th} degree non-rational B-spline curve was interpolated with a global approximation method. A parameter value, \bar{u}_k , is assigned to each Q_k and an appropriate knot vector, $U = \{u_0, \dots, u_m\}$, is selected to set up a $(n+1) \times (n+1)$ system of linear equations.

$$Q_k = C(\bar{u}_k) = \sum_{i=0}^n N_{i,p}(\bar{u}_k) P_i \quad (6)$$

P_i is a control point and \bar{u}_k is chosen with the chord length method as follows:

$$d = \sum_{k=1}^n |Q_k - Q_{k-1}| \quad (7)$$

$$\bar{u}_k = u_{k-1} + \frac{|Q_k - Q_{k-1}|}{d} \quad (8)$$

where, d is total length of chord, $k = 1, \dots, n-1$, and $\bar{u}_0 = 0$, $\bar{u}_n = 1$

The distribution of \bar{u}_k is reflected on the placement of the knots. If d is a positive real number, denote by $i = \text{int}(d)$ the largest integer such that $i \leq d$. $n + p + 2$ knots are needed in total with $n - p$ internal knots and $n - p + 1$ internal knot spans. Let

$$d = \frac{m + 1}{n - p + 1} \quad (9)$$

Then, define the internal knots by

$$\begin{aligned} i &= \text{int}(js) & \alpha &= js - i \\ u_{p+j} &= (1 - \alpha)\bar{u}_{i-1} + \alpha\bar{u}_i & j &= 1, \dots, n - p \\ u_0 &= \dots = u_p = 0, \text{ and } u_{m-p} &= \dots = u_m = 1 \end{aligned} \quad (10)$$

This was done to ensure that $Q_0 = C(0)$ and $Q_m = C(1)$.

Now let

$$R_k = Q_k - N_{0,p}(\bar{u}_k)Q_0 - N_{n,p}(\bar{u}_k)Q_m, \quad k = 1, \dots, m - 1 \quad (11)$$

Then linear least squares fitting technique is applied:

$$(N^T N)P = R \quad (12)$$

Where N is $(m - 1) \times (n - 1)$ matrix of scalars

$$N = \begin{bmatrix} N_{1,p}(\bar{u}_1) & \dots & N_{n-1,p}(\bar{u}_1) \\ \vdots & \ddots & \vdots \\ N_{1,p}(\bar{u}_{m-1}) & \dots & N_{n-1,p}(\bar{u}_{m-1}) \end{bmatrix} \quad (13)$$

R is the vector of $n-1$ points

$$R = \begin{bmatrix} N_{1,p}(\bar{u}_1)R_1 & \dots & N_{1,p}(\bar{u}_{m-1})R_{m-1} \\ \vdots & \ddots & \vdots \\ N_{n-1,p}(\bar{u}_1)R_1 & \dots & N_{n-1,p}(\bar{u}_{m-1})R_{m-1} \end{bmatrix} \quad (14)$$

And

$$P = \begin{bmatrix} P_1 \\ \vdots \\ P_{n-1} \end{bmatrix} \quad (15)$$

APPENDIX E: SAGITTAL CURVE ANALYSES RESULTS**Table E1: Radius of circular arc**

	sagittal slice [mm]									
	L1	L2	L3	L4	M1	M2	M3	M4	middle	average
B002R	23.21	24.79	23.61	24.79	21.58	21.05	21.15	21.17	22.45	22.64
B005R	24.85	23.22	23.34	22.81	21.38	18.98	18.02	17.09	23.39	21.46
B007R	26.64	29.02	22.05	23.18	18.52	21.39	18.72	16.31	23.99	22.20
B008R	20.71	20.37	20.16	22.91	20.90	21.30	21.04	16.78	20.68	20.54
B009R	20.54	19.83	22.03	23.03	20.84	20.36	21.83	16.87	20.61	20.66
B011R	21.61	26.63	31.03	28.80	22.18	15.84	15.45	16.26	21.16	22.11
B012R	24.85	26.20	25.85	26.22	23.12	22.26	21.59	22.26	24.80	24.13
B014R	21.51	22.08	22.65	23.26	20.80	19.34	19.90	24.34	21.07	21.66
B015R	18.63	22.98	23.27	22.92	18.18	17.26	19.52	24.96	17.22	20.55
B009L	27.47	23.22	22.94	20.68	15.15	15.95	19.33	16.22	26.11	20.79
B010L	35.06	29.31	30.83	28.39	35.47	29.73	26.28	25.08	32.38	30.28
B011L	17.58	20.96	29.40	30.91	14.57	15.57	17.11	17.02	14.00	19.68
B014L	24.68	24.13	23.93	20.46	18.00	17.06	16.55	26.37	23.35	21.61
B015L	26.25	25.21	24.39	23.78	28.50	20.31	20.29	23.94	29.11	24.64
B016L	36.19	32.28	27.25	29.71	31.63	29.08	28.17	23.57	20.98	28.76
mean	24.65	24.68	24.85	24.79	22.05	20.37	20.33	20.55	22.75	22.78

Table E2: Trochlear flexion angle of circular arc

	sagittal slice [°]									
	L1	L2	L3	L4	M1	M2	M3	M4	middle	average
B002R	45	45	60	60	90	90	45	60	60	62
B005R	40	50	50	60	45	65	65	50	50	53
B007R	40	60	50	55	85	66	50	55	45	56
B008R	50	55	60	60	65	55	50	65	60	58
B009R	60	50	65	65	65	55	45	70	50	58
B011R	50	55	55	80	45	45	40	60	60	54
B012R	50	50	60	50	45	50	60	50	40	51
B014R	45	60	60	60	60	55	60	55	50	56
B015R	50	50	60	65	50	50	55	55	50	54
B009L	50	60	80	80	60	70	70	50	50	63
B010L	70	60	80	70	60	65	55	60	55	64
B011L	65	55	45	60	55	60	60	70	55	58
B014L	40	50	70	65	70	65	70	50	40	58
B015L	50	45	60	55	55	50	55	40	40	50
B016L	45	45	55	50	50	55	50	55	45	50
mean	50	53	61	62	60	60	55	56	50	56

Table E3: Maximum error between data point and least squares circle

	sagittal slice [mm]									
	L1	L2	L3	L4	M1	M2	M3	M4	middle	average
B002R	0.09	0.04	0.08	0.08	0.04	0.16	0.09	0.10	0.13	0.09
B005R	0.10	0.16	0.12	0.13	0.10	0.03	0.12	0.15	0.11	0.11
B007R	0.28	0.30	0.35	0.46	0.08	0.17	0.18	0.09	0.09	0.22
B008R	0.08	0.10	0.20	0.23	0.18	0.18	0.16	0.14	0.18	0.16
B009R	0.14	0.09	0.18	0.23	0.17	0.12	0.17	0.15	0.21	0.16
B011R	0.41	0.29	0.42	0.44	0.43	0.13	0.48	0.48	0.07	0.35
B012R	0.11	0.08	0.15	0.18	0.09	0.16	0.15	0.05	0.13	0.12
B014R	0.22	0.21	0.09	0.15	0.23	0.07	0.15	0.29	0.18	0.18
B015R	0.21	0.19	0.05	0.12	0.20	0.13	0.08	0.18	0.10	0.14
B009L	0.19	0.17	0.21	0.09	0.35	0.33	0.14	0.20	0.28	0.22
B010L	0.30	0.36	0.24	0.16	0.44	0.20	0.14	0.20	0.50	0.28
B011L	0.33	0.23	0.33	0.27	0.28	0.28	0.26	0.16	0.26	0.27
B014L	0.20	0.27	0.10	0.27	0.25	0.25	0.25	0.23	0.17	0.22
B015L	0.21	0.19	0.21	0.16	0.22	0.13	0.15	0.12	0.17	0.17
B016L	0.42	0.34	0.35	0.26	0.38	0.24	0.20	0.11	0.35	0.14
mean	0.22	0.20	0.20	0.22	0.23	0.17	0.18	0.18	0.20	0.19
min	0.08	0.04	0.05	0.08	0.04	0.03	0.08	0.05	0.07	0.09
max	0.42	0.36	0.42	0.46	0.44	0.33	0.48	0.48	0.50	0.35

Table E4: Average distance between the centre points of the B-spline and circular arc

	sagittal slice [mm]									
	L1	L2	L3	L4	M1	M2	M3	M4	middle	
B002R	0.26	0.34	0.58	0.58	0.16	0.54	0.40	0.63	0.68	
B005R	0.18	1.83	0.45	0.57	0.63	0.01	0.48	0.91	0.83	
B007R	1.48	5.60	31.97	39.42	0.02	0.63	0.26	0.65	0.09	
B008R	0.40	0.37	0.27	0.86	0.46	0.32	0.33	0.26	0.88	
B009R	0.43	0.40	0.20	4.81	0.36	0.21	0.20	0.23	1.10	
B011R	0.42	3.71	2.64	0.87	4.04	0.49	2.79	0.21	8.87	
B012R	6.23	0.96	1.13	0.06	0.85	1.84	3.15	0.49	0.87	
B014R	0.32	7.68	0.30	1.28	5.80	0.44	0.74	8.52	6.41	
B015R	0.34	0.97	0.15	0.79	2.74	0.38	0.10	1.35	0.59	
B009L	4.37	3.04	6.06	0.20	7.07	7.55	0.99	3.82	1.04	
B010L	1.01	0.36	0.39	0.38	1.30	6.82	2.20	1.09	1.45	
B011L	5.18	13.45	8.71	0.29	3.68	14.30	17.11	2.05	1.45	
B014L	0.87	1.25	0.37	0.82	7.34	0.32	2.94	0.94	0.30	
B015L	1.26	2.14	2.08	1.01	9.86	0.56	3.44	5.11	2.99	
B016L	16.96	0.43	2.23	6.67	0.63	7.59	2.97	0.66	7.97	
mean	2.65	2.84	3.83	3.91	3.00	2.80	2.54	1.80	2.37	

Table E5: Centre plane location

	X-rotation	Z-rotation	Y-translation	average error between centre points
	[°]	[°]	[mm]	[mm]
B002R	-3.38	-135.03	20.99	0.05
B005R	-6.97	-146.21	18.56	0.12
B007R	-16.87	-138.21	16.88	0.50
B008R	-5.20	-139.89	18.58	0.22
B009R	-4.61	-138.91	18.66	0.21
B011R	-18.22	-149.81	17.47	0.53
B012R	-8.48	-143.51	18.91	0.27
B014R	-3.69	-138.99	16.24	0.13
B015R	-10.62	-139.31	17.36	0.48
B009L	-15.62	-151.86	24.58	0.84
B010L	-9.19	-144.02	22.30	0.64
B011L	-19.73	-76.81	13.37	0.24
B014L	-7.57	-47.71	19.06	0.64
B015L	-12.77	-153.85	18.48	0.60
B016L	-14.90	-142.85	23.49	0.87
mean	-10.52	-132.46	18.99	0.42
standard deviation	5.50	29.51	2.88	0.26

Table E6: Average % agreement between the prediction and the measured anterior-posterior (AP)

	B015L	B016L	B014L	B011L	B010L	B015R	B014R	B013R	B012R	B011R	B009R	B008R	B005R	B002R	B007R
6x6	0.63	1.13	1.76	1.79	5.30	4.17	1.65	5.82	0.77	3.52	2.19	2.62	0.52	2.83	3.65
6X7	0.56	4.16	2.15	1.26	4.81	3.45	2.12	5.22	1.53	2.51	1.49	1.30	0.40	2.45	3.11
6X8	0.62	1.43	1.37	1.53	6.10	4.32	2.63	7.57	2.05	1.28	0.85	1.09	2.21	3.15	3.11
6X9	1.00	3.96	1.01	1.77	3.45	2.66	1.98	5.62	1.08	1.71	0.73	0.70	1.05	5.14	4.44
6X10	1.74	2.82	0.76	1.95	4.19	3.35	1.80	6.31	2.69	1.47	0.86	1.84	1.38	3.88	5.14
7X6	0.68	1.92	1.21	1.74	5.89	4.22	1.79	7.12	0.82	2.29	1.32	1.65	0.59	4.31	2.91
7X7	0.67	1.87	1.23	1.06	5.15	3.59	2.03	7.27	0.77	2.07	1.60	1.67	0.68	3.14	2.72
7X8	1.09	1.38	1.40	1.72	5.68	3.39	2.66	6.63	0.77	1.92	1.26	1.60	1.66	4.11	2.68
7X9	1.75	1.53	1.04	0.99	6.51	3.90	1.69	6.17	2.54	2.29	0.88	1.31	0.55	4.81	2.67
7X10	0.98	1.30	2.61	1.34	6.49	0.78	2.50	5.61	2.38	1.55	0.80	1.29	1.68	4.98	5.13
8x6	0.56	1.27	1.60	1.25	3.92	3.99	1.79	5.90	0.98	1.85	0.65	0.99	1.11	4.33	2.72
8x7	0.57	1.25	1.63	1.14	6.21	3.12	2.15	6.34	1.24	2.52	0.81	0.90	0.98	4.31	2.59
8x8	0.51	0.97	2.28	1.63	5.02	3.06	2.55	7.12	2.10	2.18	1.14	0.73	0.86	4.31	2.54
8x9	0.51	2.24	1.72	1.90	3.86	4.30	3.38	5.75	1.63	2.00	0.93	1.29	0.55	4.14	5.59
8x10	1.25	1.57	1.95	1.95	3.79	3.96	2.93	5.78	2.91	2.03	0.77	0.37	0.64	4.25	5.16
9x6	0.52	3.63	1.38	1.21	5.31	4.22	1.92	5.60	1.62	1.26	0.58	0.92	1.02	4.35	3.35
9x7	0.67	0.99	2.31	1.61	6.37	4.42	0.23	5.75	2.01	2.45	0.84	1.63	0.90	4.63	2.59
9x8	1.51	1.66	0.46	1.10	4.24	4.13	2.33	5.78	2.58	1.98	0.87	1.24	2.64	4.71	2.59
9x9	1.51	2.80	2.69	1.99	3.81	4.32	2.19	6.25	3.43	1.44	0.42	0.38	1.14	5.21	2.54
9x10	0.53	2.37	3.07	2.11	4.78	4.12	2.50	6.09	3.66	2.28	0.30	0.37	1.14	5.01	2.53
10x6	0.63	0.99	0.68	1.50	5.60	4.32	1.09	5.28	1.24	1.86	0.80	1.31	1.06	4.68	3.34
10x7	0.61	2.24	3.74	1.35	5.84	3.57	1.22	6.08	2.69	1.54	0.41	0.50	1.21	4.68	2.68
10x8	0.92	0.99	1.25	1.09	4.90	2.41	2.45	6.15	1.14	1.59	0.30	0.63	1.01	5.03	5.70
10x9	1.22	2.12	2.15	1.57	4.90	1.88	0.19	6.15	3.19	1.95	0.31	0.37	1.27	5.03	5.99
10x10	0.53	2.77	1.05	1.85	5.21	3.98	0.20	6.02	5.71	1.66	0.31	0.33	1.25	5.03	5.94

Table E7: Average % agreement between the prediction and the measured radius of the circular arcs

	B016L	B015L	B015L	B014L	B011L	B010L	B015R	B014R	B013R	B012R	B011R	B009R	B008R	B007R	B005R	B002R
6x6	18.21	11.32	11.32	9.83	9.88	18.90	3.96	8.33	12.54	8.12	14.25	12.99	10.40	15.63	16.53	15.41
6X7	17.72	7.88	7.88	10.76	14.95	12.29	3.90	9.95	12.61	7.96	14.95	12.20	9.62	16.35	18.28	15.42
6X8	17.94	8.80	8.80	10.76	14.99	12.59	4.51	10.90	12.62	7.55	16.10	9.42	6.56	16.38	15.78	14.72
6X9	17.46	7.36	7.36	10.35	15.55	12.83	5.72	12.26	13.97	7.65	16.74	9.32	6.23	15.66	18.33	15.51
6X10	18.20	7.32	7.32	10.10	14.82	13.25	9.18	12.12	13.97	7.41	19.37	6.19	3.51	16.46	16.70	15.34
7X6	18.27	9.20	9.20	14.17	12.95	12.35	3.67	8.42	13.36	4.71	16.71	12.97	9.62	16.35	16.09	15.67
7X7	18.34	7.26	7.26	10.26	15.35	13.43	2.21	8.07	15.75	4.65	16.86	12.03	9.41	16.43	17.57	16.21
7X8	18.13	8.25	8.25	10.02	14.65	21.08	7.20	11.00	16.97	4.75	18.59	9.22	7.24	16.63	16.36	15.62
7X9	18.62	7.15	7.15	10.05	13.93	12.87	3.56	8.18	15.59	11.78	19.38	6.64	3.49	16.46	16.62	15.05
7X10	18.62	6.92	6.92	10.05	15.73	13.23	5.13	11.26	14.99	13.22	18.87	6.06	3.35	15.79	17.88	15.05
8x6	18.30	8.49	8.49	10.11	16.15	20.66	5.92	10.14	13.08	8.99	16.44	11.59	5.80	16.42	16.02	16.18
8x7	18.36	7.60	7.60	10.17	16.30	12.66	5.21	9.98	14.70	10.14	17.38	8.01	5.64	15.70	16.31	16.18
8x8	19.05	7.88	7.88	10.23	16.30	12.28	5.16	11.71	14.71	6.04	18.91	9.16	3.26	16.63	17.38	15.12
8x9	19.12	6.97	6.97	10.23	16.33	13.20	8.15	8.15	16.44	10.90	19.31	6.08	2.87	16.89	16.70	15.22
8x10	18.72	6.55	6.55	14.56	16.30	12.73	5.78	11.88	16.44	11.42	20.03	4.47	2.87	16.89	16.86	15.30
9x6	17.78	9.43	9.43	10.10	14.84	21.28	8.98	11.43	13.72	5.55	15.15	8.52	4.04	15.70	17.62	15.44
9x7	19.15	7.83	7.83	10.31	16.15	12.80	8.35	11.21	15.48	7.30	17.92	6.92	3.34	16.60	17.86	15.32
9x8	19.12	6.24	6.24	10.23	15.91	12.59	4.44	11.63	14.98	4.55	14.54	5.32	4.00	16.60	17.88	15.08
9x9	19.12	6.66	6.66	10.20	16.73	12.66	4.72	8.13	15.83	7.30	19.91	4.62	2.82	16.89	17.61	15.30
9x10	19.12	8.39	8.39	10.20	16.03	13.01	5.71	11.49	17.30	5.96	19.53	4.09	2.82	15.14	16.75	15.27
10x6	18.24	8.09	8.09	10.21	15.98	11.47	6.97	11.41	15.77	5.60	14.97	8.09	4.04	15.89	17.62	15.42
10x7	18.37	7.28	7.28	10.24	15.99	11.92	4.98	8.94	15.82	6.40	17.15	8.85	4.30	15.70	17.77	15.36
10x8	19.12	7.09	7.09	10.24	16.72	12.45	6.96	11.05	15.85	4.45	19.48	5.31	2.70	16.56	17.78	15.28
10x9	19.13	8.38	8.38	10.18	16.35	12.47	6.96	12.42	15.86	7.10	17.76	4.62	2.81	14.53	17.84	15.28
10x10	19.18	8.37	8.37	13.70	16.35	13.70	3.03	11.51	15.59	7.95	19.37	4.32	2.41	15.15	16.16	15.19

Table E8: Average % agreement between the prediction and the measured radius of the trochlear heights

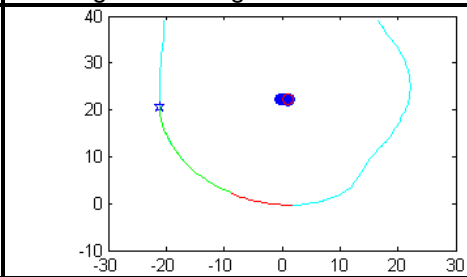
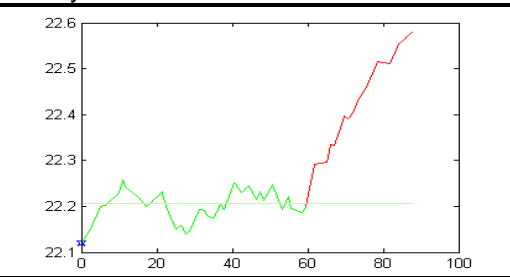
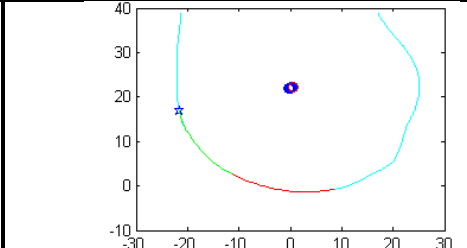
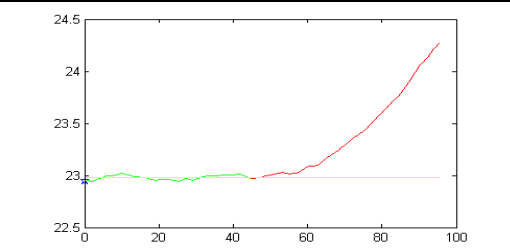
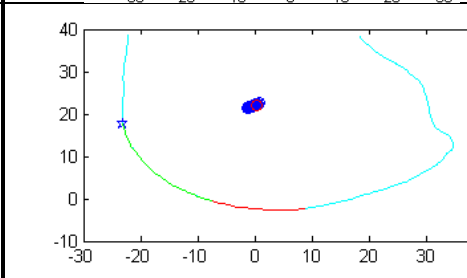
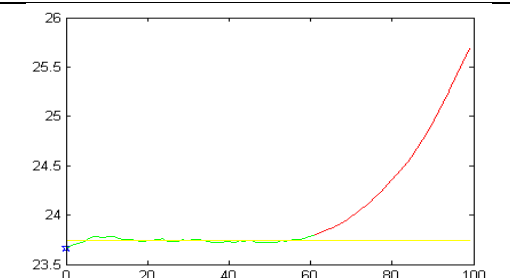
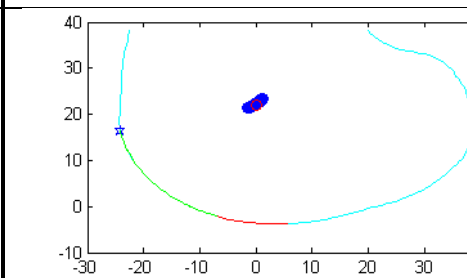
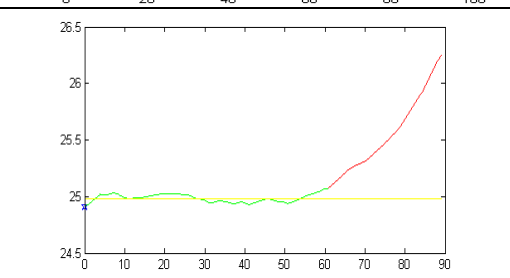
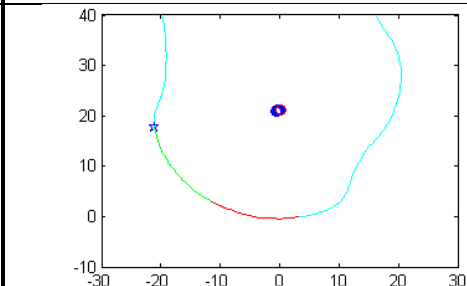
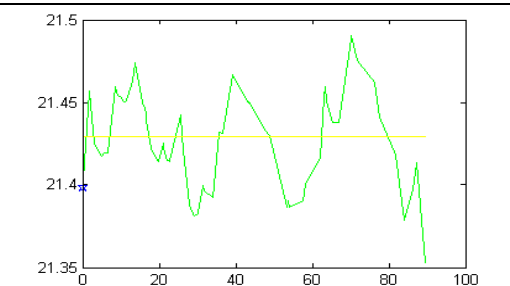
	B016L	B015L	B014L	B011L	B010L	B015R	B014R	B013R	B012R	B011R	B009R	B008R	B007R	B005R	B002R
6x6	1.01	0.79	1.15	0.98	4.31	5.29	1.07	6.24	1.25	3.00	1.14	1.74	4.83	2.50	2.81
6X7	2.71	0.53	1.65	0.66	7.30	3.96	1.23	6.22	0.82	2.52	1.87	2.23	2.84	0.60	3.10
6X8	1.63	0.53	2.07	1.11	6.24	4.55	1.99	6.26	2.14	2.65	1.26	2.24	2.43	1.79	3.24
6X9	3.74	1.39	2.76	2.25	3.66	0.73	1.40	6.46	1.77	2.82	1.04	2.17	3.80	1.14	4.93
6X10	1.13	0.53	3.45	1.34	3.96	2.44	2.40	6.56	3.62	2.58	0.87	1.55	4.10	1.17	3.90
7X6	3.21	0.81	2.50	1.44	3.22	3.85	1.91	7.45	2.40	2.52	1.49	1.49	3.00	1.63	3.76
7X7	2.13	1.09	2.53	1.56	4.95	4.54	1.79	7.45	1.24	2.77	1.36	1.73	2.43	0.43	3.35
7X8	1.80	1.87	2.05	1.19	5.14	3.64	0.82	6.71	2.37	2.76	0.67	1.72	2.41	2.17	3.49
7X9	4.21	0.56	3.18	2.19	4.34	4.80	0.62	6.60	4.27	2.86	1.13	1.58	4.04	0.96	4.54
7X10	0.75	0.49	3.18	2.53	3.82	2.52	2.18	6.46	4.78	2.75	1.07	2.21	5.29	0.85	4.45
8x6	1.39	0.69	1.46	1.80	5.16	5.03	2.01	6.71	2.86	2.66	1.36	1.72	2.43	2.16	3.78
8x7	1.18	0.63	1.47	2.10	6.40	2.75	2.01	7.24	2.03	2.59	1.35	1.72	2.43	0.49	3.69
8x8	1.18	0.70	2.33	1.99	4.36	4.21	0.57	7.17	2.00	2.53	0.70	1.10	2.43	0.96	3.70
8x9	2.94	0.89	1.18	2.15	4.16	3.90	1.86	6.95	2.18	2.47	0.72	0.83	5.04	1.65	4.54
8x10	0.93	0.70	1.77	2.25	3.88	4.21	2.07	7.10	2.23	2.60	0.72	0.83	5.10	1.15	4.95
9x6	3.68	0.78	1.69	1.60	4.51	4.04	2.99	6.79	3.13	2.37	0.77	1.07	5.25	0.84	4.58
9x7	3.90	1.34	1.75	2.10	4.20	3.97	1.56	7.02	2.40	2.76	0.72	0.83	5.08	1.17	4.69
9x8	1.94	0.58	3.99	2.27	5.28	4.77	1.56	7.02	3.14	2.66	0.81	0.83	5.05	2.63	4.55
9x9	1.51	0.61	1.83	2.28	5.20	4.60	1.81	6.45	1.94	2.56	0.39	0.66	5.11	2.37	4.72
9x10	1.44	0.39	1.27	2.22	5.32	5.07	3.29	6.43	2.14	2.52	0.39	0.66	4.53	1.10	4.74
10x6	0.96	0.66	1.77	2.09	4.62	3.85	0.16	6.61	2.27	2.72	0.77	1.07	5.36	1.22	4.91
10x7	0.78	0.36	2.99	2.21	4.55	3.33	1.69	6.58	1.71	2.67	1.13	1.46	2.63	2.88	4.56
10x8	1.03	0.51	1.77	2.54	4.63	2.45	3.13	7.14	3.74	2.67	0.43	0.49	2.40	2.44	4.82
10x9	1.03	0.36	1.77	2.28	5.20	3.78	2.43	7.00	0.61	2.62	0.39	0.32	2.40	0.99	4.57
10x10	1.03	0.42	2.01	2.54	5.57	5.07	2.07	7.14	2.71	2.65	0.45	1.50	2.38	1.51	4.74

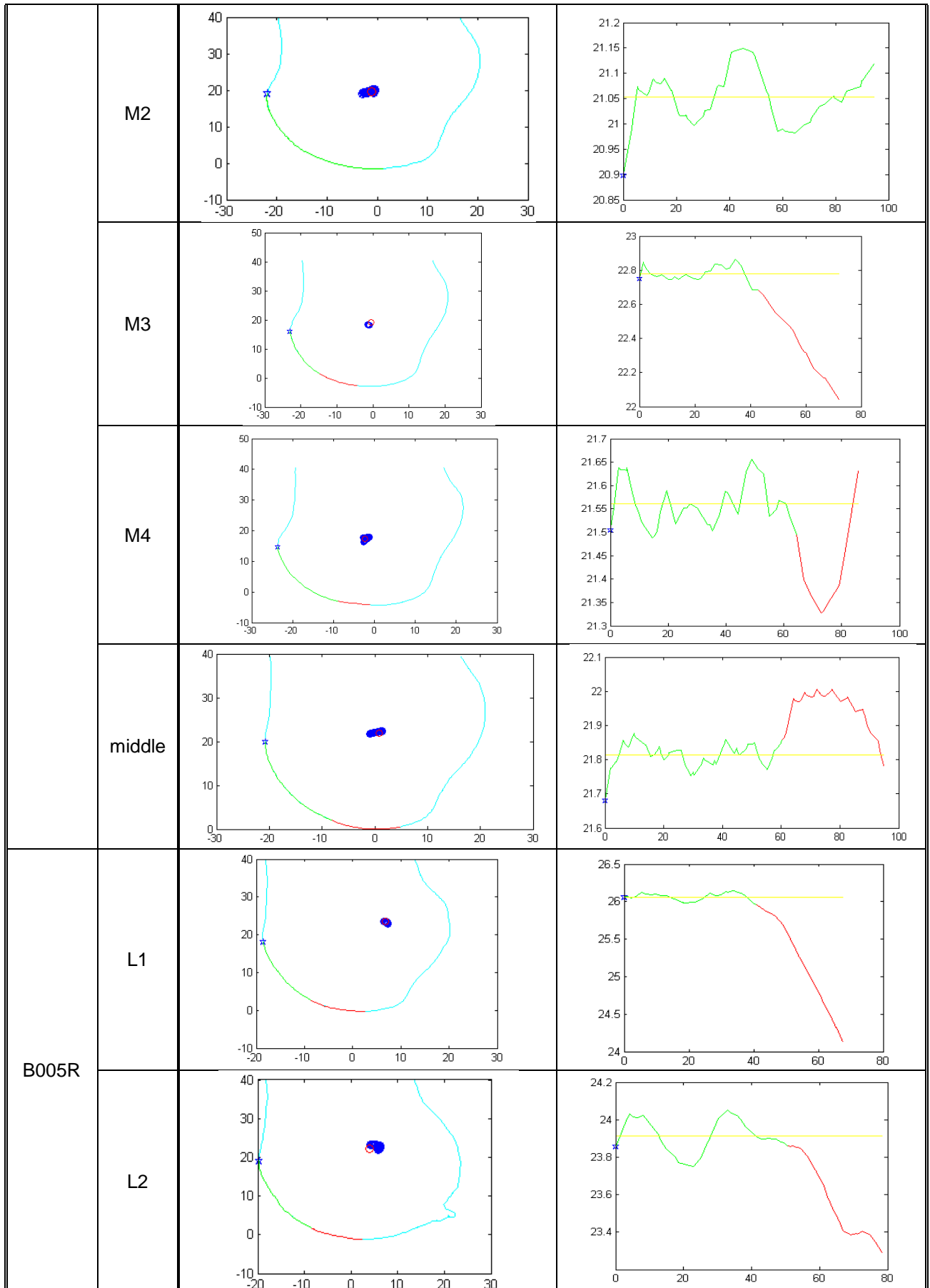
Table E8: Average % agreement between the prediction and the measured radius of the plane location

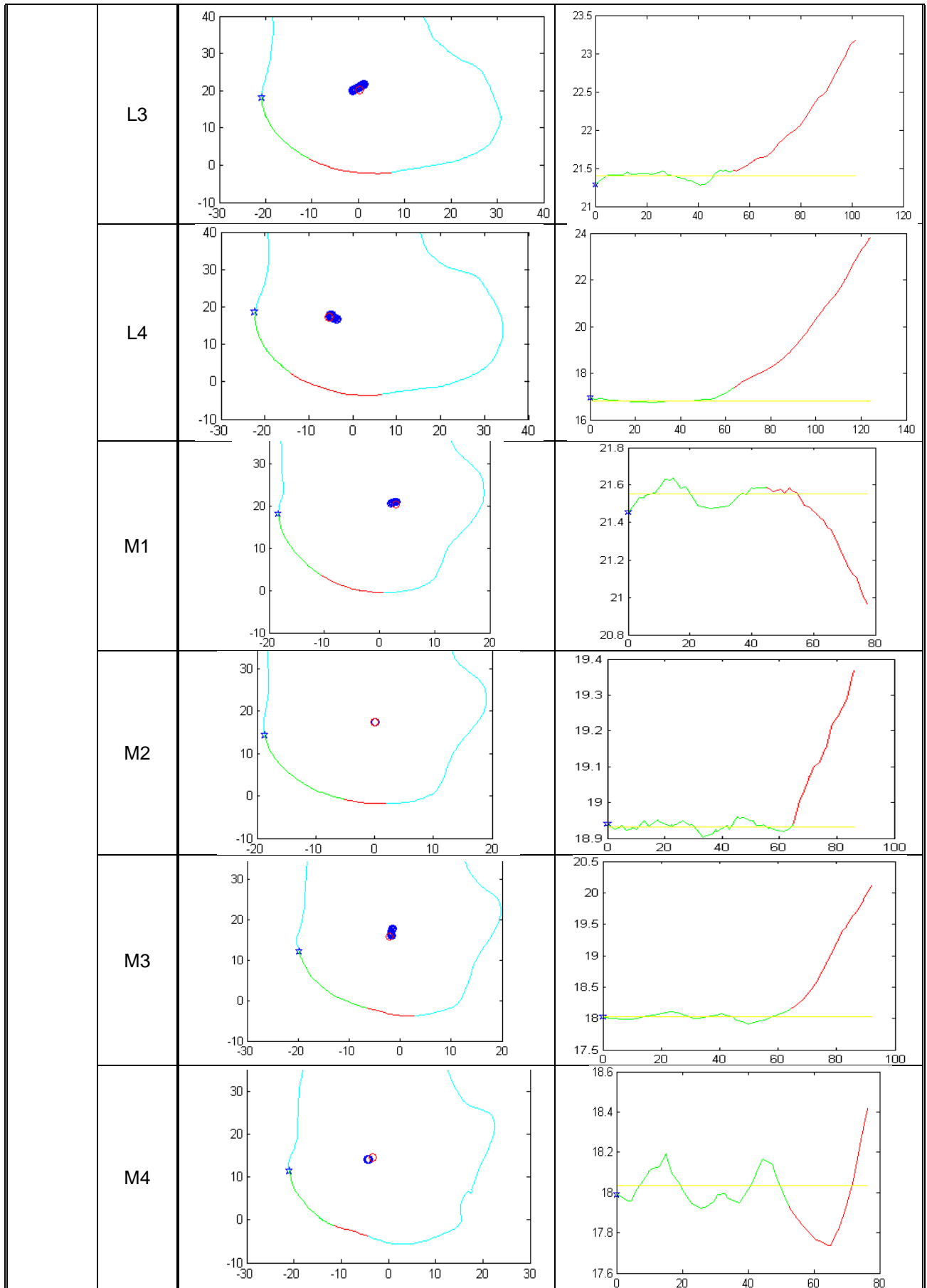
	B015L	B016L	B014L	B011L	B010L	B015R	B014R	B013R	B012R	B011R	B009R	B008R	B005R	B002R	B007R
6x6	0.63	2.82	9.29	10.90	1.28	6.66	1.55	7.06	0.71	1.35	1.72	2.26	5.91	5.28	8.06
6X7	1.34	4.42	9.65	11.01	2.84	5.42	1.55	7.04	1.97	1.61	1.72	0.95	5.91	4.91	8.23
6X8	0.89	3.86	8.51	9.96	3.34	6.16	2.17	6.97	0.81	5.65	1.70	0.70	5.97	4.92	8.27
6X9	0.67	3.49	9.38	5.96	3.34	6.15	5.01	7.11	0.80	5.69	1.71	1.88	5.85	4.96	8.35
6X10	2.07	3.54	10.13	5.98	2.72	6.38	2.37	7.11	0.74	5.83	1.36	0.94	6.00	4.84	8.40
7X6	0.74	3.28	9.21	6.60	3.04	8.69	1.83	7.13	2.17	2.45	1.70	0.76	5.93	6.22	8.37
7X7	0.65	3.31	8.25	9.55	4.13	5.69	2.09	7.61	3.28	1.03	1.59	0.67	5.65	5.93	8.86
7X8	0.61	3.16	9.94	6.15	4.13	5.54	2.08	7.13	0.76	5.54	1.70	1.00	5.88	5.13	8.66
7X9	1.63	2.79	9.99	6.12	2.37	6.15	2.43	7.61	1.76	5.69	1.69	1.03	6.05	5.48	7.59
7X10	1.62	2.81	10.80	6.25	4.15	6.24	7.11	7.72	1.66	6.24	1.35	1.03	6.00	5.48	8.63
8x6	1.00	2.15	9.28	6.04	3.87	8.57	1.83	7.16	2.15	5.50	1.65	1.32	5.68	4.78	9.50
8x7	0.99	2.76	9.79	6.68	2.71	6.60	2.10	7.43	3.56	5.54	1.64	1.04	5.78	5.15	7.88
8x8	0.62	2.76	10.13	6.17	2.82	6.66	2.17	7.40	3.75	3.94	1.69	1.06	5.83	5.15	7.62
8x9	1.67	2.79	9.88	6.14	2.30	6.30	2.37	7.14	4.56	5.69	1.36	1.16	6.05	5.10	8.71
8x10	1.67	2.78	8.44	6.15	4.16	6.29	7.46	7.77	1.73	5.67	1.32	1.17	6.06	5.10	7.74
9x6	0.73	2.67	10.79	6.81	3.74	6.17	1.47	6.99	0.77	3.43	1.49	1.67	5.99	5.71	9.51
9x7	1.82	3.39	8.78	6.40	2.08	7.86	1.53	7.79	4.33	5.54	1.78	1.05	6.08	5.86	7.70
9x8	0.78	2.68	9.14	6.10	2.08	6.59	1.43	7.77	4.36	6.19	1.34	0.96	6.09	5.16	7.62
9x9	0.78	2.94	8.59	6.09	2.14	6.59	2.50	7.76	4.37	6.24	1.32	1.16	6.09	5.16	7.63
9x10	1.66	2.84	8.59	6.21	2.22	6.80	1.47	7.76	0.86	6.24	1.45	1.16	6.06	5.19	9.57
10x6	0.53	3.35	6.46	6.06	4.02	7.39	1.45	7.16	4.03	1.18	1.46	1.05	6.08	5.49	9.51
10x7	1.82	2.59	10.51	6.55	3.39	6.08	1.40	7.42	4.53	4.30	1.47	0.99	6.04	4.60	7.73
10x8	0.80	2.59	8.50	6.67	2.14	6.46	7.48	7.77	0.88	4.38	1.34	0.96	6.15	4.11	7.75
10x9	0.99	2.61	8.97	6.69	2.14	7.69	7.50	7.77	4.80	6.19	1.30	1.16	6.21	4.33	7.63
10x10	0.74	2.77	8.44	6.50	2.16	6.56	7.27	7.88	5.83	6.19	1.51	0.98	6.07	4.29	9.76

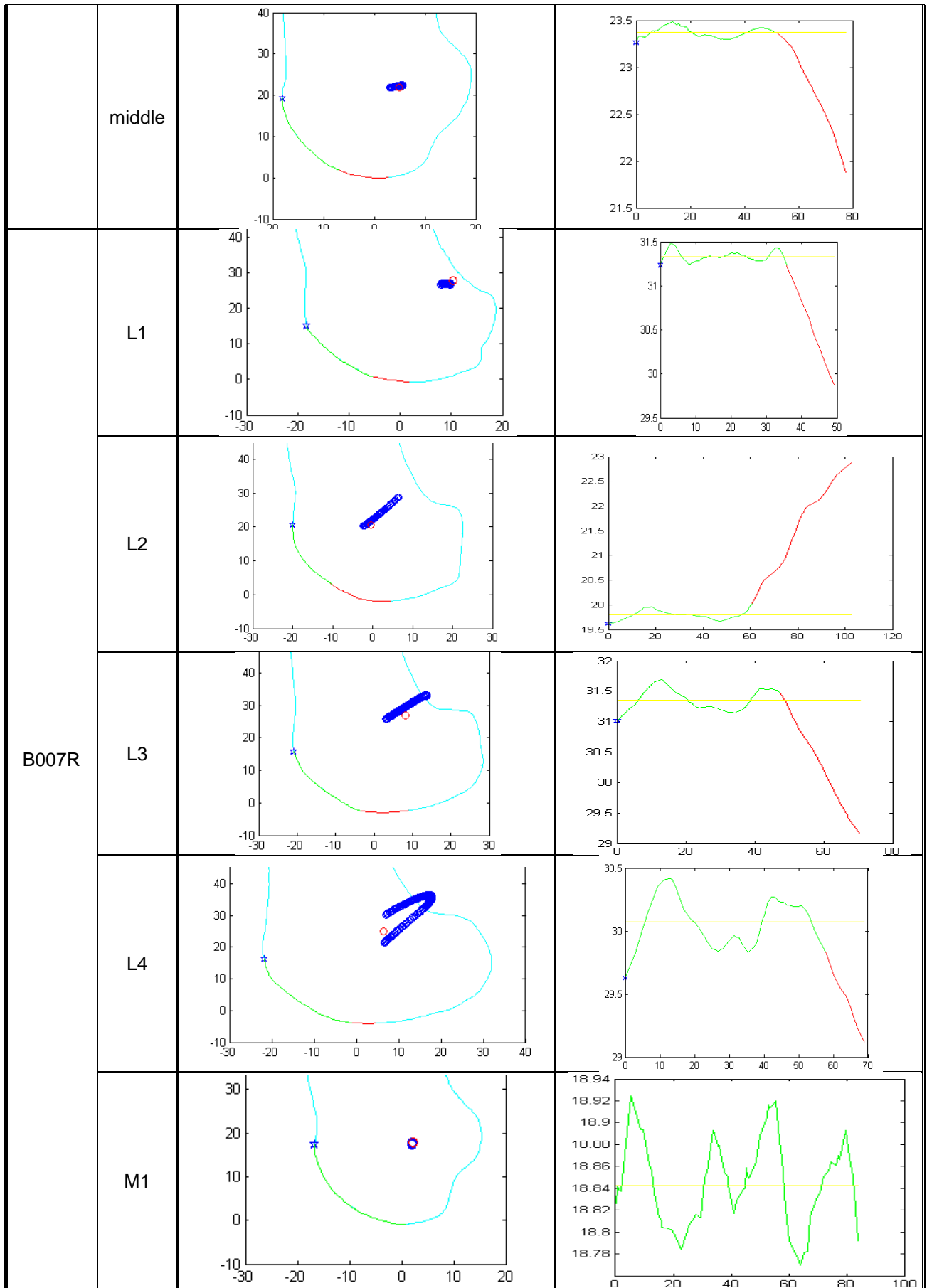
APPENDIX F: SAGITTAL CURVES OF THE NORMAL KNEES

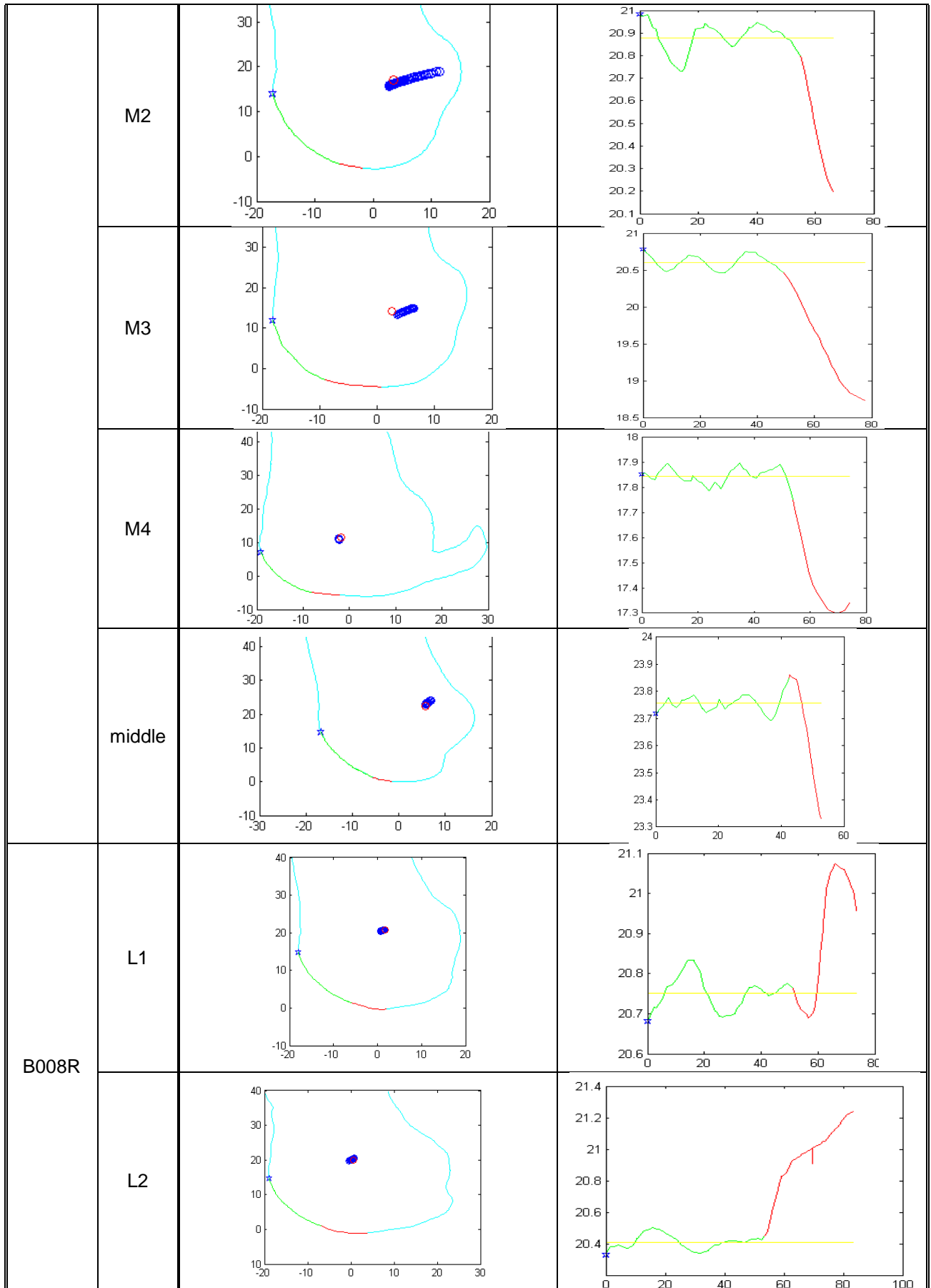
Table F1: B-spline curve and least squares circular arc fitting to the sagittal surface curves of the normal knees

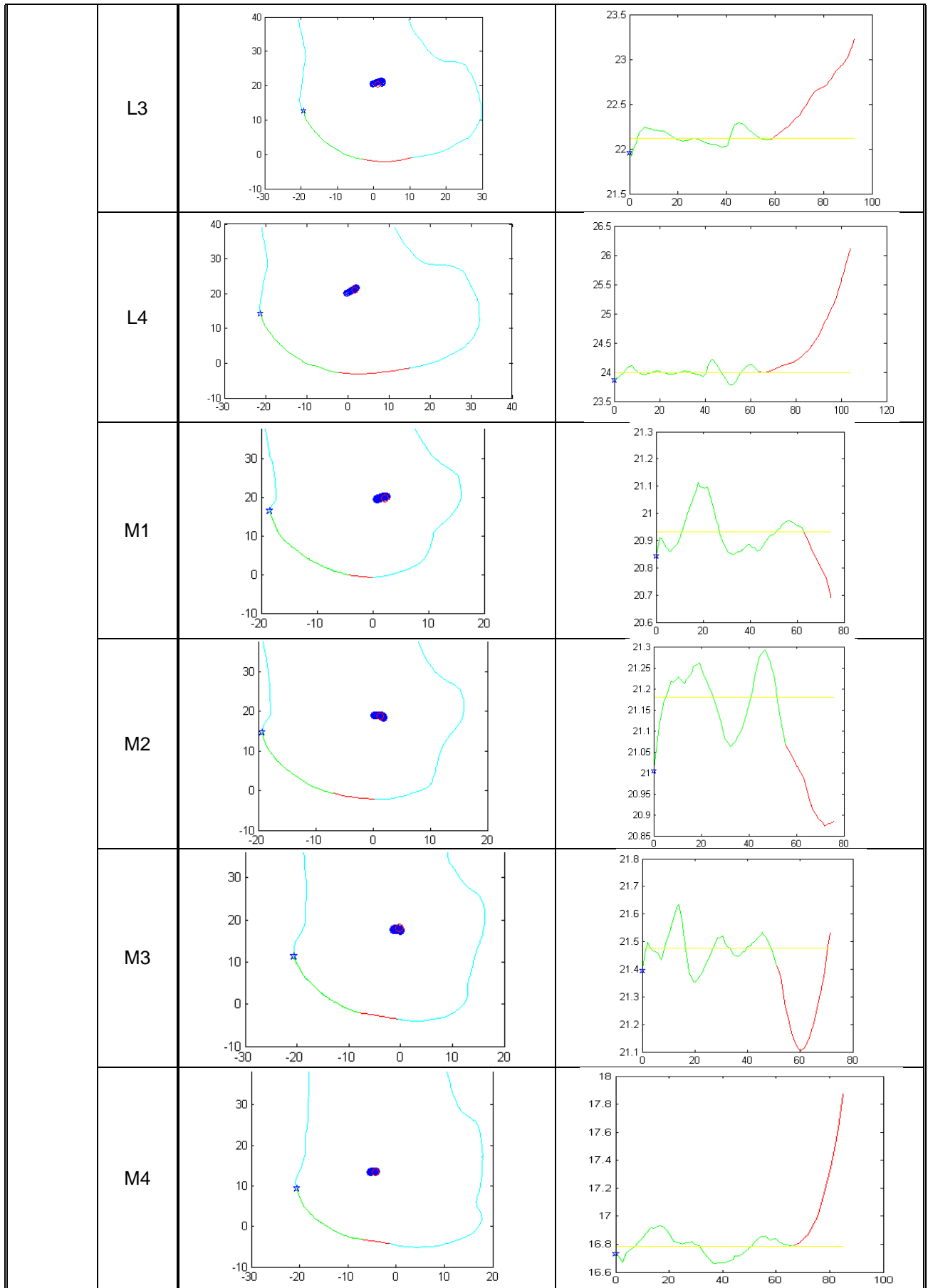
model	slice	X-coordinate [mm] vs Y- coordinate [mm]	trochlear flexion angle [°] vs distance between the centre of the arc [mm] and the data point
		blue circles: centres of the curvature (b-spline) red circle: centre of the circular arc (least squares) light blue: sagittal surface curve	green: circular section of the sagittal surface curve red: non-circular section of the sagittal surface curve yellow: radius of the circular arc
B002R	L1		
	L2		
	L3		
	L4		
	M1		

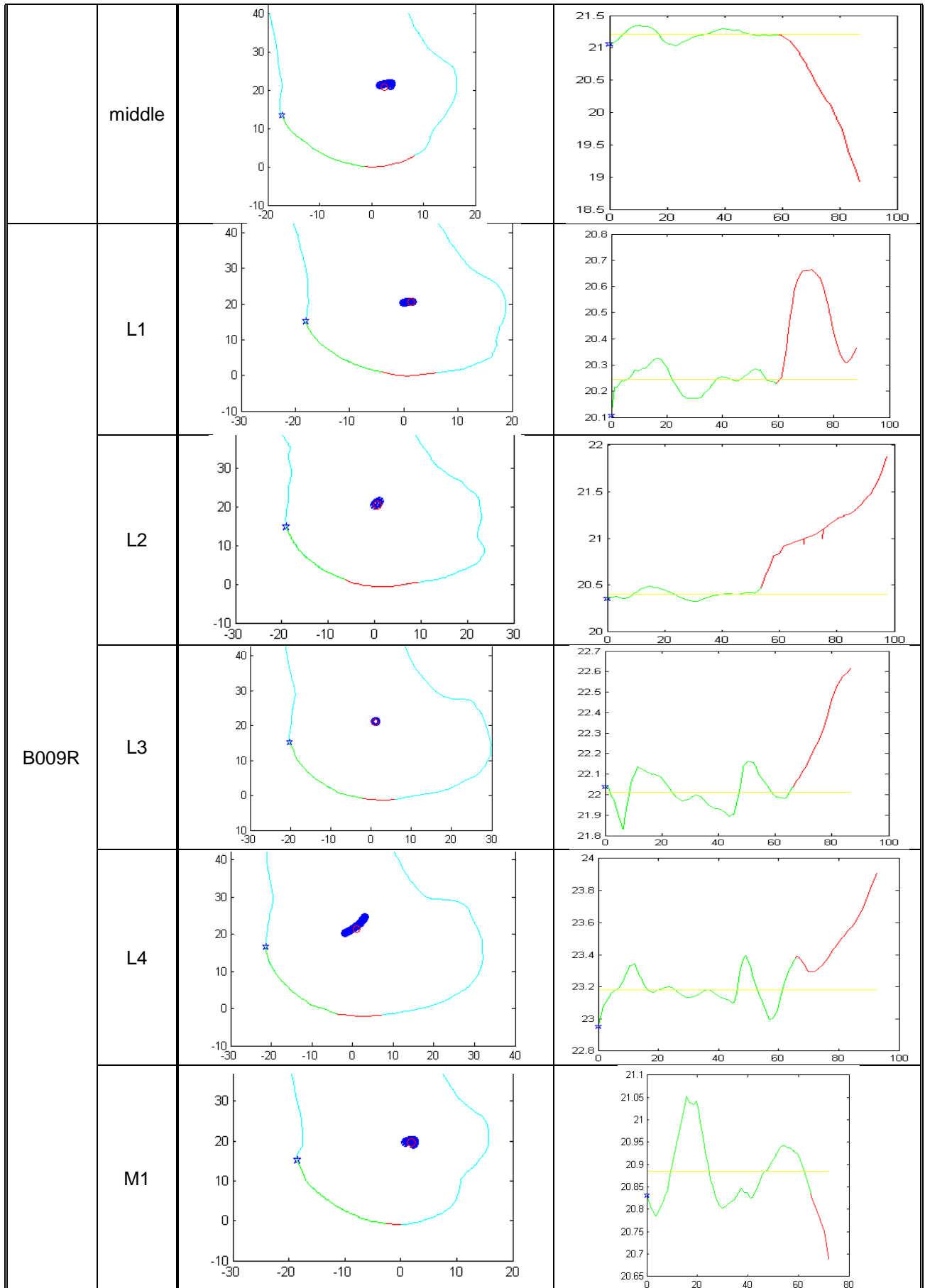


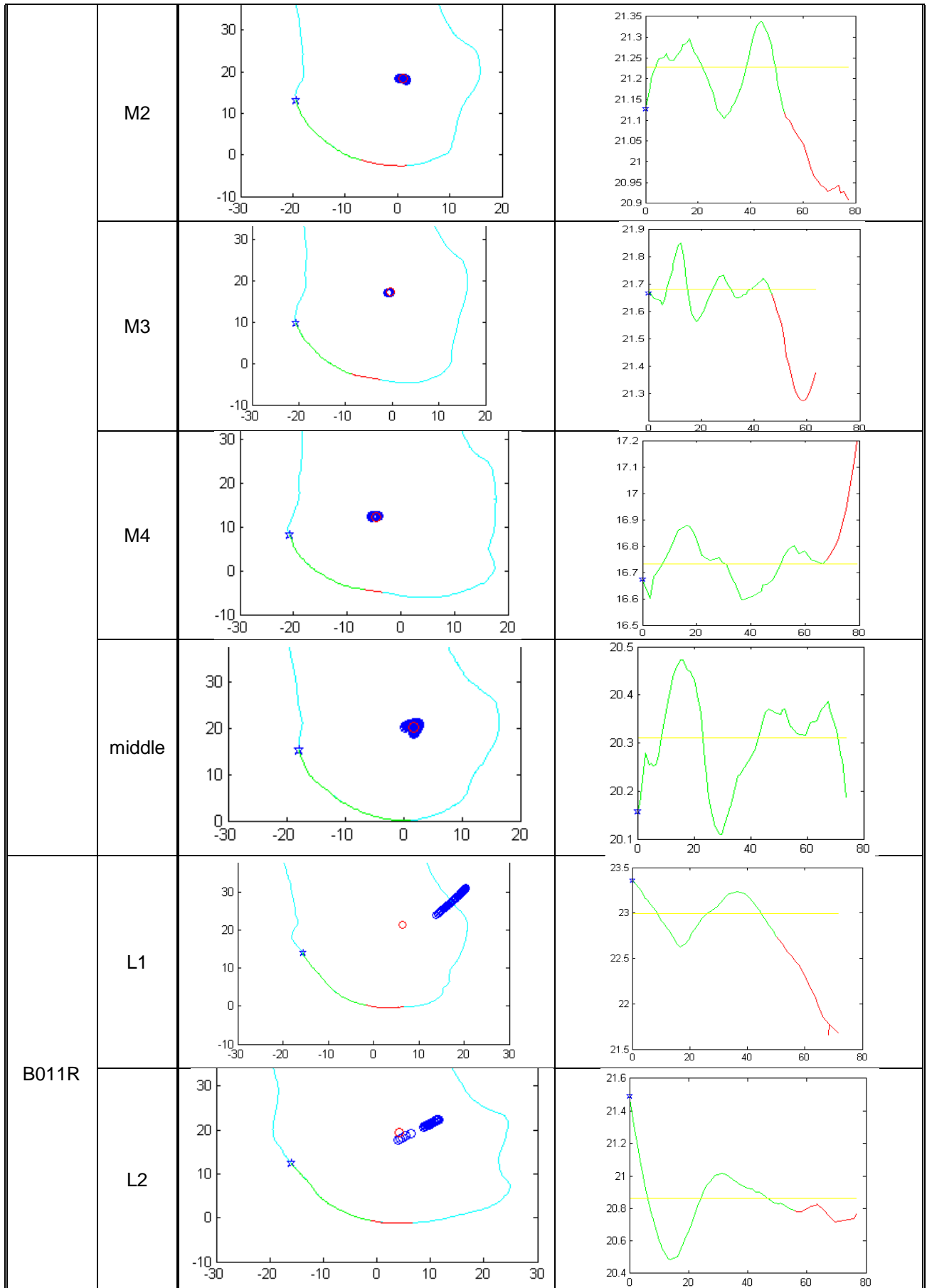


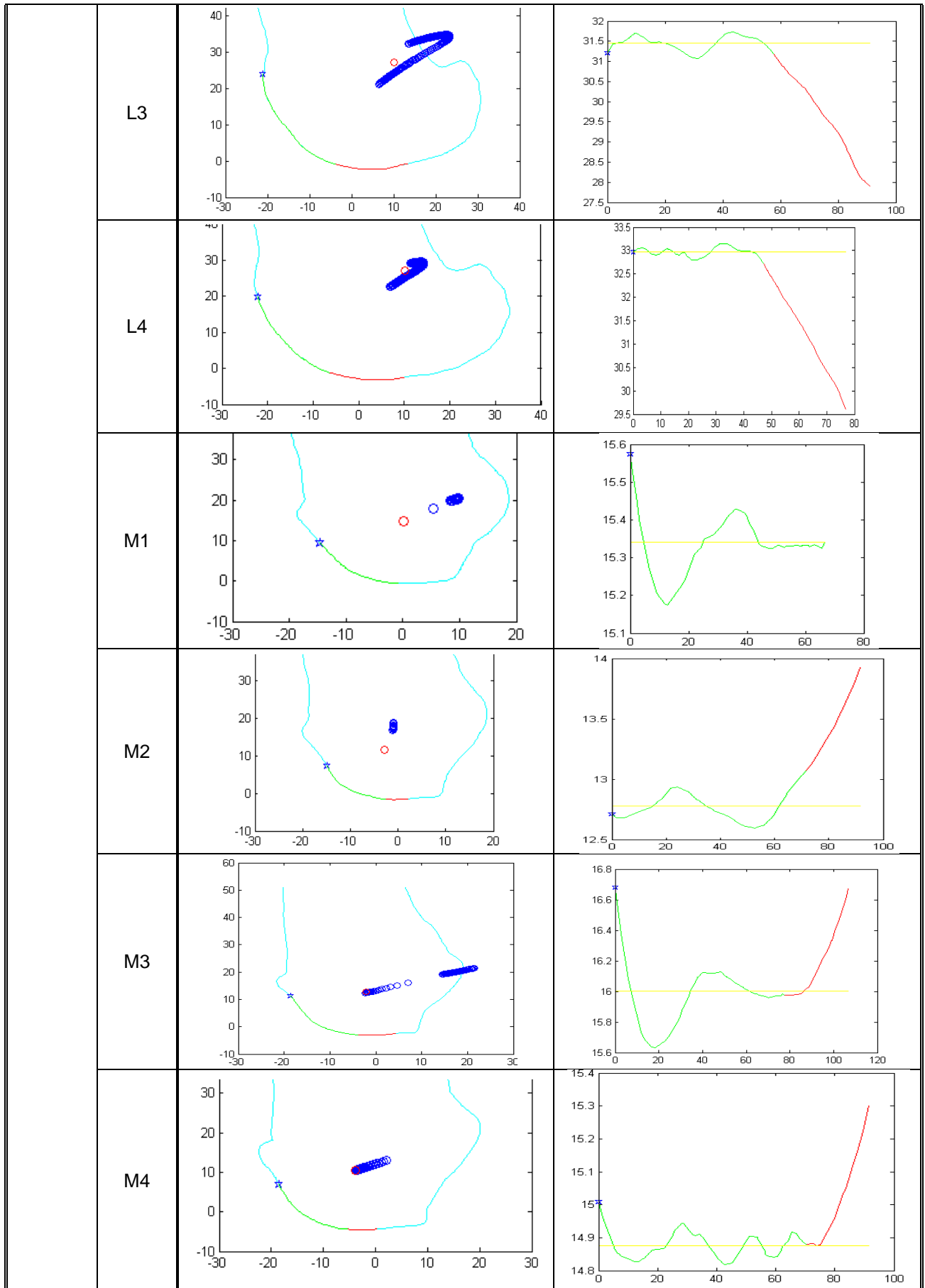


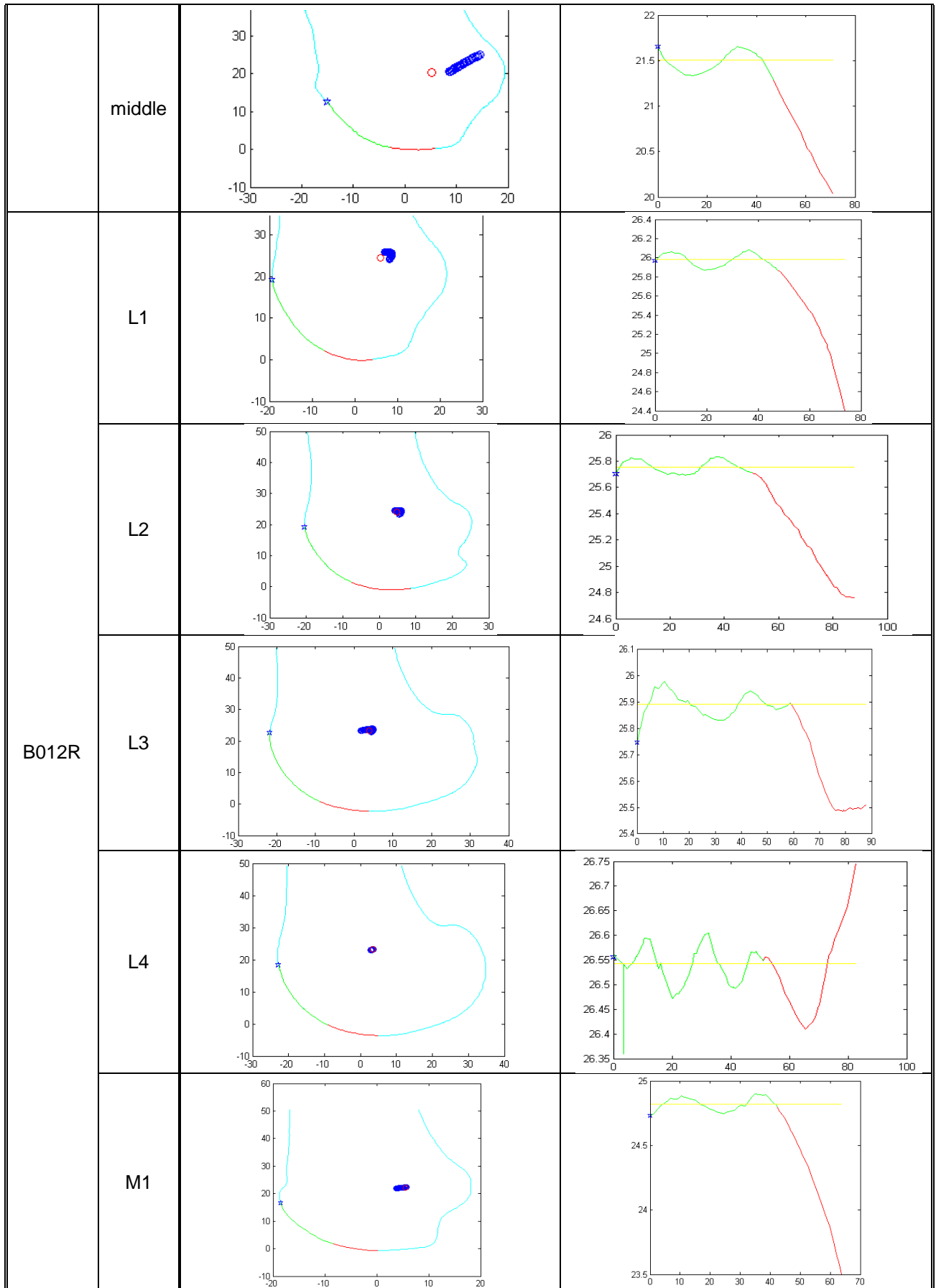


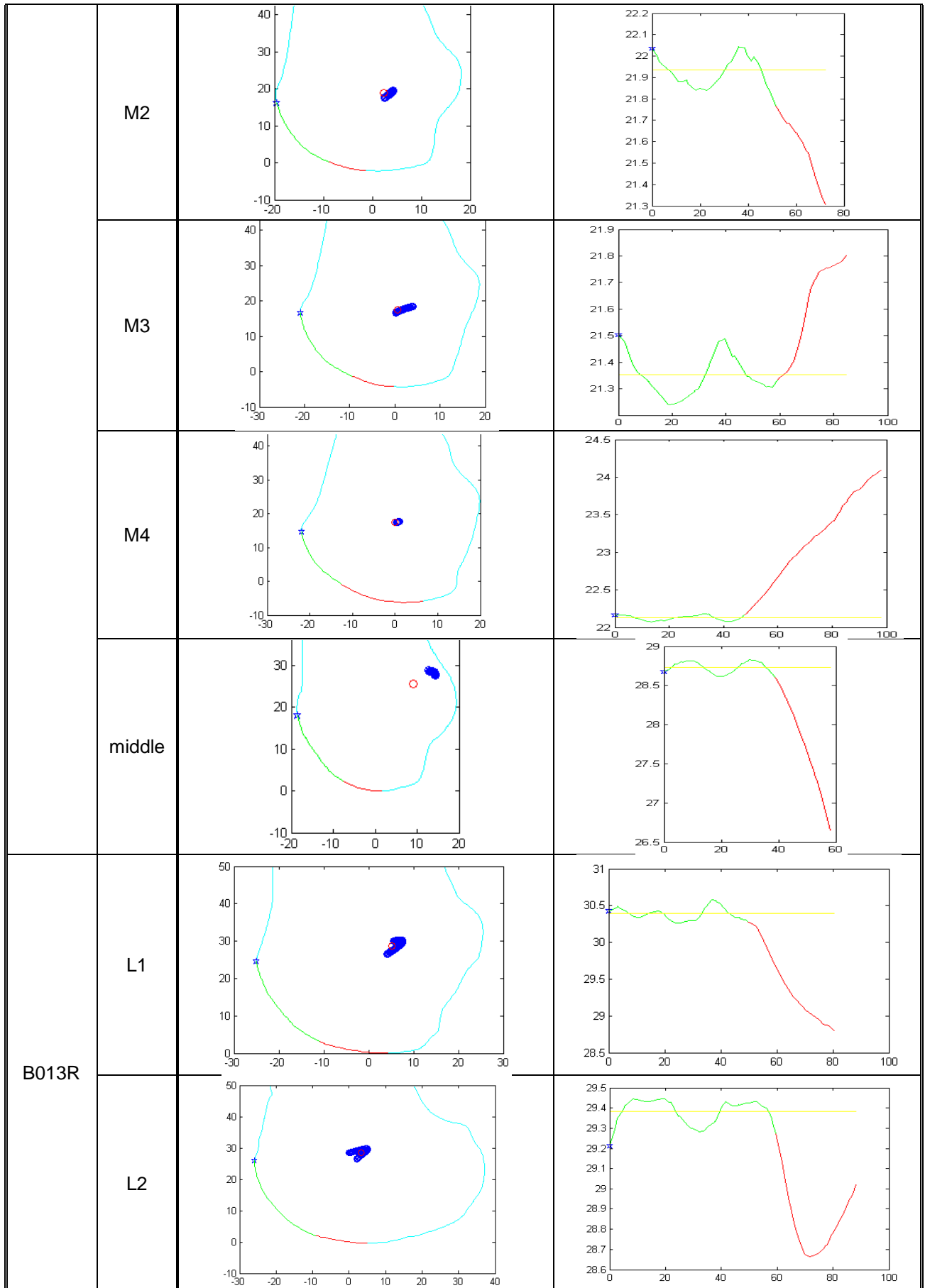


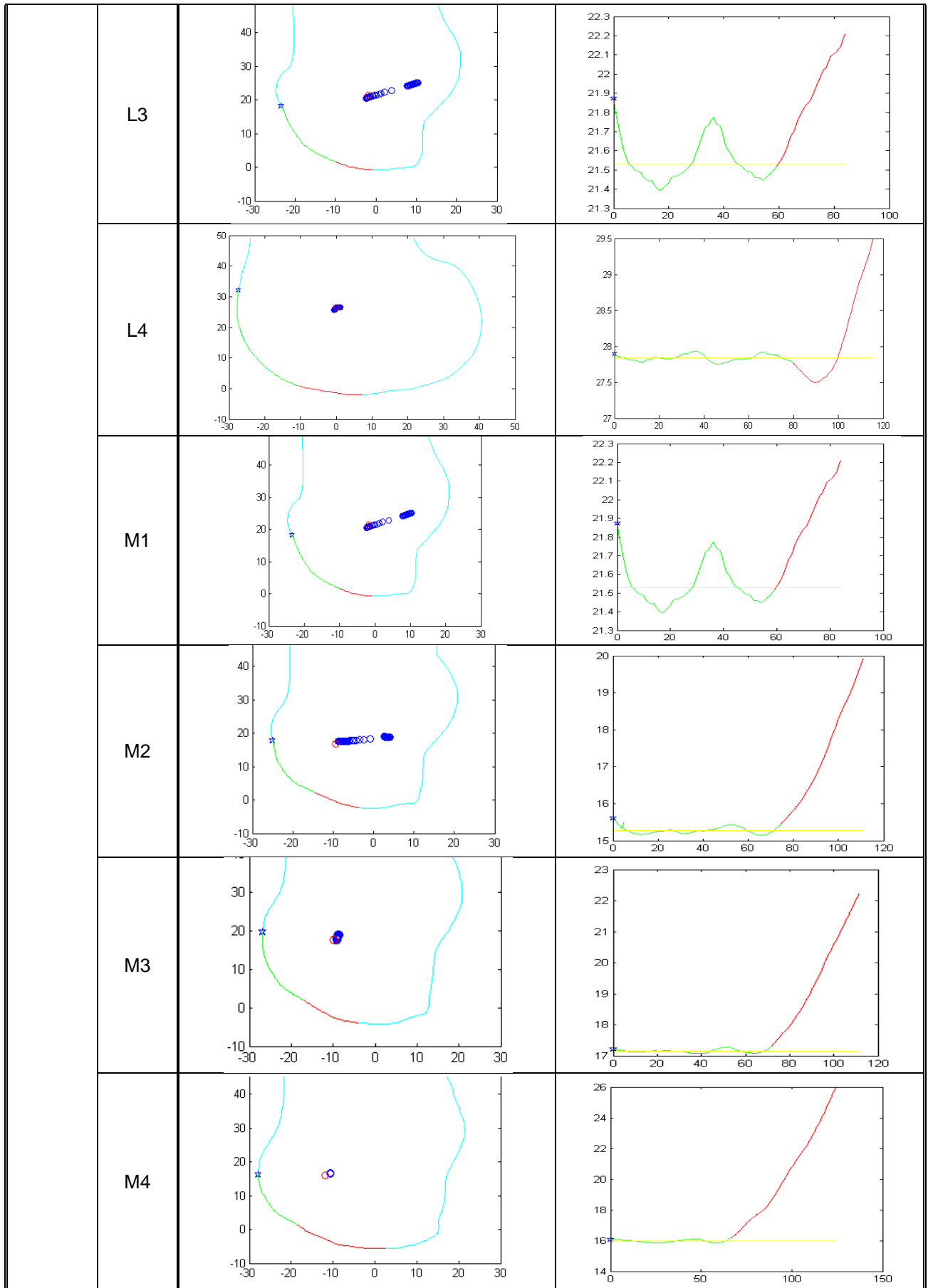


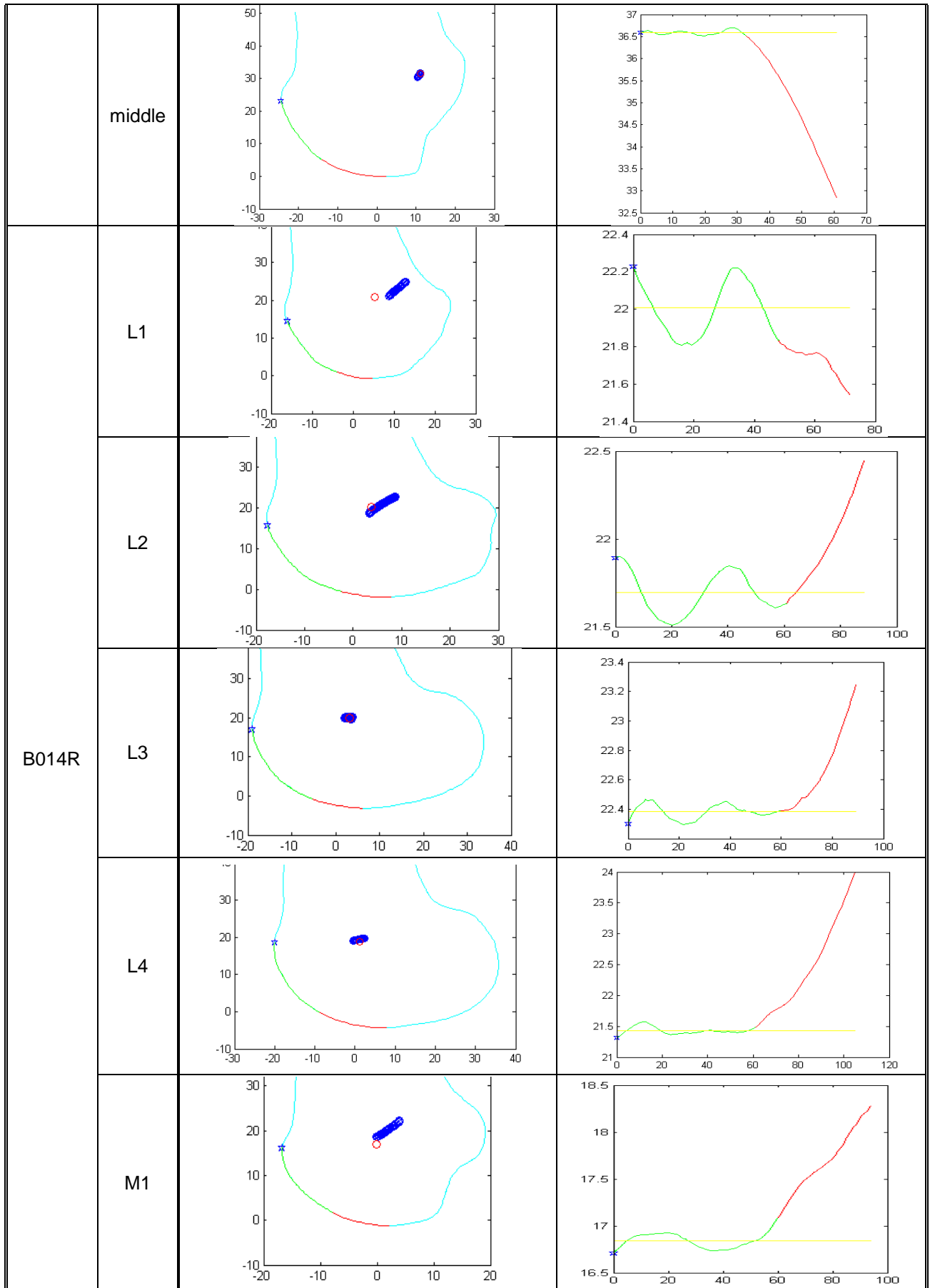


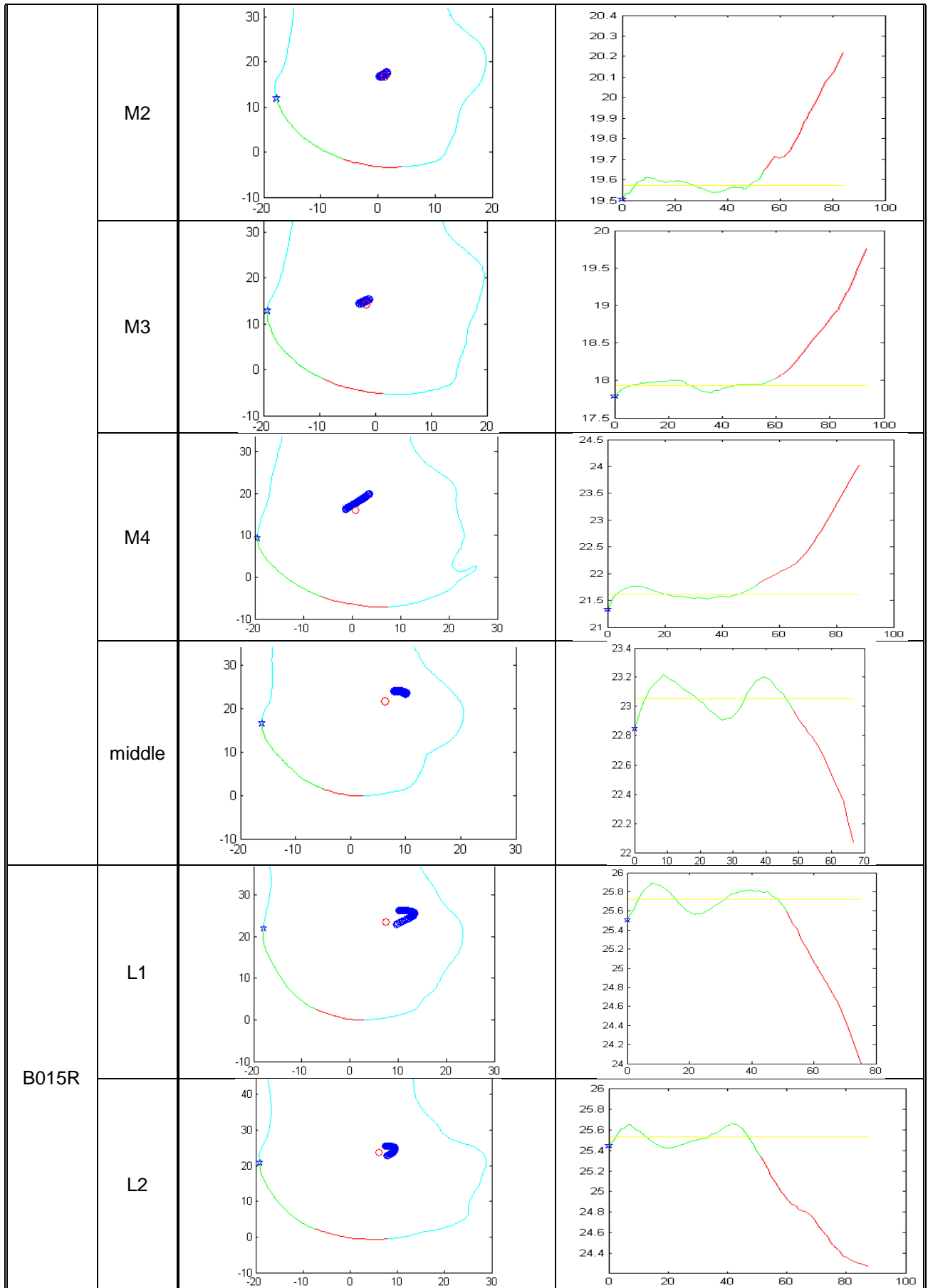


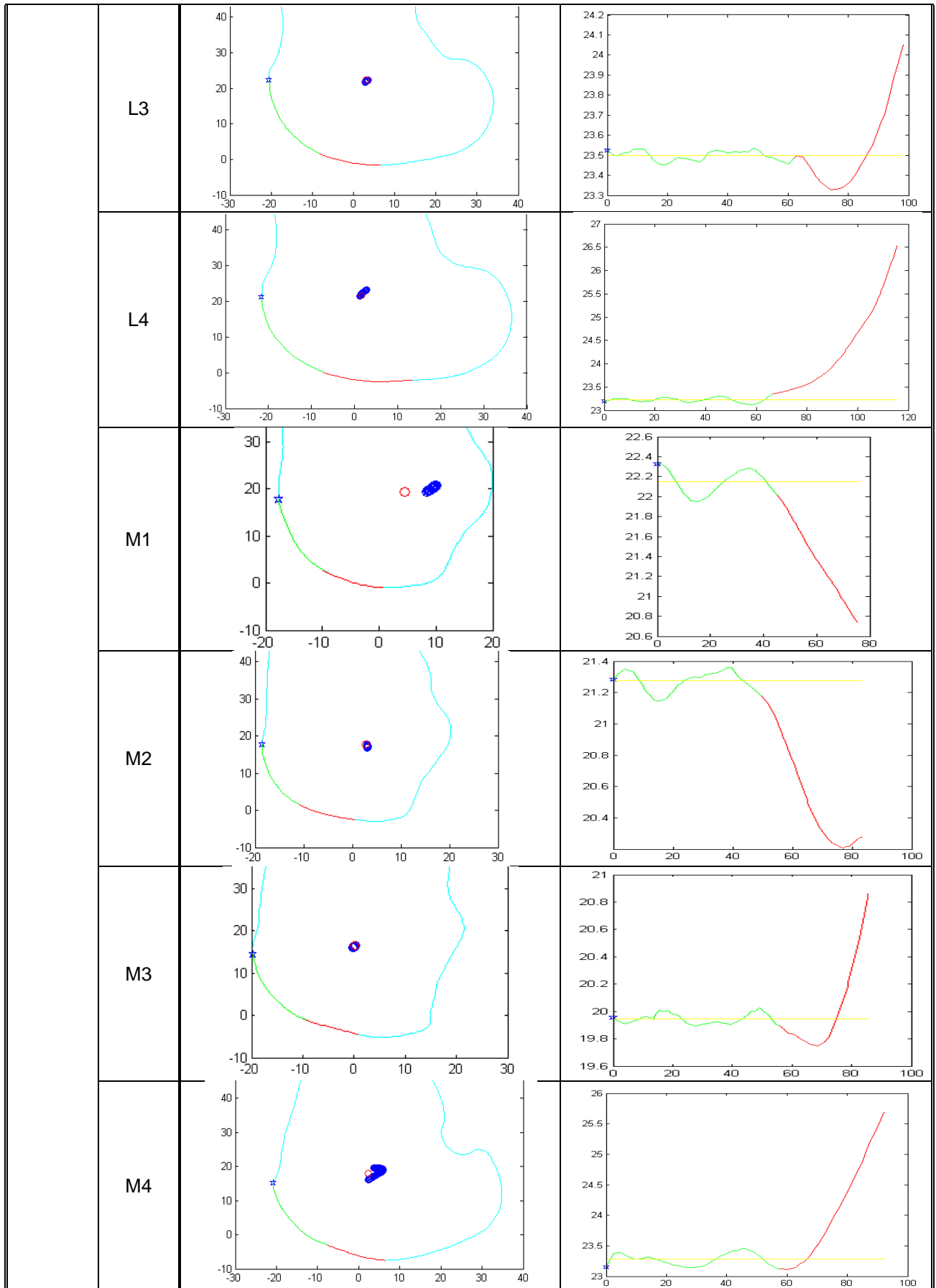


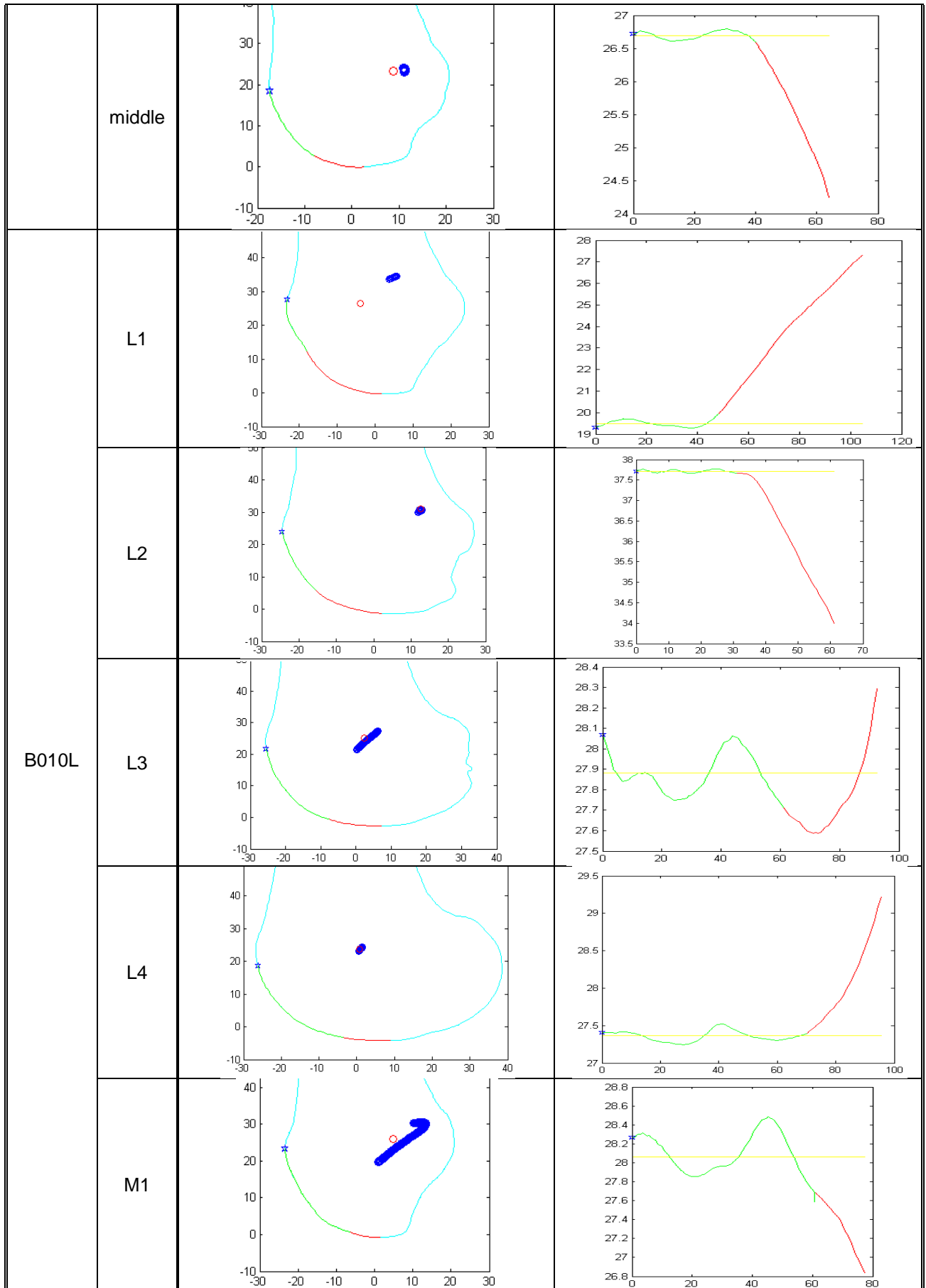


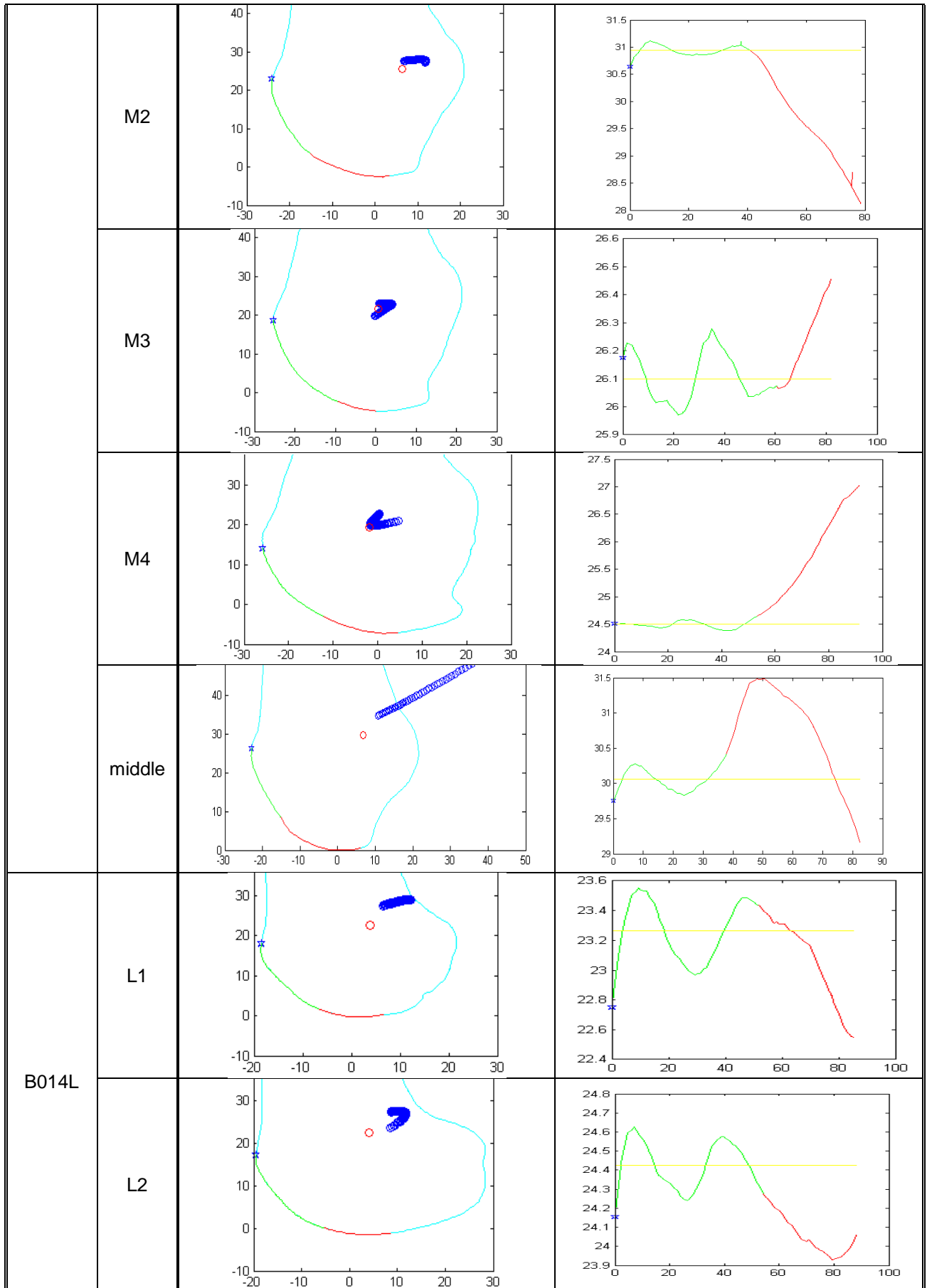


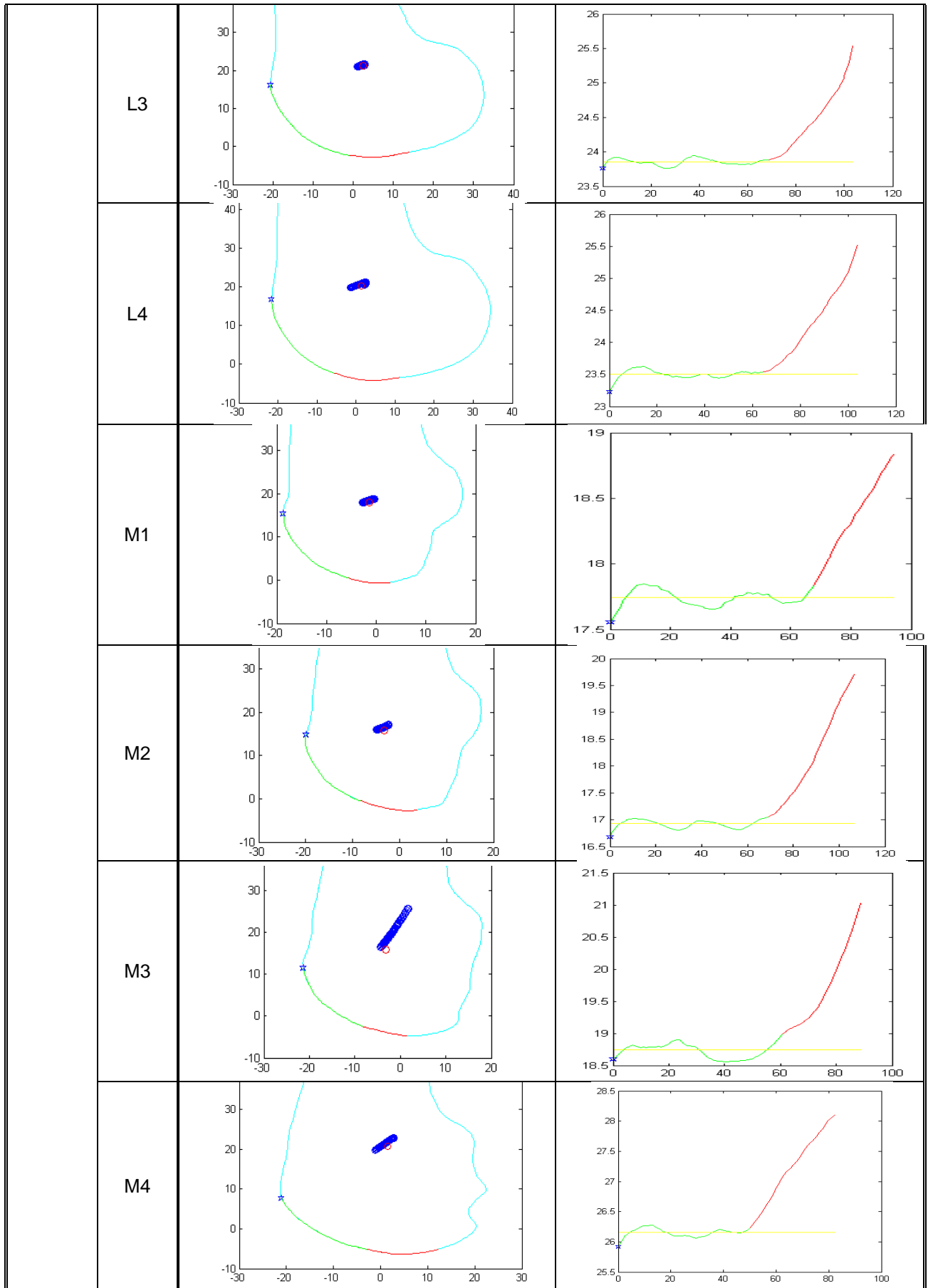


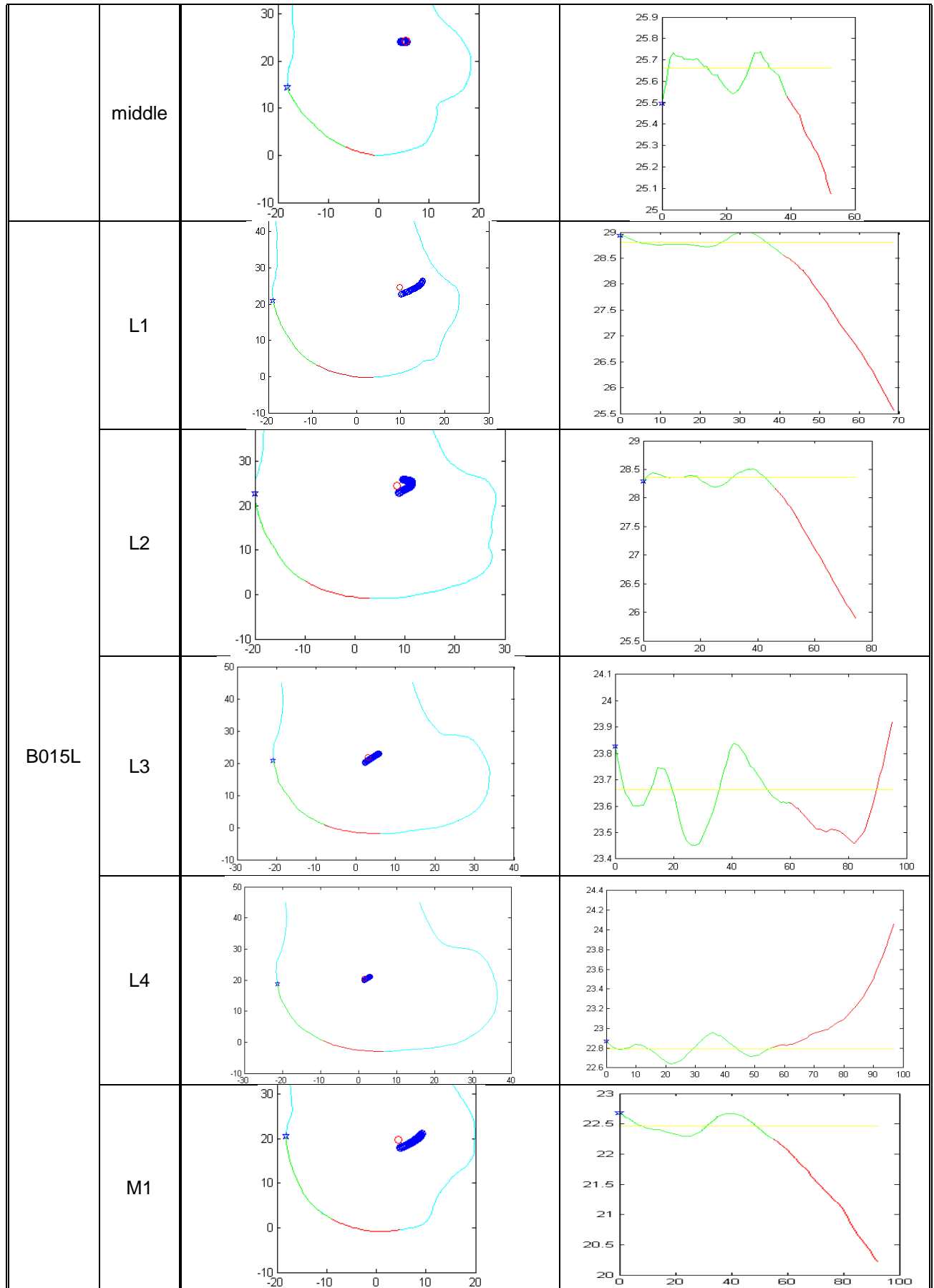


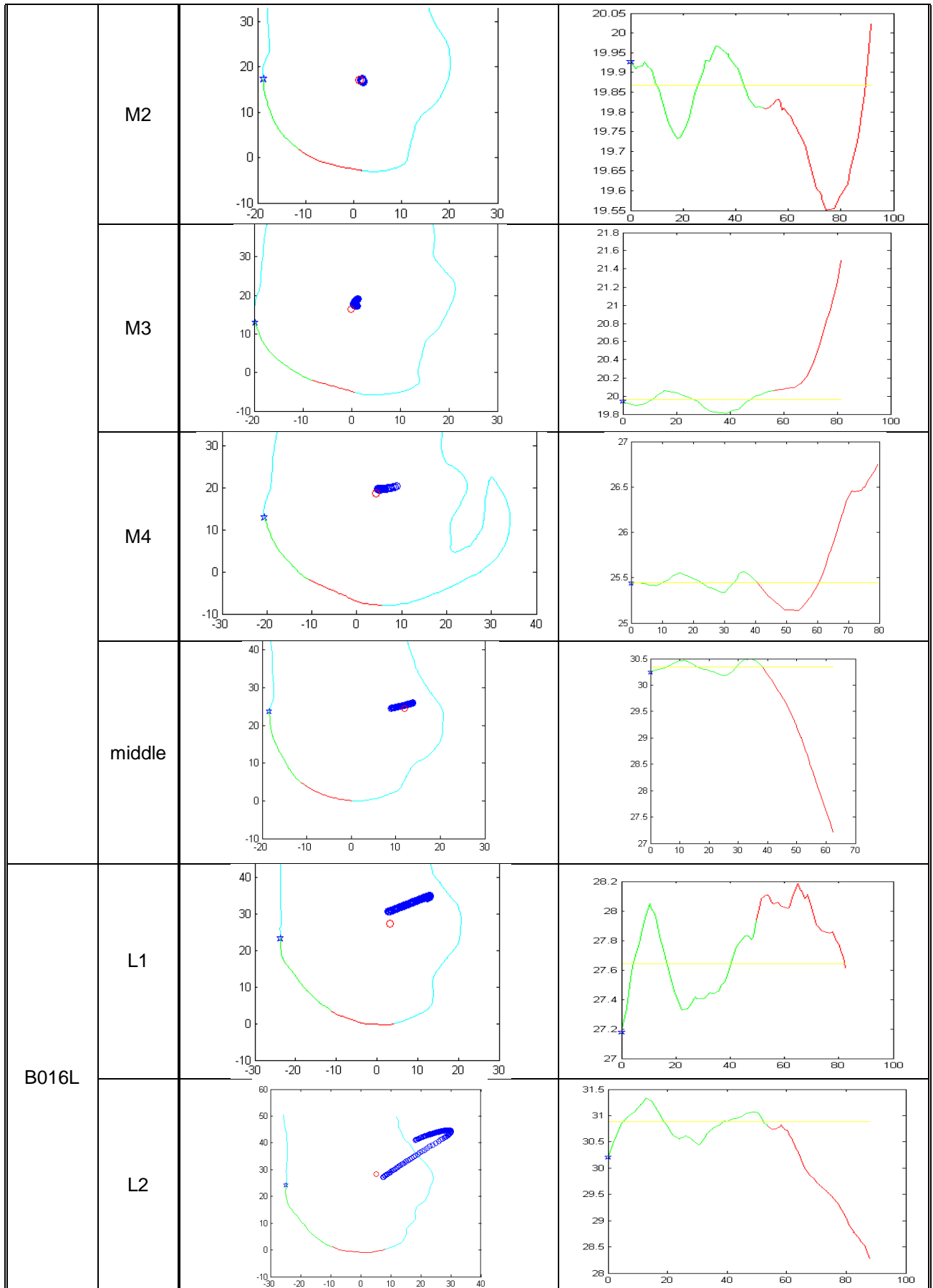


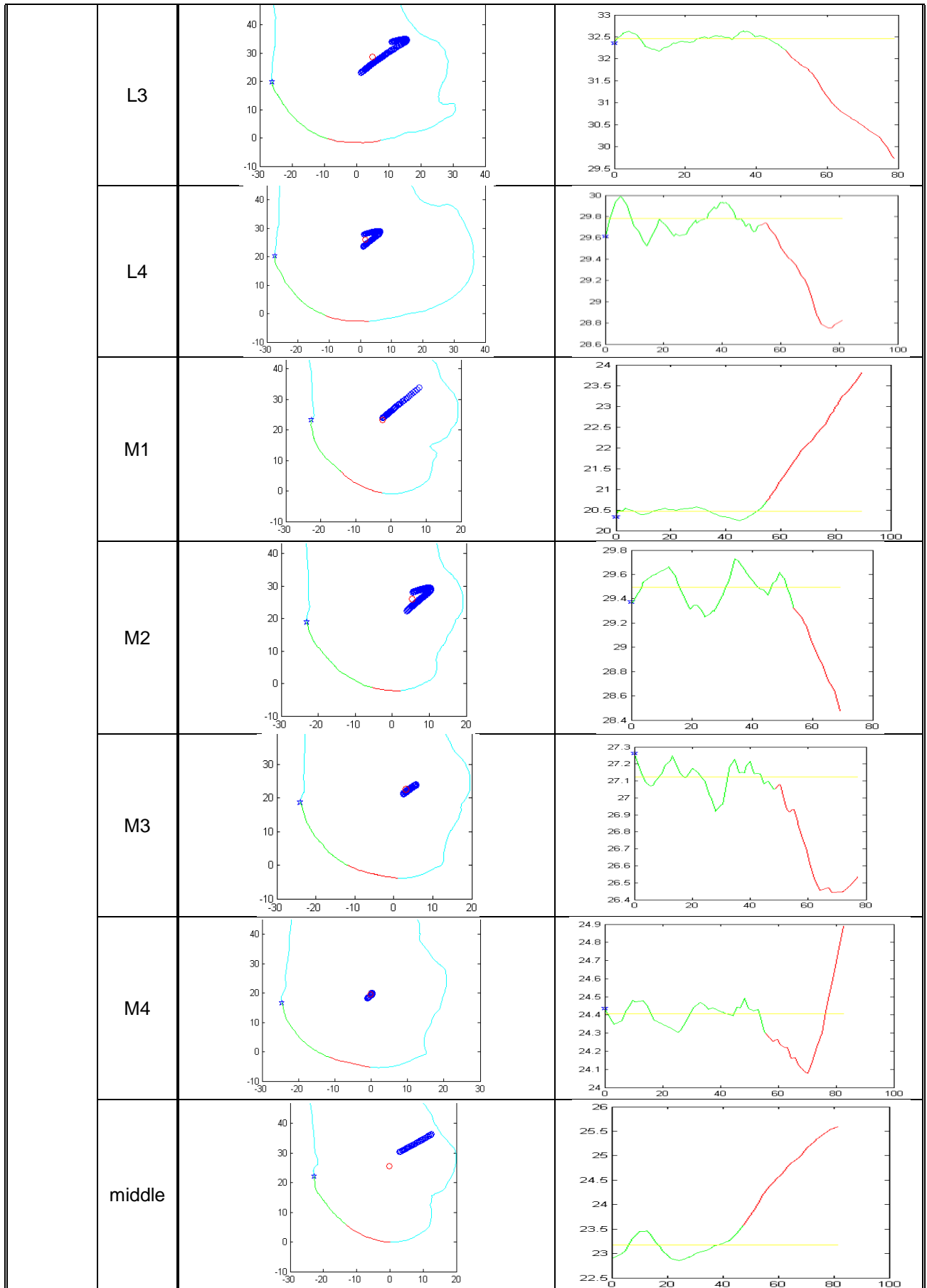












APPENDIX G: COMPARISON OF THE SULCUS ANGLE MEASUREMENT METHODS

To demonstrate that the measurements performed on a three-dimensional model is more repeatable than on the CT scans, 50 identical measurements of the sulcus were recorded for each of the two methods on the same femur. On the CT scan, the sulcus angle was measured on the measurement plane 4 (Figure 2.13), the slice which goes through the most anterior point of the trochlea. On the three-dimensional model, the measurement was performed on the measurement plane as defined in the Chapter 3.3.2.

No significant difference of the sulcus angle was shown between the two groups in sulcus angle having a confidence level higher than 99.99 % but the standard deviation of the sulcus measured on the CT scan was higher than the measurements on the three-dimensional (3D) model by 2.25 times (Table G1). The distribution of the data also shows that the measurement on the three-dimensional model was more repeatable with a smaller range (Figure G1).

Table G1: Sulcus angle measurements on a CT scan and on a three-dimensional model

	sulcus angle [°]		t-test (p value)
	CT scan	3D model	
average	136.6	139.1	< 0.0001
standard deviation	2.7	1.2	

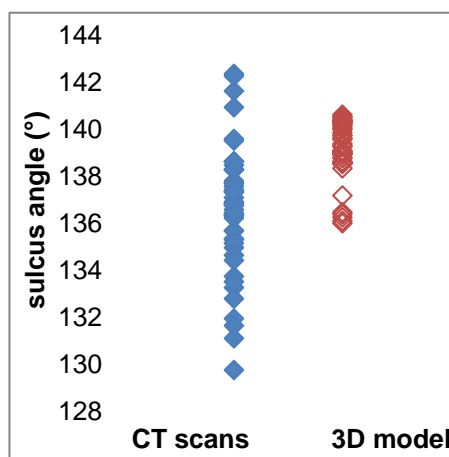


Figure G1: Sulcus angle measurements on a CT scan and on a three-dimensional (3D) model